ISTANBUL TECHNICAL UNIVERSITY ★ GRADUATE SCHOOL OF SCIENCE ENGINEERING AND TECHNOLOGY

ALTERNATIVE CONTROL STRATEGIES FOR AN ELECTROMECHANICAL ACTIVE SUSPENSION SYSTEM

M.Sc. THESIS

Sevsel Gamze KABIL

Department of Mechanical Engineering

Automotive Programme

JANUARY 2012

ISTANBUL TECHNICAL UNIVERSITY ★ GRADUATE SCHOOL OF SCIENCE ENGINEERING AND TECHNOLOGY

ALTERNATIVE CONTROL STRATEGIES FOR AN ELECTROMECHANICAL ACTIVE SUSPENSION SYSTEM

M.Sc. THESIS

Sevsel Gamze KABIL
(503091746)

Department of Mechanical Engineering

Automotive Programme

Thesis Advisor: Assist. Prof. Dr. Ozgen AKALIN

JANUARY 2012

İSTANBUL TEKNİK ÜNİVERSİTESİ ★ FEN BİLİMLERİ ENSTİTÜSÜ

BİR ELEKTROMEKANİK AKTİF SÜSPANSİYON SİSTEMİ İCİN ALTERNATİF KONTROL STRATEJİLERİ

YÜKSEK LİSANS TEZİ

Sevsel Gamze KABİL
(503091746)

Makina Mühendisliği Anabilim Dalı

Otomotiv Programı

Tez Danışmanı: Y. Doc. Dr. Özgen AKALIN

OCAK 2012

Sevsel Gamze KABIL, a **M.Sc.** student of ITU **Institute of Science and Technology** student ID 503091746, successfully defended the **thesis** entitled "**ALTERNATIVE CONTROL STRATEGIES FOR AN ELECTROMECHANICAL ACTIVE SUSPENSION SYSTEM**", which she prepared after fulfilling the requirements specified in the associated legislations, before the jury whose signatures are below.

Thesis Advisor :	**Assist. Prof. Dr. Özgen AKALIN** İstanbul Technical University	....
Jury Members :	**Prof. Dr. Ahmet Güney** İstanbul Technical University	....
	Assist. Prof.Dr. Erdem UZUNSOY Yıldız Technical University	....

Date of Submission : 15 December 2011
Date of Defense : 30 January 2012

FOREWORD

Firstly, I would like to thank my thesis advisor Assist. Prof. Dr. Ozgen AKALIN for his guidance and encouragement during my studies. This work was completed while I was working at Volkswagen AG as a trainee. I am very much thankful to Dr. Alexandra NIERSMANN, Dipl. Ing. Sascha ZEIPERT and Dipl. Ing. Andreas RIECKMANN of Volkswagen AG for their technical guidance and help.

I would like to thank Dipl. Ing. Matthias TOMECKI for his support, help and motivation.

Finally and most importantly, I would like to thank my family especially my mother for their patience.

December 2011

Sevsel Gamze KABIL
(Mechanical Engineer)

TABLE OF CONTENTS

Page

ABBREVIATIONS

ABC	**:** Active Body Control
AC	**:** Alternating Current
Aktakon	**:** Aktive Aufbau Kontrolle (Active Body Control)
CAN	**:** Controller Area Network
CG	**:** Center of gravity
DC	**:** Direct Current
DOF	**:** Degree of freedom
ECU	**:** Electronic Control Unit
e-ABC	**:** Electromechanical Active Body Control
LMI	**:** Linear Matrix Inequality
MPC	**:** Model Predictive Control
PID	**:** Proportional Integral Derivative controller
PSD	**:** Power Spectral Density
RMS	**:** Root Mean Square
Rpm	**:** Revolution per minute

LIST OF TABLES

LIST OF FIGURES

Page

LIST OF SYMBOLS

c_b	:	Body damping coefficient [N/m]
c_{bf}	:	Front body damping coefficient [N/m]
c_{br}	:	Rear body damping coefficient [N/m]
c_w	:	Tire damping coefficient [N/m]
c_{wf}	:	Front tire damping coefficient [N/m]
c_{wr}	:	Rear tire damping coefficient [N/m]
D	:	Dimensionless damping ratio [-]
D_{act}	:	Damping ratio of actuator [-]
F_{act}	:	Actuator force [N]
F_{act_f}	:	Front actuator force [N]
F_{act_r}	:	Rear actuator force [N]
F_{A_f}	:	Front accumulator spring force [N]
F_{A_r}	:	Rear accumulator spring force [N]
F_{Db_f}	:	Front damping force of sprung mass [N]
F_{Db_r}	:	Rear damping force of sprung mass [N]
F_{Dw_f}	:	Front damping force of unsprung mass [N]
F_{Dw_r}	:	Rear damping force of unsprung mass [N]
$\|F_{dyn}\|_{rms}$	:	RMS value of the dynamic wheel load [N]
F_{res}	:	Result force of actuator [N]
F_{Sb_f}	:	Front spring force of sprung mass [N]
F_{Sb_r}	:	Rear spring force of sprung mass [N]

$\boldsymbol{F_{sp}}$	:	Suspension bearing force [N]
$\boldsymbol{F_{stat}}$	:	Static force of actuator [N]
$\boldsymbol{F_{Sw_f}}$	:	Front spring force of unsprung mass [N]
$\boldsymbol{F_{Sw_r}}$	:	Rear spring force of unsprung mass [N]
$\boldsymbol{F(t)}$	:	Actuator force [N]
$\boldsymbol{F_w}$	:	Wheel load [N]
$\boldsymbol{h}$	:	Roadway excitation (input of simulations) [m]
$\boldsymbol{h_f}$	:	Front roadway excitation [m]
$\boldsymbol{h_r}$	:	Rear roadway excitation [m]
$\boldsymbol{\dot{h}}$	:	Roadway excitation velocity [m/s]
$\boldsymbol{\dot{h}_f}$	:	Front roadway excitation velocity [m/s]
$\boldsymbol{\dot{h}_r}$	:	Rear roadway excitation velocity [m/s]
$\boldsymbol{i}$	:	Suspension compression ratio [-]
$\boldsymbol{i_f}$	:	Front suspension compression ratio [-]
$\boldsymbol{i_r}$	:	Rear suspension compression ratio [-]
$\boldsymbol{J_y}$	:	Pitch moment of inertia [$kg \cdot m^2$]
$\boldsymbol{k_A}$	:	Accumulator spring Stiffness [N/m]
$\boldsymbol{k_{Af}}$	:	Front accumulator spring Stiffness [N/m]
$\boldsymbol{k_{Ar}}$	:	Rear accumulator spring Stiffness [N/m]
$\boldsymbol{k_b}$	:	Body spring stiffness [N/m]
$\boldsymbol{k_{bf}}$	:	Front body spring stiffness [N/m]
$\boldsymbol{k_{br}}$	:	Rear body spring stiffness [N/m]
$\boldsymbol{k_w}$	:	Tire stiffness [N/m]
$\boldsymbol{k_{wf}}$	:	Front tire stiffness [N/m]
$\boldsymbol{k_{wr}}$	:	Rear tire stiffness [N/m]

l_f	:	Front wheelbase [m]
l_r	:	Rear wheelbase [m]
$l_{suspension}$	:	Suspension bearing lateral distance from chassis [m]
l_{wheel}	:	Wheel lateral distance from chassis [m]
m_b	:	Sprung mass [kg]
m_{bf}	:	Front sprung mass [kg]
m_{br}	:	Rear sprung mass [kg]
m_w	:	Unsprung mass [kg]
v	:	Longitudinal velocity of the vehicle [m/s]
$v_{act,z}$	:	Vertical velocity of the actuator [m/s]
$\mathbf{w}$	:	Maximum rotational speed of the electromotor [rpm]
ω_b	:	The undamped natural frequency of the vehicle body [rad/s]
ω_d	:	The damped natural frequency of the vehicle body [rad/s]
$\omega_{0,act}$	:	Natural frequency of actuator [rad/s]
ω_w	:	Natural frequency of wheel [rad/s]
z_{act}	:	Spring seat relative displacement [m]
z_{actf}	:	Front spring seat relative displacement [m]
z_{actr}	:	Rear spring seat relative displacement [m]
z_b	:	Vertical body displacement [m]
z_{bf}	:	Front vertical body displacement [m]
z_{br}	:	Rear vertical body displacement [m]
$\dot{z}_b$	:	Vertical body velocity [m/s]
$\dot{z}_{bf}$	:	Front vertical body velocity [m/s]
$\dot{z}_{br}$	:	Rear vertical body velocity [m/s]
$\ddot{z}_b$	:	Vertical body acceleration [m]

$\ddot{z}_{bf}$	:	Front body acceleration $[\mathrm{m/s^2}]$
$\ddot{z}_{br}$	:	Rear body acceleration $[\mathrm{m/s^2}]$
z_w	:	Vertical wheel displacement [m]
z_{wf}	:	Front vertical wheel displacement [m]
z_{wr}	:	Rear vertical wheel displacement [m]
$\dot{z}_w$	:	Vertical wheel velocity $[\mathrm{m/s}]$
$\dot{z}_{wf}$	:	Front vertical wheel velocity $[\mathrm{m/s}]$
$\dot{z}_{wr}$	:	Rear vertical wheel velocity $[\mathrm{m/s}]$
$\ddot{z}_w$	:	Vertical wheel acceleration $[\mathrm{m/s^2}]$
$\ddot{z}_{wf}$	:	Front vertical wheel acceleration $[\mathrm{m/s^2}]$
$\ddot{z}_{wr}$	:	Rear vertical wheel acceleration $[\mathrm{m/s^2}]$
$\lVert\ddot{z}_b\rVert_{rms}$	:	RMS value of the vertical vehicle body acceleration $[\mathrm{m/s^2}]$
α	:	Actuator’s spindle pitch [m]
φ	:	Pitch angle $[\mathrm{rad}]$
$\ddot{\varphi}$	:	Pitch acceleration $[\mathrm{rad/s^2}]$
σ	:	Decaying constant
$\Delta z_{pitch_{f,r}}$	:	Relative pitch motion [m]
$\Delta z_{b_{f,r}}$	:	Relative vertical chassis motion [m]

ALTERNATIVE CONTROL STRATEGIES
FOR AN ELECTROMECHANICAL ACTIVE SUSPENSION SYSTEM

SUMMARY

In recent years, various types of active suspension systems have been developed and introduced into the market, in order to improve the ride and handling characteristics of vehicles. Most of these systems are based on hydraulic actuators, which involve certain disadvantages as high energy consumption, dirt contamination or restricted suitability for hybrid vehicles.

Therefore, in order to eliminate these disadvantages, a new active body control system was developed, in which the conventional springs and dampers are retained, and the spring seat position is controlled via electromechanical actuators. To exploit the full potential of this innovative suspension system, a convenient control strategy needs to be designed that represents the goal of this thesis.

First of all, a MATLAB/Simulink model has been created, which embodies the most relevant dynamic properties of the vehicle for the purpose of reducing the number of tests in reality as those take more time and are riskier.

Initially, several different control strategies have been evaluated in MATLAB/Simulink for understanding the reaction logic of each controller and hereby its impact on the test vehicle.

Subsequently, the best control parameters have been determined for each controller model in order to get the best ride comfort possible. Finally, supported by the results of the simulations, the controller strategies were validated in the test vehicle.

The significant findings that result from this work show that the Groundhook strategy deteriorates the ride comfort in comparison to the passive suspension system, resulting from the controller strategy focusing on driving safety and not on ride comfort. The P-Controller (minimizing the vertical body acceleration itself) or especially the Skyhook controller is able to improve the ride comfort substantially. With State-Space controller the best ride comfort of the test vehicle is obtained. This already very good behavior can be exceeded by the State-Space strategy particularly when combining it with a Skyhook controller. The combined State-Space / Skyhook strategy generates a ride comfort in the test vehicle, which seems even more enhanced than anticipated by the objective PSD values.

Consequently, this control is recommended to be applied for the active electromechanical suspension system. In order to obtain even more improved ride comfort with the combined controller, some issues are recommended additionally. These are differing the control parameters (constants), adding the resulting actuator displacements by using another summation structure (for example instead of adding the displacement of 100% Skyhook with 100% State-Space control’s, 60% Skyhook

with 90% State-Space control) or combining an additional controller such as P-Controller might be beneficial.

BİR ELEKTROMEKANİK AKTİF SÜSPANSİYON SİSTEMİ İÇİN ALTERNATİF KONTROL STRATEJİLERİ

ÖZET

Günümüzde konvansiyonel taşıtlar başta olmak üzere en yaygın olarak kullanılan süspansiyon çeşidi pasif süspansiyon olmakla birlikte, elektrikli ve hibrit araçlara yönelinmesiyle çeşitli mekatronik aktif süspansiyon sistemlerine de ihtiyaç duyulmaya başlanmıştır. Geçtiğimiz yıllarda taşıt sürüş konforunu iyileştirmek amacıyla çeşitli aktif süspansiyon sistemleri geliştirilmiş ve markette yer bulmaya başlamıştır. Şu an için prototipleri üretilmiş ve kullanılan, "low bandwidth (slow active)" ve "high bandwitdh (fully active)" olmak üzere iki çeşit aktif süspansiyon sistemi bulunmaktadır.

Enerji gereksinimleri, çalışma frekans aralıkları ve hız kısıtlamaları farklı olan bu iki konseptten talebe göre uygun olan seçildikten sonra konfor ve güvenlik açısından en iyi sonuç alınabilecek kontrolcülerle bu sistemler desteklenmektedir. Bu aktif sistemlerin çoğu hidrolik kontrol elemanları içermekte olup, yüksek enerji tüketimi, hidrolik sistemin yağ vb. akışkanlarla çalışması sonucu kir tutabilmesi ve hibrit (ya da elektrikli) araçlara sınırlı uyumu gibi dezavantajları bulunmaktadır.

Bu sebeple yine geçtiğimiz yıllarda, bu dezavantajlardan kurtulabilmek için süspansiyon yay yatağı (spring seat) pozisyonunu 5 Hz'e kadar kontrol eden elektromekanik kontrol elemanı içeren yeni bir aktif gövde kontrol (e-ABC) sistemi geliştirilmiştir.

Bu sistem iki yay içermekte olup bir tanesi normal bir konvansiyonel sistemdeki gibi süspansiyon yayı iken, diğeri statik yüklerin taşınmasından sorumlu 'akümülatör yayı' olarak tanımlanan yardımcı bir yaydır. Bu yayın varlığı sayesinde elektromekanik aktif süspansiyon sistemi hidrolik sisteme göre daha az ilave yakıt tüketimine sebep olmaktadır ve sistemdeki yay yatağının hareketine müdahale etme yeteneğine sahip kontrol elemanı sadece dinamik yüklerin karşılanmasında kullanılmaktadır.

Bu yenilikçi sistemin tam performansından faydalanabilmek amacıyla temel olarak iyi bir sürüş konforu elde etmek için en uygun kontrol stratejisinin tasarımı bu yüksek lisans tezinin hedefidir.

Bu bağlamda, öncelikle gerçekte yapılacak ve riskli olabilecek test sayısını aza indirgemek, dolayısıyla aracın zarar görmesini engellemek ve zamandan tasarruf etmek için taşıtın dinamik özelliklerini yansıtan bir MATLAB/Simulink modeli oluşturulmuştur. Bu Simulink modeli bir yarım taşıt modelidir. Sağ ve sol tekerlekler bir orta düzlemde tek bir tekerlek olarak kabul edilerek tek izli bir model oluşturulmuştur. Model altı ana bloktan oluşmaktadır. Bunlar gövde, kontrolcü, yay, sönüm elemanı, tekerlek, girdi ve çıktı bloklarıdır. Stokastik girdi verisi olarak test sürüşlerinin gerçekleştirildiği pistin x ve z düzlemindeki değerleri kullanılmış ve bu testler 60 km/h hızla yapılmıştır. Simulink modeli yarım taşıt modeli olduğundan

taşıtın yalpa hareketi ihmal edilmiştir. Ayrıca taşıt gövde elastisitesi ve lastik sönüm sabiti de ihmal edilen parametreler arasındadır.

İlk olarak, araç üzerindeki etkilerini ve aracın cevabını anlamak amacıyla MATLAB/Simulink'te Skyhook, Groundhook, State-Space, P-Kontrol ve 'Skyhook ile State-Space'in birlikte çalıştırılmasıyla elde edilen kombine kontrol' gibi birçok farklı kontrol stratejisi ve bloğu tasarlanmıştır.

Daha sonra, araçtan en iyi konfor değerini elde edebilmek için bu stratejilerin ilgili kontrol bloklarında kullanılmak üzere en uygun kontrol parametreleri, simülasyonlarin birçok kez tekrarlanmasıyla veya MATLAB içerisinde çeşitli döngüler (loop) yardımıyla belirlenmiştir. Seçilen uygun kontrol parametreleri ile yine simülasyonlarla, süspansiyon sisteminin limit ve sınırları sınanarak test esnasında herhangi bir tehlikeye mahal verilmemesi sağlanmıştır. Sonuç olarak, simülasyonlardan elde edilen en iyi sonuçları veren kontrol parametreleri aracın yazılımına (dSpace programı) entegre edilerek araç üzerinde testler yapılmıştır. Bu testlerin sonuçları konfor için, en basit değerlendirmelerden biri olduğu varsayılan taşıt gövde düşey ivmesinin Güç Spektrum Yoğunluğu (PSD) değerlerine göre karşılaştırılmıştır. Karşılaştırma ve değerlendirmeler yapılırken PSD eğrisinin maksimum değerleri baz alınmıştır. Taşıt gövde ivmesinin PSD diyagramına bakıldığında bu maksimum değer, 0-5 Hz. arasında elde edilmekte olup, yol pürüzlülüğünün taşıt gövdesine etkisini göstermektedir. Bu frekans değerleri arasındaki PSD eğrisinin en yüksek değeri ne kadar düşükse sürüş konforunun o kadar iyi olduğu söylenebilir.

İncelenen kontrol strajelerini konfor açısından kötüden iyiye doğru gidecek şekilde özetlemek gerekirse:

Genellikle konfor için değil yol tutuş güvenliği için kullanılan Groundhook stratejisi simülasyonlarla ve taşıt üzerinde incelenmiştir. Tahmin edildiği gibi Groundhook kontrol prensibi ile sürüş konforu açısından pek olumlu sonuçlar elde edilememiştir. Tekerlek düşey hızını kontrol girdisi olarak kullanan bu strateji konfor açısından pasif süspansiyondan bile kötü değerler vermektedir.

Yine konforu iyileştirme amaçlı, taşıt gövdesinin direk olarak Güç Spektrum Yoğunluğu diyagramlarınla karşılaştırılan gövde düşey ivmesini kontrol girdisi olarak kullanan ve istenen gövde düşey ivmesini sıfır olarak kabul eden P-kontrolcüsü ile çeşitli simülasyonlar yapılmış olup, simülasyonlarda kullanılan en elverişli parametreler sayesinde oldukça düşük PSD (Güç yoğunluğu spektrumu) değerleri elde edilmiştir. Ancak testler esnasında bu kontrol prensibinin yüksek elektrik gereksinimi nedeniyle bu elverişli kontrol parametreleri kullanılamadığından pasif süspansiyondan daha iyi ancak neticede ortalama bir konfor değeri elde edilmiştir.

Kontrol girdisi olarak taşıt gövdesinin düşey hızını kullanan Skyhook kontrol stratejisi için öncelikle sensörlerle ölçülen taşıt gövde düşey ivmesi, kontrolcüde kullanılmak üzere düşey gövde hızına dönüştürülür. Kontrolcüde, istenen değer ile gerçek değer arasındaki fark kullanılmaktadır. Bu stratejide, istenen gövde düşey hızı sıfır olarak kabul edilmiştir. Kontrol bloğunda, gerekli süspansiyon yay yatağı hareketi hesaplandıktan sonra bu değer elektromotor tarafından sisteme etki ettirilir ve bu kontrolcüyle de aynı şekilde çeşitli simülasyonlar yapılıp, taşıt konforu için en iyi sonuçları veren kontrol parametreleri belirlenmiştir. Sonrasında bu belirlenen parametreler taşıtın yazılımına entegre edilmiş olup, (simülasyondakine eşdeğer) kontrol bloğunda kullanılarak testler gerçekleştirilmiştir. Test taşıtının verdiği konfor cevap karakteristiğine göre testlerden daha iyi sonuç alınabilecek şekilde en elverişli kontrol parametreleri belirlenmiş ve bu doğrultuda prototip taşıt ile testler tekrarlanmıştır.

Sonrasında, bu incelenmiş kontrol prensiplerinin hepsinden daha karmaşık olarak değerlendirilebilecek (“State-Space”) durum kontrolcüsü taşıta uygulanmıştır. Bu kontrolcüde diğer kontrolcülerde olduğu gibi sadece bir değil altı adet sensör verisine ihtiyaç duyulmaktadır. Taşıt hareket denklemleri yazıldıktan sonra ortaya çıkan sistem matrisi gereği ihtiyaç duyulan veriler: taşıt gövde ve tekerlek düşey hızları, taşıt gövde ve tekerlek düşey göreceli yer değiştirmeleri, yay yatağı yer değiştirmesi ve hızıdır. Bu stratejiyi anlamanın en iyi yolu sistemin kutup diyagramına bakmaktır. Sistem matrisinden elde edilen bu diyagramda altı adet kutup bulunmaktadır. State-Space konrolcü ile her bir kutbun yerini değiştirmek (ötelemek) ve yeni bir taşıt dinamik davranışı elde etmek mümkündür. Sanal eksene yani y eksenine en yakın olan kutuplar baskın kutuplar olup, taşıt gövdesinin dinamik hareketine en çok bu pollerin ötelenmesi etki etmektedir. Çeşitli farklı frekans ve sönüm oranı değerleri ile bu baskın pollerin yerleri değiştirilerek taşıt gövdesinin dinamik cevabı incelenmiş ve bu kontrolcü ile yapılan testler ve simülasyonlardan alınan sonuçların en iyi konfor değerlerini verdiği gözlemlenmiştir.

Son olarak da en iyi sonucun alındığı iki kontrol prensibi, Skyhook ve durum kontrolcüleri kombine edilip, her iki kontrol prensibinin en elverişli kontrol sabitleri bu kontrolcüde kullanılmıştır. Toplam kontrol elemanı hareketi, Skyhook ve durum kontrolcülerinde hesaplanan yay yatağı pozisyonlarının %100 toplamı şeklindedir. Yapılan simülasyonların ardından prototip taşıt üzerinde de bu en elverişli parametrelerle testler yapılmış ve bu tez çalışması sırasında denenmiş olan kontrol stratejilerindeki en iyi sonuç elde edilmiştir.

Bu tez çalışmasının sonucunda, yapılan değerlendirmeler neticesinde en iyi sonucun alındığı Skyhook / State-Space birleşiminden oluşan kontrolcü konfor açısından önerilmekte olup bu kontrolcünün konfor açısından daha da iyileştirilebilecek bir potansiyel vadettiği düşünülmektedir. Daha iyi bir sürüş dinamiği ve konforu elde edebilmek için örneğin kontrol parametreleri değiştirilebilir ki bu tezde Skyhook ve State-Space’in yalnız başına çalıştıkları durumdaki konfor için en uygun sonucu veren kontrolsabitleri alınıp birleştirilmiş kontrolcüde kullanılmıştır. Ancak ikisinin birlikte çalışma durumunda her iki kontrol sabitinin birbirine uyumlu ve konfor için de daha elverişli kontrol değerleri olabilir.

Bunun yanı sıra yine bu tezdeki birleştirilmiş kontrolcüde yay yatağı hareketlerinin %100’ü işleme alınmakta ancak bu iki kontrolcünün hesapladığı yay yatağı hareketlerinin değişik kombinasyonları ile hesaplamalar yapılabilir. Örneğin Skyhook’un hesapladığı yay yatağı hareketinin %60’ı hesaba katılırken, State-Space’in %90’ı kullanılabilir.

Son olarak önerilebilecek madde ise bu iki birleştirilmiş kontrolcüye ilave olarak başka bir kontrolcünün kullanılması olabilir. Üç kontrolcünün de aynı anda birleştirilerek kullanımı ile daha iyi bir sürüş konforunu sağlamak mümkün olabilir.

Konfor algısı insandan insana farklılık göstermekle birlikte ISO standartları kılavuzu ile yaklaşık değerlendirmeler yapılabilmesine rağmen yine de öznel bir kavram olarak kabul edilmektir. Bu yüksek lisans tezi göstermiştir ki ‘low-bandwitdh’ (düşük band aralıklı) süspansiyon sistemi kontrolünde henüz bir tabu bulunmamakla birlikte çeşitli kontrol strateji ve sistemlerinin kombinasyonuyla sürüş konforu ve güvenliği açısından en uygun kontrolcünün seçimi yine konfor kavramı gibi öznel olacaktır.

1. INTRODUCTION

1.1 Motivation

Frequently, the vehicle's frame and furthermore its components, which include suspension, wheels, brakes and steering have been easily described as chassis in the past. Nowadays, this oversimplified characterization ignores the matter of fact that the chassis provides a complex assembly of elements, which determine the dynamic attributes of a vehicle. Essentially, it has two important functions:

- Sustain permanent contact between wheels and roadway in order to achieve good ride safety and handling [1].
- Isolate the vehicle from oscillations induced by road disturbances to increase the level of ride comfort and to reduce physical fatigue of the driver [1] [2].

By choosing the spring stiffness and damper coefficient of a passive suspension system, vehicle's dynamic behavior can be adjusted. A soft spring and damper setup enables excellent ride comfort, a stiff spring and damper setup ensures a controllable vehicle. In this case, comfort and safety requirements are conflicting. This contrariety can be eased by applying an actively produced control force through actuators (active suspensions) or by adjustable damping (semi-active suspensions) in mechatronic suspensions [1].

Figure 1.1 illustrates this situation in a conflict diagram of different vehicle suspension configurations. The root mean square (RMS) value of the vertical vehicle body acceleration $\|\ddot{z}_b\|_{rms}$ is one of the simple values, which enable to interpret the ride comfort behavior of a vehicle: A low RMS value is equivalent to a comfortable vehicle suspension. On the other hand, good ride safety and handling corresponds with a low RMS value of the dynamic wheel load $\|F_{dyn}\|_{rms}$ [1].

As shown in Figure 1.1, spring and damper settings affect the suspension performance significantly. The conventional (passive) system embodies a standard choice for the spring and damper. In order to obtain improved ride comfort, the spring stiffness and the damper coefficients could be lowered, however the suspension deflection limits would not supply this demand. A semi-active system, which is capable of varying the damping, allows improving either ride comfort or safety. However, even if the spring stiffness could be extremely lowered, the orientation has to be determined as safety or comfort again. The Pareto front visualizes the inability to improve one requirement without worsen the other [1] [3].

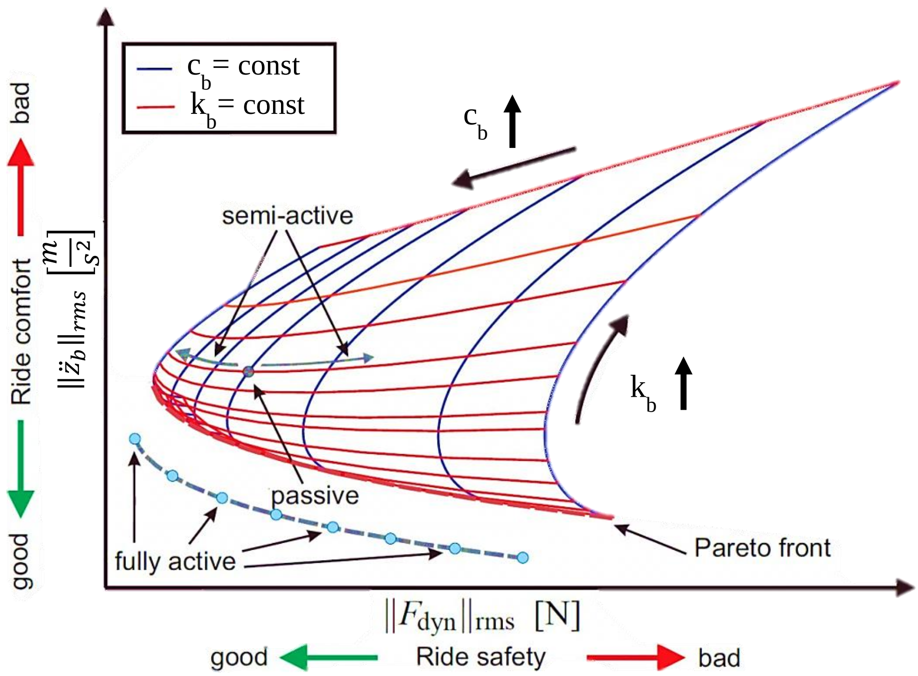

Figure 1.1 : Conflict diagram of different vehicle suspension configurations [3].

On the other hand fully active mechatronic suspension systems can optimize ride comfort and safety at the same time. Consequently, they are able to generate a new favored Pareto front curve (grey dashed curve), which represents once more a compromise of ride comfort and safety as the previous curve. Instead of variations of spring stiffness or damping, such as in the conventional suspensions, these cyan bullets show different suspension controller strategies [3] [4] [5].

1.2 Literature Survey

Mechatronic suspension systems can be categorized in following five groups. The first group is “Automatic level control systems”. They keep the distance constant between the chassis and the road, regardless of different loading. One of the most famous systems is the Nivomat (hydraulic system) by Sachs [3] [6] [7].

The second group consists of “Adaptive suspension systems”, which enable slow variations of spring and damper properties. Porsche Panamera presented 2009 a corresponding system with air springs [3]. 1989 $Citroën$ uses an adaptive suspension system called “Hydractive Suspension”, in which solenoid valves provide suspension stiffness. The system adapts flexibility and damping, therewith, the priority changes to comfort or safety [8] [9].

“Semi-active suspensions” represent further enhanced suspension systems. They have the possibility of fast adjustment of the damper with associated bandwidth of up to 40 Hz. The force is generated by a semi-active element depending on the direction of relative displacement of the chassis and this is the main property of semi-active suspension systems. There are three main types of semi-active suspensions, which are noticeable: electrohydraulic dampers, magnetorheological dampers and electrorheological dampers. The level of energy dissipation can be changed by semi-active dampers, but not be provided [3] [10]. The semi-active dampers are contemporarily utilized among others at the Audi R8, BMW 7 series, Porsche 911 or Mercedes Benz E-class [3].

“Active suspension systems” can be divided into Fully Active Systems and Slow Active Systems and show the most enhanced dynamic behavior. Fully active systems are able to react up to 30 Hz. A linear electromagnetic motor work parallel to the primary spring and controls the system by applying a suspension control force (they omit passive damping). However, in a suspension like the Bose system, the main disadvantage of this system is their high energy consumption [1] [3] [6] [10] [11].

In slow active suspension systems, an additional actuator, which can be an electromotor (VW e-ABC: electromechanical active body control) or a hydraulic cylinder (Mercedes ABC: active body control), can generate the desired suspension by adjusting the main spring mount for each wheel. Both systems operate within the bandwidth of approximately up to 5 Hz [3] [10]. These systems enable to reduce heave, roll and pitch motions of the vehicle and can be combined with other chassis control systems, such as preview control [12] [13].

VW’s e-ABC system has several advantages compared to the hydraulic system. An accumulator spring, which is used in parallel to the electromotor, reduces the electric power demand caused by static vertical load [12]. On the other hand, hydraulic systems require generally a permanently driven pump. Hereby, e-ABC, with a recuperation ability of the electrical actuator, provides a significant decrease of energy demand compared to Mercedes ABC system [12] [14].

For exploiting the full potential of these suspension systems, applying effective control algorithms is essential. A selection of some of the most important control principles is presented in the following.

Current control systems for vehicle suspensions consist of two groups: Linear control methodologies such as classical PID, H_2 etc. and Nonlinear systems, mainly based on Lyapunov's methods or sliding control [15]. In this chapter, several various active suspension controls from literature will be mentioned.

As mentioned before, Mercedes Benz ABC is a slow active suspension with the aim of absorbing the motions of pitch, roll and heave. This system's ECU uses four primary algorithms. (a) A Skyhook algorithm minimizes the absolute vehicle chassis' acceleration value, which is independent of road unevenness, through using the vertical body acceleration sensor's signals. (b) A lateral acceleration intervention reduces the roll moment during dynamic steering maneuvers. (c) A longitudinal acceleration intervention reduces the pitch during braking or acceleration. (d) An Aktakon (Aktive Aufbau Kontrolle = Active Body Control) algorithm controls pitch, roll and heave motions with feedback control, which monitors and processes the relative displacements between the vehicle's body and each individual wheel. The difference between desired and actual value of this relative displacement enables the vehicle to generate a desired position and to keep it there (leveling regulation). At the same time suspension behavior and therewith the subjective ride comfort characteristics of the vehicle are also concurrently controlled up to 5 Hz by generating and applying a control force in its ABC system [16] [17] [18].

In Mercedes Benz concept car F700 with ABC, a preview system has already been introduced. The vehicle is equipped with laser scanners and LIDAR sensors to collect the road profile input [19] and by this means, it 'prepares' the system for incoming disturbances. For these kind of suspensions, the examined control approaches such as 'MPC (Model Predictive Control)' and 'Multi-Objective $H\infty/GH_2$ preview control' are explained in [20] [21]. According to Mehra et al. (1997), "MPC design includes the restrictions on state control and output variables. It generalizes the approaches based on feedback linearization and dynamic inversion from single step control to multiple step control over a receding prediction horizon."

Multi-Objective $H\infty/GH_2$ preview control assists the suspension working space, to change freely in given limits. A LMI (Linear Matrix Inequality) approach is the basis for Multi-Objective control design with sufficient design tools. The optimization is also convenient on a wide range of road disturbances. When it is required, the $H\infty$ norm of its (sub)system is minimized. During worst-case disturbances, the GH_2-norm measure is employed to accomplish the system constraints. It enables adequate stability margins taking into consideration the pole location constraints. It is designed in the discrete time domain, "in order to avoid performance degradation by discretizing the controller." [21].

Alleyne and Hedrick (1995) explained that a Skyhook force, which is determined from the states of system, with a sliding control law is applied to the active suspension element in order to reduce the acceleration of passenger compartment. The nonlinear dynamics of the electro-hydraulic actuator is taken into consideration and the desired system dynamics are described. Under various nonlinear controller types, the performances of the system are compared with each other. One of these types is the sliding control method (with special case of robust feedback linearization), another type is a standard method coupled with nonlinear control law and a further type is a modified adaptive algorithm coupled with the sliding control method.

Alleyne and Hedrick (1995) mentioned that it is difficult to generate the control force between sprung and unsprung masses as desired. In order to solve this active suspension problem, a different problem reformulation, based on setting a specified displacement between sprung and unsprung masses, is offered. The problem is converted into a 'displacement-tracking' problem from 'force tracking' problem due to this reformulation. It is realized that when this reformulation is accomplished, the capability of the servo-control methodology is improved despite the fundamental limitations on control-plant structure of a 1 DOF (degree of freedom) experimental system. In this study, two control methods (a model reference adaptive controller and a robust controller) are utilized and their performances are compared.

Ramsbottom and Crolla (1999) interpreted the active suspension problem as one of combined tuning and set-point tracking, and accordingly, cooperated ride control and leveling control abilities. It suggests a scheme involving a variant of the self-tuning pole-assignment algorithm.

Leite and Peres (2005) discussed the robust control design problem by using state feedback gains for an active suspension of a quarter-vehicle model. According to Leite and Peres (2005), the examined controllers guarantee “robust pole location of the closed-loop system inside a circular region on the left-hand side of complex plane”. There are three defined Linear Matrix inequalities for presence of a robust stabilizing state feedback gain: (i) The quadratic stability based gain, (ii) a condition, which uses an augmented space modified in order to deal with the pole location specification, and (iii) a condition uses an extended number of equations and produces a parameter-dependent state feedback gain. The sprung mass, the damper coefficient and the spring constant are considered as uncertain parameters associated with an identified interval (polytopic uncertainty) in the suspension model.

Lauwerys et al. (2005) introduced a robust linear controller in a quarter car test-rig for an active suspension without a physical (nonlinear) model of a car or the shock-absorber. Although robust linear control design techniques ($H\infty$ and μ synthesis) are in charge of the model uncertainties, which are presented by the linear model approximation of the nonlinear dynamics, linear black box models are identified by means of frequency domain identification techniques.

1.3 Objectives

Electromechanical active suspension systems show considerable advantages over conventional hydraulic actuated active suspension systems, due to their lower power consumption, reliability, suitability for electric power trains, etc. The literature survey showed that new control strategies needed to be developed for these new active suspension systems. Therefore, the objective of this study is to obtain better ride comfort by designing a controller model for an electromechanical slow active suspension system.

Aimed at this kind of suspension, the control principle will be based on controlling the force through controlling the movement of body spring seat. Several control strategies will be examined in order to acquire the most effective type for slow active suspension systems by pursuing the following:

- Creating a MATLAB/Simulink model, which represents the dynamic properties of the test vehicle.
- Simulating several different control strategies in MATLAB/Simulink.
- Finding convenient controller parameters, which enable the best ride comfort behavior.
- Validation and adjustment of these results in the test vehicle.

2. VEHICLE SUSPENSION SYSTEMS

It is considered that the “suspension system” is a general definition and it includes the combined functions of vibration dampers, suspension springs and stabilizers. In vehicles, suspension systems are mainly responsible for the following tasks, which are very significant for the overall function of the chassis:

- Ride comfort,
- Driving behavior,
- Roll, pitch and yaw tendencies of the vehicle.

Through these tasks, the vehicle structure and the passengers as well are protected by the suspension system from the effect of disturbing vertical displacements, yaw and pitch fluctuations. Furthermore, the suspension system assists the wheels to sustain contact with the road. This is the basis for an effective force transfer, required for power transfer, road holding, acceleration, braking and eventually:

- Driving safety [1] [22].

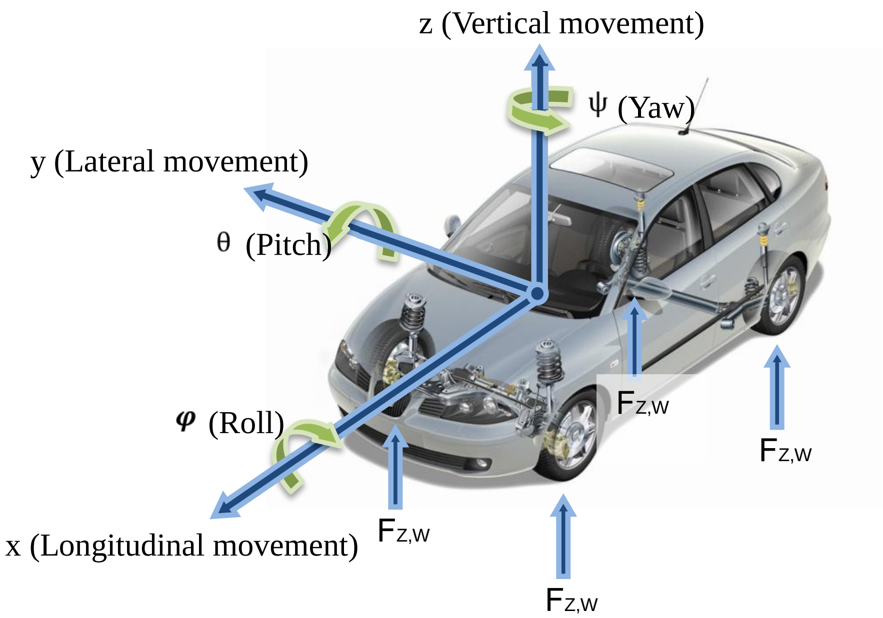

Figure 2.1 : Suspension system motions [1].

On Figure 2.1 the motions of the vehicle, the angles of motions and the forces, which affect these explained tasks, are delineated.

2.1 Relation of Suspension and Comfort

While driving, the well-being of the passengers describe the ‘ride comfort’. The leading reasons for disturbances of the passengers are the oscillations that influence the passengers by generating vibration, noise or both. These vibrations can be caused by the roadway excitation, each single elements of the chassis or the powertrain. In order to prevent the transmission and penetration of disturbances into the passenger’s compartment, suspension systems are used [1].

For ride comfort, the mostly used measure is the Root Mean Square (RMS) value $\|\ddot{z}_b\|rms$ as mentioned on page 1 or the Power Spectral Density (PSD) of the vertical vehicle body’s acceleration. By isolating the body movements, which are induced by the roadway or the dynamics of the vehicle, the suspension system attempts to enhance the ride comfort. If the suspensions of the seats are neglected, the vertical acceleration of the vehicle body mass quantifies the ride comfort regarding vertical vibrations. Principally, ride comfort is a consequence of the human sensitivity for vibrations and it is dependent on the frequency range. E.g., 4-8 Hz is the most influential frequency range for vertical excitations [3] [23] [24] [25].

In order to interpret the comfort feeling of the passengers, first, the description of ‘vibrations’ will be clarified.

2.2 Vibrations

The vibrations generated by the maneuvers and the excitations of the road induce firstly the wheels and then the vehicle chassis, through the suspension system. The springs and dampers cannot be comprehended disassociated from each other in a suspension system, because during driving, numerous chassis parameters influence each other. This means that the dampers and springs together transmit the reduced vertical displacement to the vehicle chassis [1]. “When the vehicle drives over a bump, the suspension springs and vibration dampers are compressed. The resulting shock to the vehicle is absorbed by the suspension. The springs, however, tend to relax again, thereby releasing the energy stored within them.” [1]

Each vehicle has some characteristics, which have great effects on the dynamics and the comfort feeling of the vehicle. These are defined as the resonance or natural frequencies of the chassis and the wheels [24].

In suspension systems, vibration dampers are used in order to decrease the amplitude and disturbance of oscillations. The sprung and unsprung masses oscillate in different frequency ranges. Figure 2.2 shows the reduction, which is caused by the dampers (red curves), of road-induced vibrations (undamped vibrations: blue curves) [1].

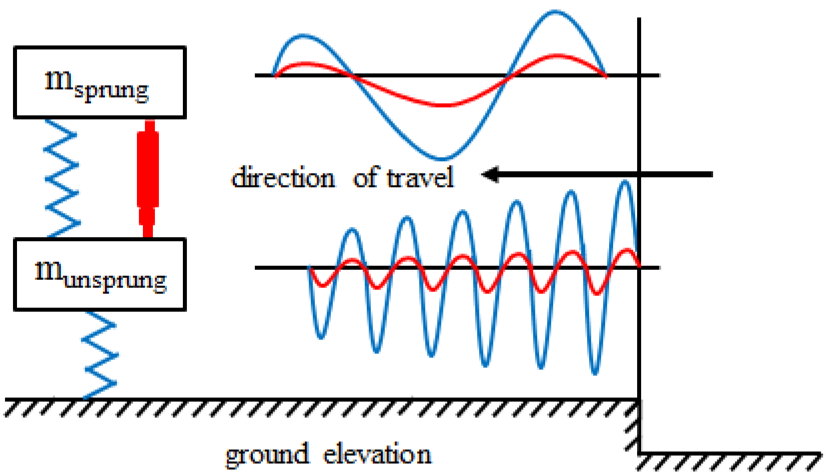

Figure 2.2 : Vibration reduction [1].

Figure 2.3 depicts a quarter vehicle model to clarify the following natural frequency equations.

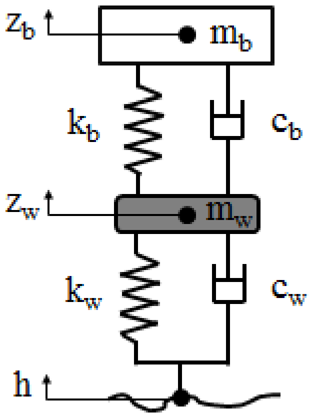

Figure 2.3 : Quarter vehicle model [26].

The undamped natural frequency of the vehicle body is calculated by using formula 2.1 [24]:

$$\omega_b{}^2 = \frac{k_b}{m_b} \tag{2. 1}$$

The undamped natural frequency of the wheels is obtained through formula 2.2 [24]:

$$\omega_w{}^2 = \frac{k_b + k_w}{m_w} \tag{2. 2}$$

As mentioned above, there will be decaying oscillations between axle and body mainly because of the damping as illustrated in Figure 2.2. This decaying oscillation, mostly called “damped natural frequency”, is characterized by two values ‘σ’ and ‘ω_d’. ‘σ’ indicates how fast the oscillation decays and is therefore referred to as decaying constant calculated through formula 2.3 [24]:

$$\sigma = \frac{c}{2m} \tag{2. 3}$$

The damped natural frequency ‘ω_d’ is calculated with formula 2.4 [24]:

$$\omega_d = \sqrt{\omega^2 - \sigma^2} \tag{2. 4}$$

As a further variable, the dimensionless damping is shown in formula 2.5 [24]:

$$D = \frac{\sigma}{\omega} = \frac{c}{2\sqrt{km}} = \frac{c\omega}{2k} = \frac{c}{2m\omega} \tag{2. 5}$$

With this abbreviation, damped natural frequency is acquired as in formula 2.6 [24]:

$$\omega_d = \omega\sqrt{1 - D^2} \tag{2. 6}$$

During substituting these equations into equations of motions, there is another point to take into consideration called the suspension compression ratio “i”. That correlation represents the relationship between the displacement of the wheel and corresponding suspension deflection (see Figure 2.4). This ratio is dependent upon the alignment, instant position and kinematics of the suspension components and it is not constant but generally less than “1”. The instant compression or rebound position of the suspension affect this “i” ratio [1].

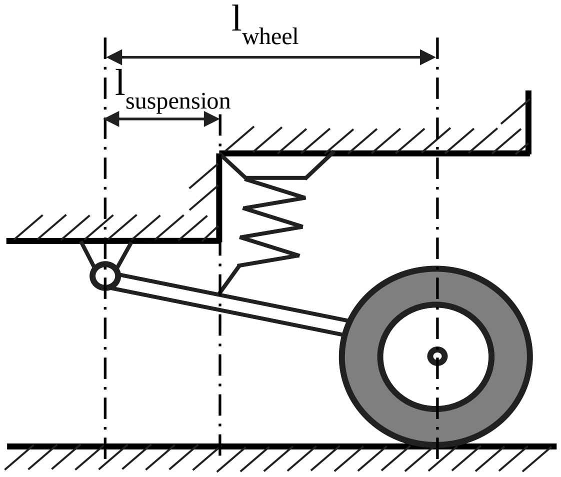

Figure 2.4 : Delineation of axle geometry and suspension leg [1].

On the axle, the force correlation can be assumed with the depicted theorem in Figure 2.5.

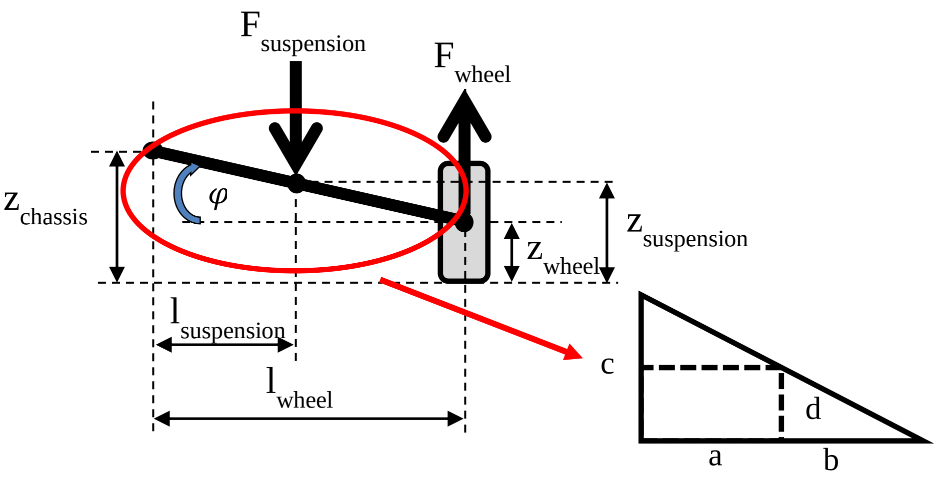

Figure 2.5 : Definition of Suspension bearing force through moment equilibrium [1].

According to the presentation above, formula 2.7 is written [27]:

$$\frac{c-d}{c} = \frac{a}{a+b} = \frac{l_{suspension}}{l_{wheel}} = i \qquad \textbf{(2. 7)}$$

The balance of the wheel load and the spring or damper force is calculated by using formula 2.8 [1]:

$$F_{suspension} \cdot i = F_{wheel} \qquad \textbf{(2. 8)}$$

For a particular compression or rebound position, the spring stiffness or damping constant for a single wheel of an independently suspended axle can be determined by using the following equations [1] [27]:

$$k_{relative\ to\ wheel} = \frac{dF_w}{dz_w} = \frac{d(F_{sp} \cdot i)}{dz_w} = k \cdot i^2 + \frac{di}{dz_w} \cdot F \tag{2. 9}$$

$$c_{relative\ to\ wheel} = \frac{dF_w}{d\dot{z}_w} = \frac{d(F_{sp} \cdot i)}{d\dot{z}_w} = c \cdot i^2 + \frac{di}{d\dot{z}_w} \cdot F \tag{2. 10}$$

After the principles of vibration are comprehended, another important point will be mentioned as ‘the appropriate vehicle model’ according to the purpose.

2.3 Vehicle Models

Currently, there are three different vehicle models to describe the vertical dynamic behavior of the vehicle and for each model there is another interest of motion. Principally, pitch, roll and heave motions of the chassis are the main vertical dynamic degrees of freedom (DOF) of a vehicle [3].

2.3.1 Quarter vehicle models

The quarter-vehicle model solely analyzes the heave motions of a corresponding sprung and unsprung mass [28]. Typically, a passive quarter-vehicle model contains the sprung mass, unsprung mass, the suspension system (in order to set up the sprung and unsprung masses together), a tire model, which includes parallel spring and damper configuration. The sprung mass represents the mass of the chassis with passengers and loading. The unsprung mass represents the tire, wheel, break and mass of wheel carrier and suspension system [3].

In Figure 2.6, different suspension quarter-vehicle models are shown, which are introduced in a control-oriented perspective with increasing complexity [3] [10]. In addition to components of passive (conventional) suspensions, semi-active suspensions contain adjustable damping. Furthermore, active (slow, fully active) suspensions introduce actuators in the suspension working space and these actuators (electrical or hydraulic) enable increasing and reducing system energy by applying a force between the sprung and unsprung mass [3] [29].

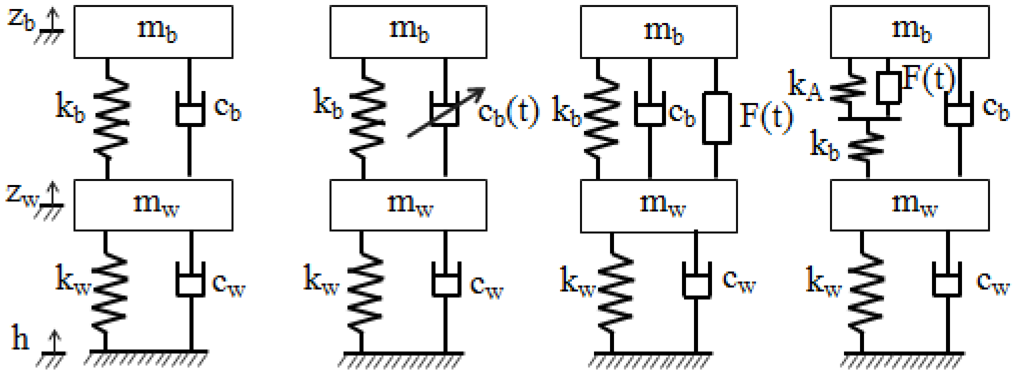

Figure 2.6 : Quarter-vehicle models of a passive, semi-active, fully and slow active suspension system [3] [12].

2.3.2 Half vehicle models

Besides observing the vertical heave motion, half vehicle models inquire into the pitch motion of a vehicle. In principle, half vehicle models unite two quarter-vehicle models (front and rear) joined by a rigid frame. These rigid frame assumptions disregard vehicle chassis and frame deflections. Generally, they involve the change of height, regarding the pitch angle around the vehicle's center of gravity (CG) [29].

The half-vehicle model is a convenient model for comfort interpretation in the frequency range of interest (i.e. 0-30 Hz), if the motions of the two rear or front wheels can be assumed to be coupled [3] [10]. Therefore, in this thesis, a half vehicle model is utilized and it is detailed in the 'Model Development' section.

2.3.3 Full vehicle models

In a full vehicle model, the complete dynamic behavior of the entire vehicle is considered [3] [29]. Quarter or half vehicle models simplify the investigation by ignoring turning or yaw motions, full vehicle models on the other hand, provide to examine all: pitch, roll and heave motions of the vehicle. Full-vehicle models consist of four quarter-vehicle suspension models, combined by a stiff frame [29].

After defining these current vehicle models, some selected controlled suspension systems will be shortly mentioned.

2.4 Mechatronic (Controllable) Suspension Systems

Considering the actuator types containing

- the actuator bandwidth,
- the power demand of the actuators,
- the controllability range,
- i.e. the constraints for the actuator forces,

it is possible to categorize the mechatronic suspension systems in following five groups [3] [24] [10].

2.4.1 Automatic level control systems (Load leveling)

These types of control systems can be based on air springs and compressors. They keep the distance constant between the chassis and the road regardless of different loading [3] [6]. Hereby, regardless of the vehicle's load level, with adequate suspension deflection, a soft, comfort oriented suspension setup can be acquired. The electrical consumption is usually between 100-200W and the bandwidth is within 0.1-1 Hz [3] [10]. The most famous example of that type control active control strategies is Nivomat by Sachs with its spring and damping function [7].

2.4.2 Adaptive suspension systems

These kinds of suspension systems enable solely slow variations of spring and damper properties. More sportive road holding is obtained by lowering down the center of gravity of the vehicle when driving with high velocity. In Porsche Panamera (2009 model) it is presented with air springs [3]. 1989 $Citroën$ uses an adaptive suspension system called "Hydractive Suspension", in which solenoid valves provide suspension stiffness. The system adapts flexibility and damping, therewith, the priority changes to comfort or safety [8] [9]. The power demand is mainly contingent on the required energy for changing the stiffness [3].

2.4.3 Semi-active suspensions

Semi-active suspension systems have the possibility of fast adjustment of the damper (shock absorber) characteristics with associated bandwidth of up to 40Hz. The force is generated by a semi-active element depending on the direction of relative displacement of the chassis and this is the main property of semi-active suspension systems. The level of energy dissipation can be changed by semi-active dampers but not be provided. Furthermore, their power demand is very low within the range of 20-40 W for each damper [3] [10]. The semi-active dampers are contemporarily utilized among others at the Audi R8, BMW 7 series, Porsche 911 or Mercedes Benz E-class [3]. There are three main types of semi-active suspensions, which are noticeable:

2.4.3.1 Electrohydraulic dampers

Compared to the classical passive element, instead of passive valves the electrohydraulic device comprises electronic valves. This kind of dampers, which are usually equipped with solenoid valve, absorb or dissipate energy by throttling a viscous (hydraulic oil) flow through an orifice amongst two or more chambers inside the damper. The level of dissipation can be varied by adjusting the cross-section of the orifice (see Figure 2.7) [3] [10] [30].

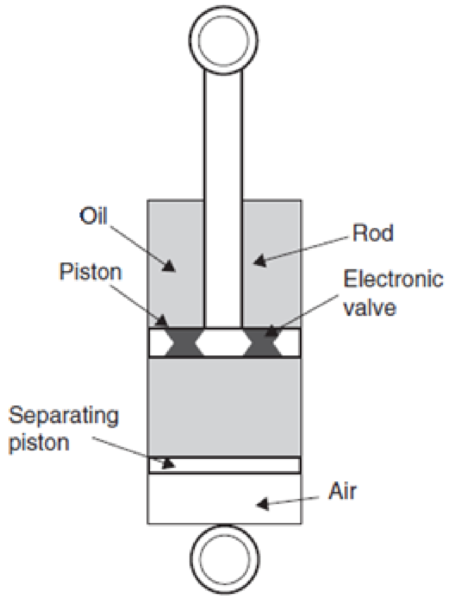

Figure 2.7 : Schematic representation of an electrohydraulic shock absorber [10].

2.4.3.2 Magnetorheological dampers

These types of dampers have several remarkable features such as stability, reliability, low power requirements. By applying a magnetic field, it is possible to form chains with magnetic particles in the fluid (see Figure 2.8, B is the magnetic field). It reacts in less than a few milliseconds related to the viscosity of a magnetorheological fluid [10] [31].

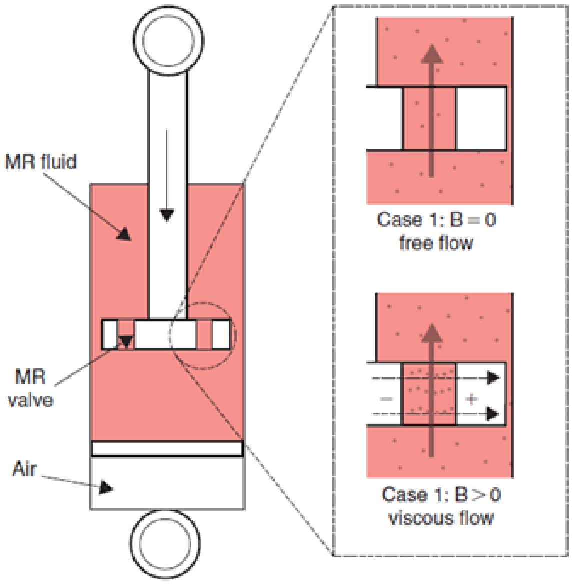

Figure 2.8 : Schematic representation of a magnetorheological damper behavior [10]

2.4.3.3 Electrorheological dampers (ER Dampers)

With electrorheological dampers (see Figure 2.9), it is possible to change the viscosity suddenly by applying an electric field [32]. The particles in the fluids, compared to magnetorheological dampers are less abrasive. Therefore, the durability of the seals is further enhanced [3] [33].

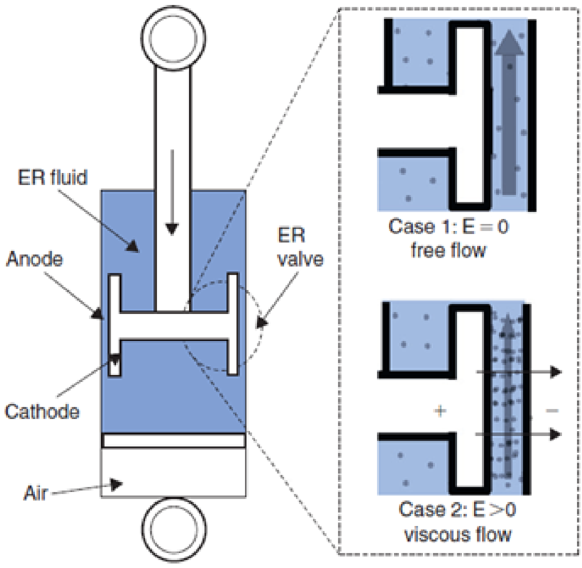

Figure 2.9 : Schematic representation of an electrorheological damper: with and without electric field (E is the electric field) [10]

2.4.4 Fully active systems (High bandwidth active systems)

There are two types of active suspension systems according to control bandwidth. They will be explained in the following.

A linear electromagnetic motor, which is able to react in milliseconds up to 30 Hz, omits the passive damper. The actuators work parallel to the primary spring and they control the system by applying a suspension control force as shown in Figure 2.10. The main disadvantage of these system is their high energy consumption 4-20 kW [1] [3] [10] [6].

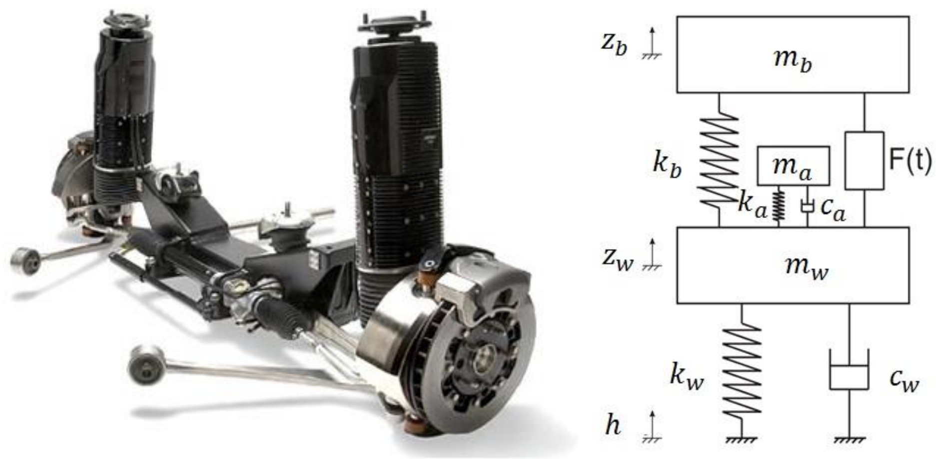

Figure 2.10 : High bandwidth active suspension system by BOSE and its quarter-car model [3] [11].

2.4.5 Slow active systems (Low bandwidth active systems)

Slow active suspension systems are the main focus of this thesis and will be explained in this section more in detail. In that kind of suspensions, an additional actuator, which can be an electromotor or a hydraulic cylinder, combined with the suspension, adjusts the slow active suspension and can generate suspension force. Generally, the actuators are in series to the primary spring as shown in Figure 2.11 (Mercedes ABC system with hydraulic cylinders). ABC operates within the range of 1-5 kW energy demand and the bandwidth of this system is approximately up to 5 Hz. Disturbances, which represent a higher frequency than 5 Hz, cannot be taken into account by the actuator [3] [10].

Resolution of the conflict between road safety and driving comfort is the main goal of these suspensions. The control system uses the information of numerous sensors, to compute the commands for the actuators (displacement of spring base) [13].

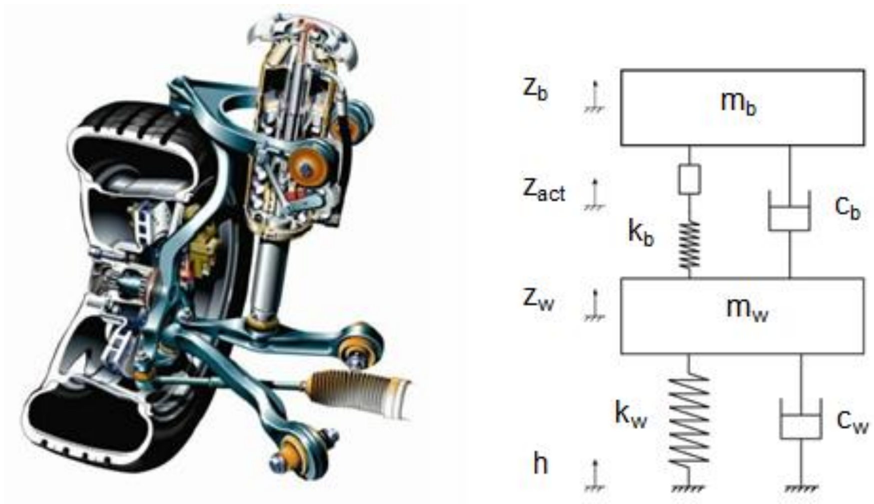

Figure 2.11 : ABC system by Mercedes Benz and its quarter-car model [3] [34].

The ride comfort characteristics and the vehicle's dynamics behavior can be adjusted with appropriate controller parameters. Thus, the system can respond to various handling requirements. By selecting comfort or sport mode, the handling characteristics can be switched manually. The main function of this system is, along with the dampers, to improve ride comfort and to carry the vehicle body [13] [14].

This system enables to reduce heave, roll and pitch motions of the vehicle. Furthermore, while driving a curve (roll motion); it reduces the effect of centrifugal force as shown in Figure 2.12, it means no anti-roll bars are required. The actuators obtain all compensations of roll motions. In addition, depending on the unevenness of the road, ride leveling can be re-adjusted to attain a better handling safety and ride comfort. Moreover, this system can be combined with other chassis control systems, such as preview control to enable further improvements [12] [13].

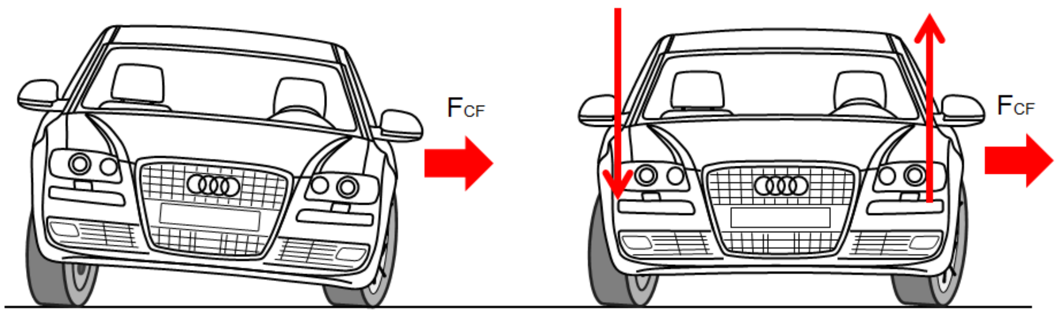

Figure 2.12 : Roll motion caused by road bends [35].

In this master thesis as an alternative to Mercedes Benz's system, an electromechanical Active Body Control (e-ABC) system is used by applying an electromotor with a spindle drive instead of a hydraulic cylinder to adjust the main spring mount for each wheel [12] [13]. In the following, this e-ABC system will be clarified.

2.4.5.1 Function and configurations

With the assist of actuator forces produced by an electromotor at each wheel, e-ABC controls the vehicle body movements. The position of the actuator, wheels and car body are recorded by sensors and processed in the control unit [12] [14].

As shown in Figure 2.13, the actuator works in conjunction with two serial connected springs, a spindle drive and with a parallel connected hydraulic damper. The main spring (its stiffness shown as 'k_b') is adjusted by the electric drive to pull and push direction. An accumulator spring (its stiffness is shown as 'k_A') is used in parallel to the electromotor, in order to reduce the electric power demand caused by static vertical load. The electromotor itself is used only for compensating the dynamic load [12].

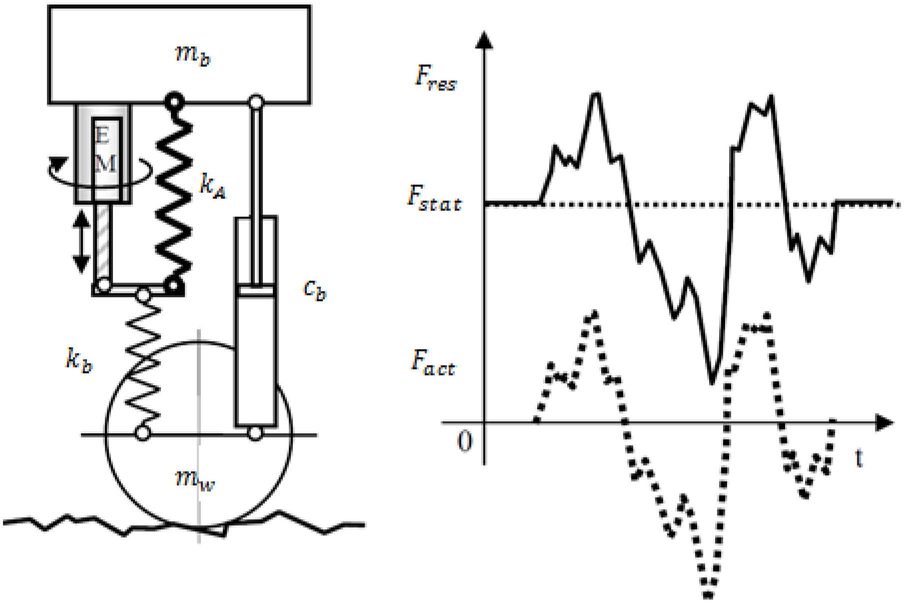

Figure 2.13 : Required dynamic and static actuator forces [14].

It has several advantages compared to hydraulic systems. For instance, the average energy consumption is zero, when power dissipation is neglected. Solely the varying in the stationary load of the vehicle causes enduring setting forces. The required energy can be provided permanently by the electrical system of the vehicle, due to the fact, that these forces are minor [12].

The suspension of the vehicle body is affected by the change of spring load and its speed of change up to 5 Hz. That limit is a further reason for the relatively low energy consumption of this slow active system [12] [14].

Furthermore, hydraulic systems require generally a permanently driven pump. E-ABC on the other hand, with the recuperation ability of the electrical actuator, provides a significant decrease of energy demand compared to Mercedes ABC system [22].

2.4.5.2 Internal structure of the spring strut module

With the design, the required dynamic behavior and simultaneously restricted package specifications can be compromised. The main parameters like spindle ratio, motor torque, electrical current peak and least rotor inertia are taken into account [12] [14].

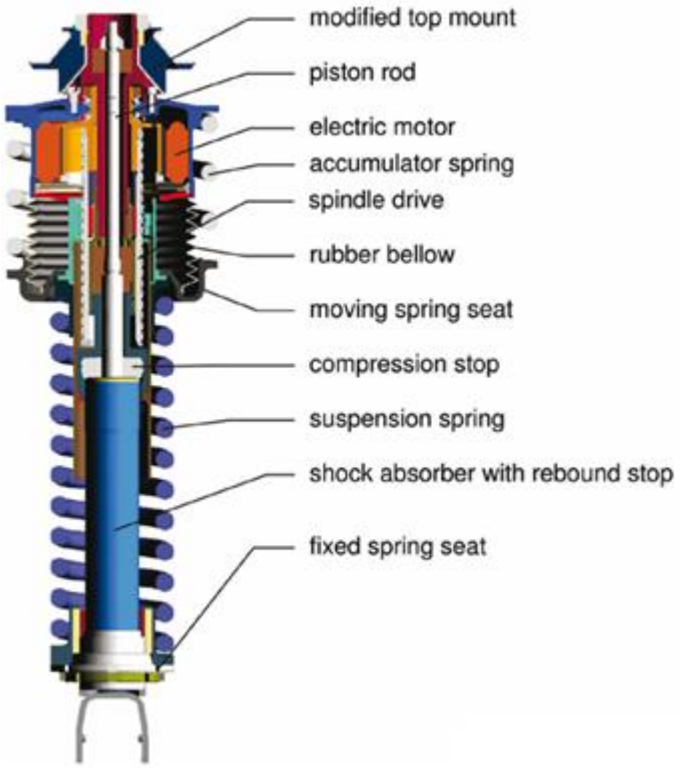

Figure 2.14 : Sectional view on the design of a spring strut module [14].

Figure 2.14 delineates a sectional view of the strut assembly with the electromechanical actuator. Two coil springs, the suspension travel and the actuator travel settle the length of the strut. The required motor torque, spring stiffness and actuator travel of the accumulator spring determine the outer diameter. To provide a cost-effective manufacture, the entire drivetrain of the actuator is identical on both axles [3] [14] [13].

2.4.5.3 System design and control

In order to process the control algorithms and record data, a prototype vehicle is in use with four actuators, several sensors and a double-layer high-capacity condenser, dSPACE hardware [12] [14].

In Figure 2.15, this system is delineated in the prototype vehicle. The vehicle is controlled by two dSPACE Autoboxes (3). The first dSPACE Autobox is responsible for the vehicle control and the second dSPACE Autobox controls the four electric motors. The CAN-Bus system is used for the communication of the boxes. Power loss in AC power cables is reduced by close positions of the actuators to their power electronics (1). A high-capacity condenser (2), stabilizing the voltage, is located in the center of the vehicle. “The electromechanical system works with a 12 V on-board net. The condenser is connected parallel to the electrical system of the vehicle with a capacity of 100 F and is used as a storage device in order to stabilize the voltage [14].”

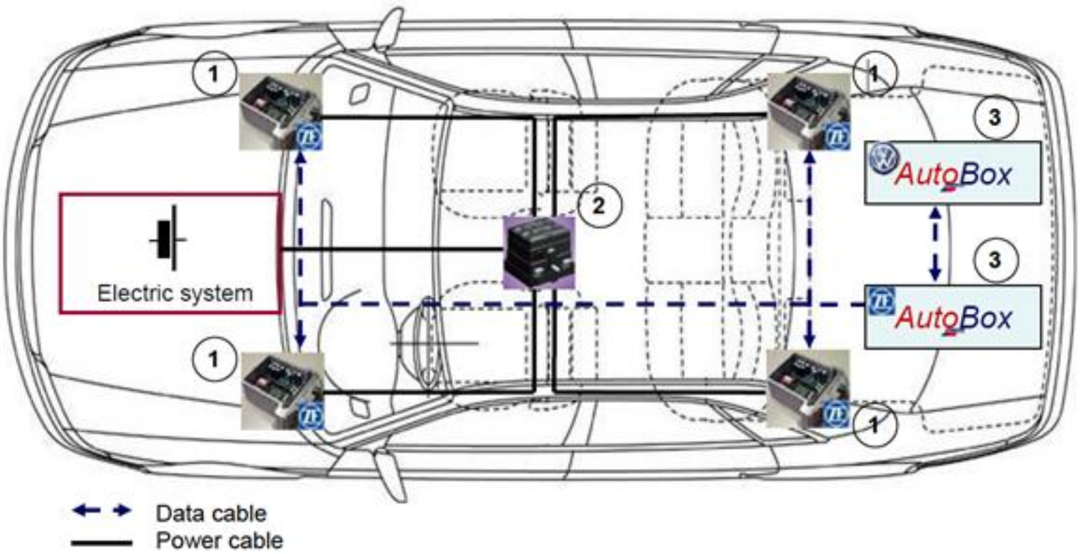

Figure 2.15 : Demonstrator vehicle [14].

From the Autobox, which is responsible for vehicle dynamics, is sent the required motor torque. This box obtains data about actual rotational speed, rotational angle, motor torque of each actuator (as shown in Figure 2.16). Furthermore, it obtains data such as temperatures of motors, power electronics, status flags, etc. [12].

Figure 2.16 delineates the block diagram of the entire vehicle controller. Spindle position controllers compute the desired motor torque. “The parameters of the spindle position are calculated with a linear model of the actuator and a given dynamic behavior. The behavior corresponds to a PT_2 system with an eigenfrequency of 5.8 Hz and a damping ratio of 0.9.” [12]

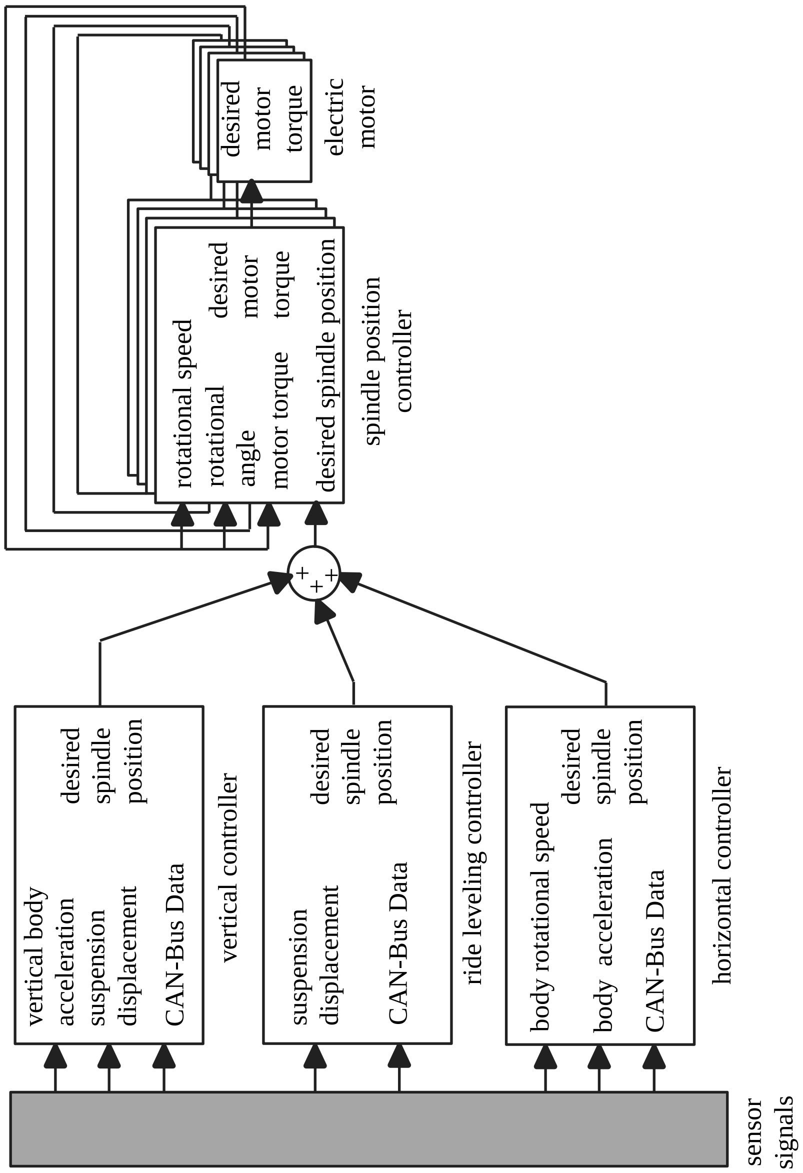

Figure 2.16 : Block diagram of vehicle controller [12].

PT_2 describes the behavior of a dynamical system, which reacts proportional (P-constant) to its input signal: i.e. a higher input signal generates a higher output signal.

Another fact worth mentioning is the time delay of this element. Figure 2.17 illustrates this behavior: The PT_2 system is stimulated at zero sec. with a step function (input value of “1”), however, the answer reaches its final stage (amplitude) of “1” after 2-3 sec. (second and third curve) or approximately after 6 sec (first curve). In this case, the final stage of “1” represents the P-constant of this dynamical system.

Furthermore, as depicted in this figure, a PT_2 element is able to oscillate, due to the reason that there are two storages, which transmit energy to each other. E.g. in a mechanical system, a spring under tension releases its stored energy into the mass which will be accelerated. In the next moment, this mass is decelerated by the spring and the stored energy of the moving mass is transferred back into the spring. This process continues until the energy is consumed (converted into thermal energy). Only a damping ratio between a value of zero and one enables oscillation. This is the reason why the first curve is not able to oscillate, since its damping ratio is bigger than one. The time delay of PT_2 is dependent on the frequency and on the damping ratio of the PT_2 element. In Figure 2.17, the second and third curves embody the same damping ratio of ‘0,3’, the frequency differs (second curve 1,0 Hz and third curve 1,3 Hz) [36].

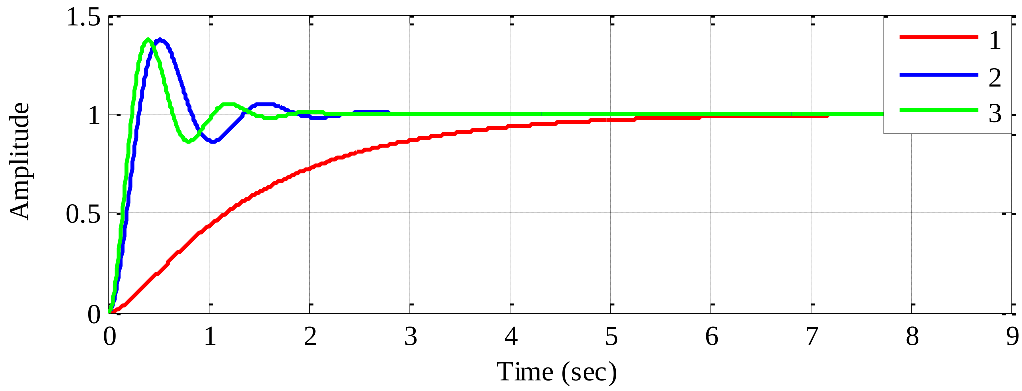

Figure 2.17 : Step responses of three options.

As a consequence of road roughness and driving maneuvers, such as acceleration, braking, or steering, the vehicle body is forced to move around the lateral and longitudinal axes. These movements are reduced by means of controlled spindle positions [23].

The total desired spindle position is determined with a summation of three controllers (horizontal, ride-leveling, vertical controllers) desired values (see Figure 2.16) [12].

The desired spindle positions, as a result of driving maneuvers, are computed by the horizontal controller and the desired vehicle level is computed by the ride-leveling controller.

The desired spindle position, arising from road disturbances, is calculated in the vertical controller by processing the sensor signals of the body acceleration (strut domes) and of the suspension deflection [37].

2.5 Control Types and Purposes of Suspension Systems

After comprehending the types of controllable suspension systems, Figure 2.18 shows a comparison of these systems [1] [3] [10]. According to requirements and desires the most appropriate type are chosen by the manufacturers.

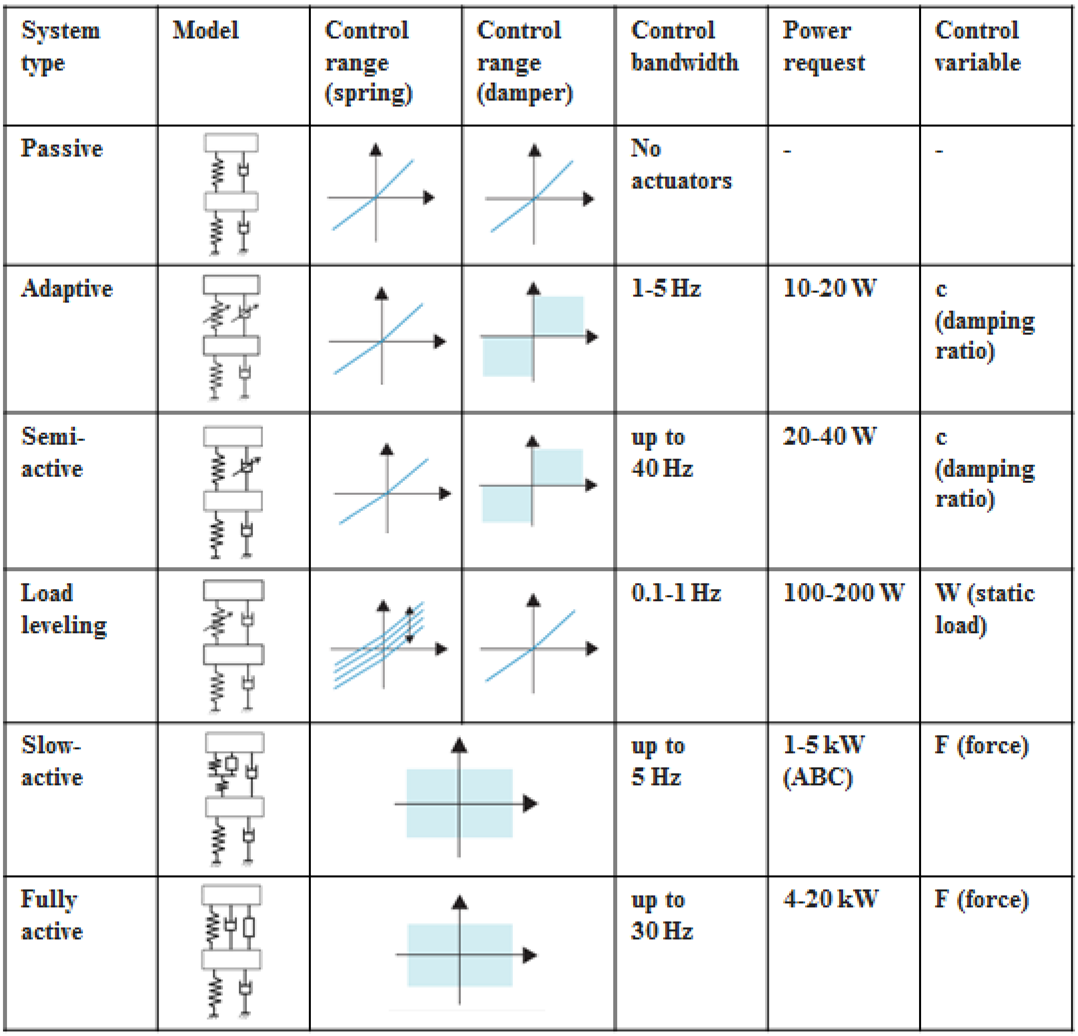

System type	Model	Control range (spring)	Control range (damper)	Control bandwidth	Power request	Control variable
Passive				No actuators	-	-
Adaptive				1-5 Hz	10-20 W	c (damping ratio)
Semi-active				up to 40 Hz	20-40 W	c (damping ratio)
Load leveling				0.1-1 Hz	100-200 W	W (static load)
Slow-active				up to 5 Hz	1-5 kW (ABC)	F (force)
Fully active				up to 30 Hz	4-20 kW	F (force)

Figure 2.18 : Classification of electronically controlled suspension.

After some controllable suspension systems are explained and compared, the reasons for using an active suspension system will be mentioned.

2.5.1 Purpose of active suspension control

2.5.1.1 Driving comfort

Maximum comfort according to driver and passengers can be defined as the minimum disturbance, which occurs because of the mechanical and acoustical vibrations, in perceivable frequency range for humans. For mechanical vibrations, it is considered that the comfort perception of humans is the acceleration of the vehicle chassis. Therefore, it is strived to keep body acceleration lowest as possible [19].

2.5.1.2 Road safety

For the improvement of road safety, an intervention in the wheel dynamics is necessary. With greater vertical movements of the wheels, the transmitted force between the vehicle and the road will be inadequate. It can cause that the vehicle loses contact with the road [19].

2.5.1.3 Leveling (Horizontalization)

The leveling of the vehicle provides a limited pitch and roll angle of the vehicle during road disturbances, longitudinal and lateral dynamic driving maneuvers. A support is required for the occurred pitching and rolling moments. A good leveling provides improved driver reaction, because the horizon between the vehicle and the road surface changes less. A perfectly leveled vehicle is still not desirable, because boundaries of the vehicle should be recognized by the driver at the right time [19].

2.5.1.4 Self-leveling (Constant ride height)

The automatic level control ensures the maintenance of a constant ride height regardless of load condition and thus provides that the suspension travel of the vehicle remains [19].

2.5.1.5 Energy consumption

Through control interventions the energy consumption of the suspension has to be kept as low as possible in order to avoid unnecessarily increase of the fuel consumption [19].

3. DEVELOPMENT OF SIMULATION MODEL

The main focus of this chapter is to explain the Simulink model which is used in order to optimize driving comfort of the test vehicle. The purpose of using a Simulink model is to reduce the number of tests with the vehicle in reality, as those take more time and are riskier than simulations (especially components of the active suspension system can be damaged).

3.1 Vehicle Simulation Model

A half-vehicle simulation model is used in MATLAB/Simulink to evaluate the slow active suspension‘s comfort characteristics and several different control strategies are examined by combining to this model. The initial Simulink model developed by Volkswagen AG was further improved during this thesis. In order to obtain an enhanced vertical comfort of the vehicle, it is sufficient to simulate the model with the related main parameters of its suspension system. Therefore, the assumptions, neglects and simplifications, which have been made to simplify the model, are explained in the next section.

3.1.1 Assumptions and simplifications

The half vehicle model is a simplified vibration system replacement of the entire vehicle. During these simulations, a single-track model (see Figure 3.1) is used and the masses of the body and the wheels are taken into consideration.

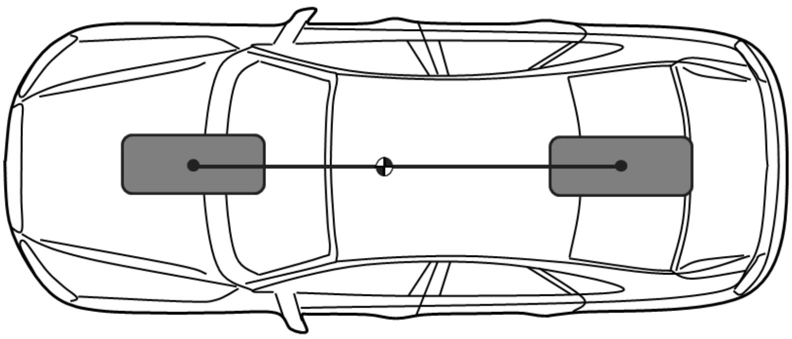

Figure 3.1 : Single-track model of a half vehicle model [26].

Figure 3.1 and Figure 3.2 show the model that provides a graphical representation of the simplifications. The unsprung masses include the masses of the wheels, tires and brake systems and hereafter are represented as "m_w". The sprung mass consists of the vehicle mass and the mass of suspension components and hereinafter is presented as body mass "m_b". The damping of the tires and the elasticity of the body are neglected.

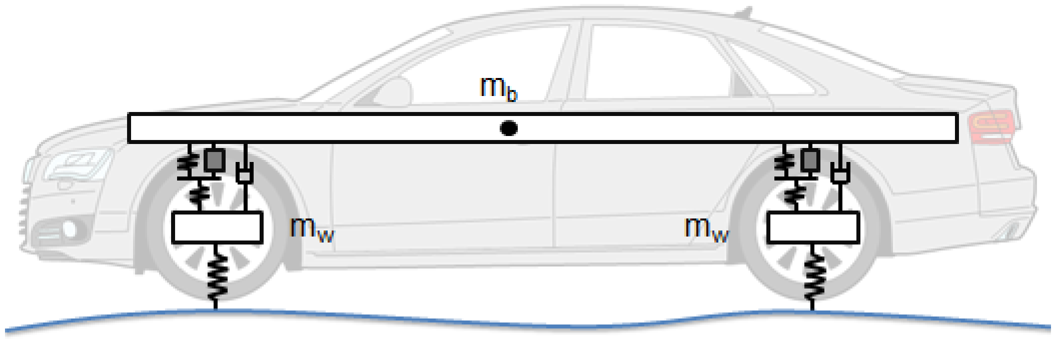

Figure 3.2 : Masses and suspension system of half vehicle model [10].

In order to adapt this half-vehicle model in MATLAB/Simulink, first the system's equations of motions will be explained, before the directions should be determined as positive or negative. For this purpose, the actuator movement should be also comprehended. The quarter vehicle model of this system is delineated in Figure 3.3.

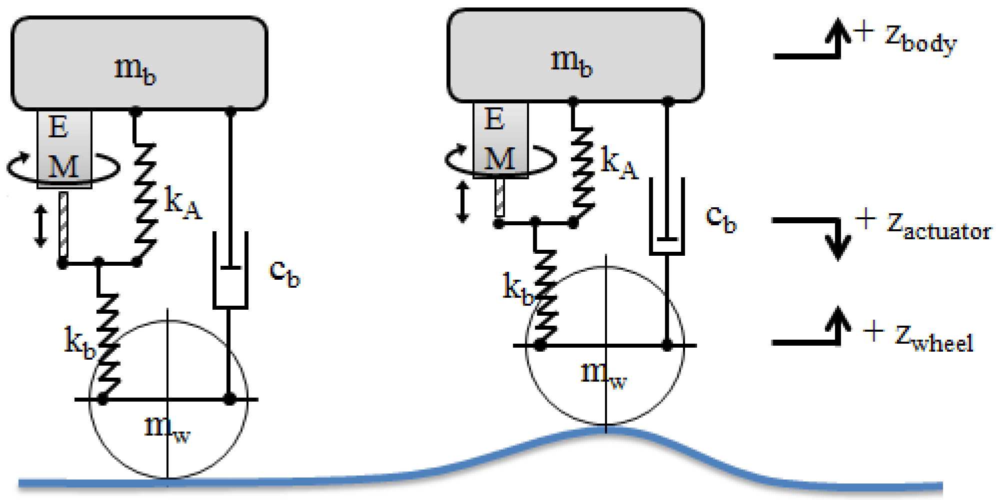

Figure 3.3 : Actuator working principle [12].

The principle of the actuator is to induce the body spring seat upwards or downwards according to the wheels motion. As shown in Figure 3.3 when the wheel runs over a bump, the body spring seat is moved upwards by the actuator (electromotor). In order to get a better driving comfort, this actuator should move as much as necessary. However, there are some constraints. The spring seat movement, the maximum rotational speed of the motor 'w' and the spindle pitch 'α' are bounded in given limits. By using formula 3.1, the vertical speed of the actuator '$v_{act,z}$' is calculated:

$$v_{act,z} = \pm\left(\frac{w}{60} \cdot \alpha\right) \qquad \textbf{(3.1)}$$

Furthermore, the positive 'z' directions are shown in Figure 3.3. I.e. when the main spring seat moves upwards, the sign of direction will be shown as negative "-". After the actuator working principles and constraints have been comprehended, the half vehicle model's free body diagram is presented in Figure 3.4.

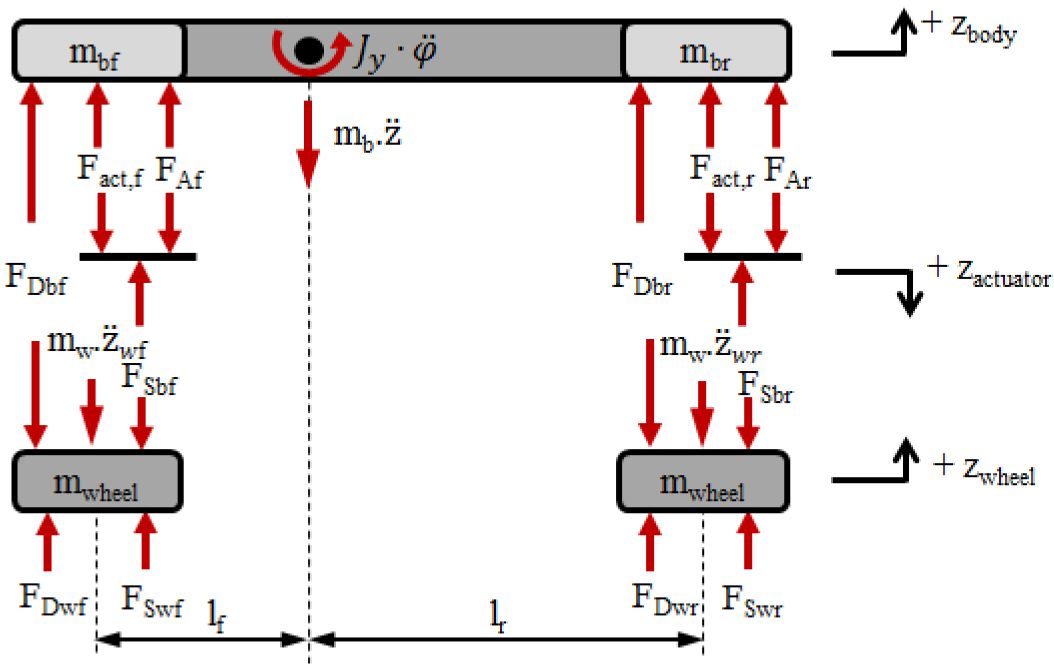

Figure 3.4 : Free body diagram of the half vehicle model [26] [35].

To set up the equations of motions (the following formulas of this section are obtained from [28]), it is assumed that the balance of forces (in "z" direction) and the moment equilibrium are situated around the center of gravity. The gravitational forces are not shown, since they are assumed to be compensated by static deflections. Hence, the balance of forces in "z" direction is calculated by using formula 3.2:

$$-m_b\ddot{z}_b + F_{Db_f} + F_{A_f} + F_{act_f} + F_{Db_r} + F_{A_r} + F_{act_r} = 0 \qquad \textbf{(3.2)}$$

The total spring force is calculated with the forces on the spring leg as shown in formula 3.3:

$$F_{A_{\mathrm{f},r}} + F_{act_{f,r}} = F_{Sb_{f,r}} \qquad \textbf{(3.3)}$$

The duty of the accumulator spring is to carry the static weight of the vehicle as explained in section 2.4.4.2, Figure 2.13. In this way, the required dynamic actuator force can be assumed as equal to the dynamic force of the body spring as shown in formula 3.4:

$$F_{act_{f,r}} = (F_{Sb_{f,r}})_{dyn} \qquad \textbf{(3.4)}$$

Consequently, the structure of the vertical body acceleration is calculated by using formula 3.5:

$$m_b \ddot{z}_b = F_{Db_f} + F_{Db_r} + F_{Sb_\mathrm{f}} + F_{Sb_r} \qquad \textbf{(3.5)}$$

The damper and spring forces that affect the sprung mass are shown in formula 3.6 and 3.7:

$$F_{Db_{f,r}} = (-\dot{z}_{bf,r} + \dot{z}_{wf,r})c_{bf,r} \qquad \textbf{(3.6)}$$

$$F_{Sb_{\mathrm{f},r}} = (-z_{bf,r} + z_{wf,r} + z_{actf,r})k_{bf,r} \qquad \textbf{(3.7)}$$

Both forces are assumed to be proportional to the relative displacement $\Delta z_b = (z_b - z_w)$ or to the relative velocity $\Delta \dot{z}_b = (\dot{z}_b - \dot{z}_w)$ with spring stiffness 'k' and damping constant 'c', which is shown in Figure 3.5

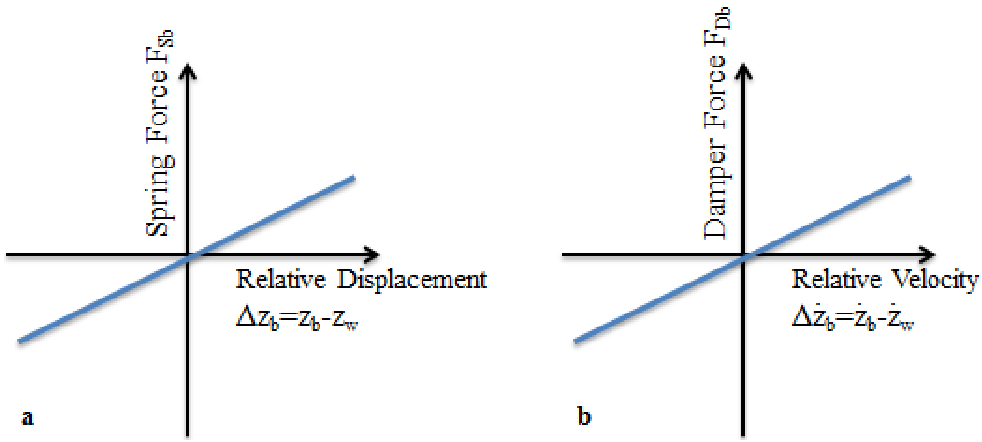

Figure 3.5 : Delineation of spring stiffness and damping coefficient [28].

If these forces (formula 3.3 – 3.7) are substituted in equation 3.3, the vertical body acceleration of the vehicle is obtained (formula 3.8):

$$\ddot{z}_{bf,r} = -\frac{c_{bf,r}}{m_{bf,r}}\dot{z}_{bf,r} + \frac{c_{bf,r}}{m_{bf,r}}\dot{z}_{wf,r} - \frac{k_{bf,r}}{m_{bf,r}}z_{bf,r} + \frac{k_{bf,r}}{m_{bf,r}}z_{wf,r} + \frac{k_{bf,r}}{m_{bf,r}}z_{actf,r} \quad \textbf{(3.8)}$$

The vehicle body movement, relative to the wheels is assumed as formula 3.9:

$$\Delta z_{bf,r} = z_{bf,r} - z_{wf,r} \quad \textbf{(3.9)}$$

At the end the vertical body acceleration is obtained by formula 3.10:

$$\ddot{z}_{bf,r} = -\frac{c_{bf,r}}{m_{bf,r}}\dot{z}_{bf,r} + \frac{c_{bf,r}}{m_{bf,r}}\dot{z}_{wf,r} - \frac{k_{bf,r}}{m_{bf,r}}\Delta z_{bf,r} + \frac{k_{bf,r}}{m_{bf,r}}z_{actf,r} \quad \textbf{(3.10)}$$

And the structures of vertical acceleration of unsprung masses are calculated by using formula 3.11:

$$m_w\ddot{z}_{w_{f,r}} = -F_{Db_{f,r}} - F_{Sb_{f,r}} + F_{Dw_{f,r}} + F_{Sw_{f,r}} \quad \textbf{(3.11)}$$

Following equations, 3.12 and 3.13, define the forces of unsprung masses:

$$F_{Dw_{f,r}} = (\dot{h}_{f,r} - \dot{z}_{w_{f,r}})c_{wf,r} \quad \textbf{(3.12)}$$

$$F_{Sw_{f,r}} = (h_{f,r} - z_{w_{f,r}})k_{wf,r} \tag{3.13}$$

Formula 3.6, 3.7, 3.12 and 3.13 are substituted in the wheel's equations of motion (formula 3.11) as seen in formula 3.14:

$$\begin{aligned} m_w \ddot{z}_{wf,r} = -c_{bf,r} \cdot \left(-\dot{z}_{bf,r} + \dot{z}_{wf,r}\right) - k_{bf,r}\left(-z_{bf,r} + z_{wf,r} + z_{actf,r}\right) \\ + k_{wf,r}\left(-z_{wf,r} + h_{f,r}\right) + c_{wf,r}\left(-\dot{z}_{wf,r} + \dot{h}_{f,r}\right) \end{aligned} \tag{3.14}$$

The wheel motion, relative to the ground, is assumed as in formula 3.15:

$$\Delta z_{wf,r} = z_{wf,r} - h_{f,r} \tag{3.15}$$

Finally, the vertical wheel acceleration is calculated by using formula 3.16:

$$\begin{aligned} \ddot{z}_{wf,r} = +\frac{c_{bf,r}}{m_{wf,r}}\dot{z}_{bf,r} - \frac{c_{bf,r}}{m_{wf,r}}\dot{z}_{wf,r} + \frac{k_{bf,r}}{m_{wf,r}}\Delta z_{bf,r} - \frac{k_{bf,r}}{m_{wf,r}}z_{actf,r} \\ - \frac{k_{wf,r}}{m_{wf,r}}\Delta z_{wf,r} + \frac{c_{wf,r}}{m_{wf,r}}\left(\dot{h}_{f,r} - \dot{z}_{wf,r}\right) \end{aligned} \tag{3.16}$$

After obtaining the wheel and body (center of gravity) motions, the front and rear axle's motions will be calculated by supplementing the pitch moment to the model. In order to calculate the pitch angle, the pitch pole is assumed to be at the center of gravity (see Figure 3.6). It is agreed that the pitch angle is negative during braking. The equation of moment balance is as presented in formula 3.17:

$$-J_y \cdot \ddot{\varphi} + \left(F_{Db_f} + F_{Sb_f}\right) \cdot l_f - \left(F_{Db_r} + F_{Sb_r}\right) \cdot l_r = 0 \tag{3.17}$$

And the pitch acceleration is calculated with formula 3.18:

$$\ddot{\varphi} = \frac{\left(F_{Db_f} + F_{Sb_f}\right) \cdot l_f - \left(F_{Db_r} + F_{Sb_r}\right) \cdot l_r}{J_y} \tag{3.18}$$

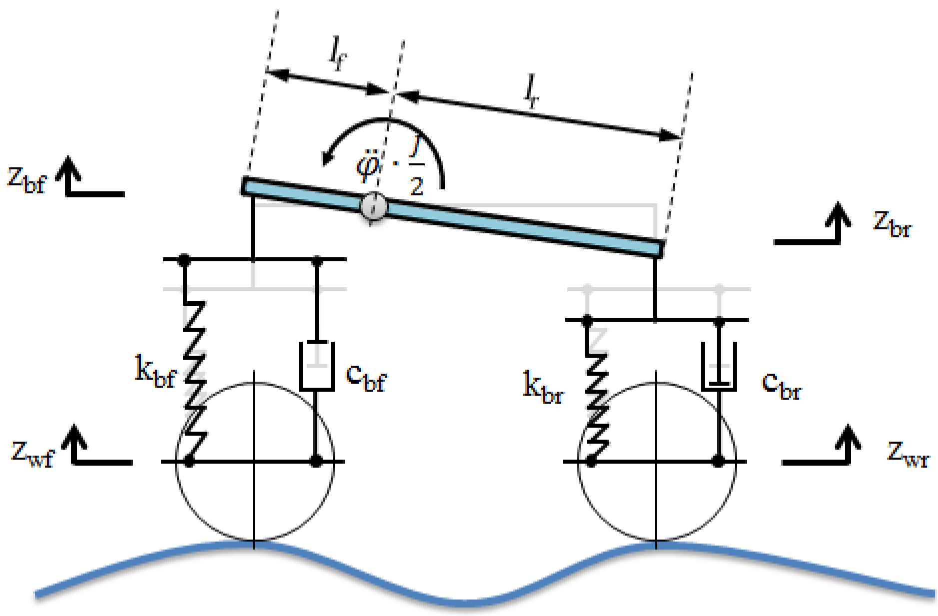

Figure 3.6 : Pitch angle delineation [38].

Once the pitch angle is calculated, relative chassis displacements at front and rear axles are acquired with the trigonometric equation presented in formula 3.19:

$$\Delta z_{pitch_{f,r}} = l_{f,r} \cdot \sin(\varphi) \tag{3.19}$$

For small pitch angles, following formula can be applied:

$$\sin(\varphi) \approx \varphi \tag{3.20}$$

The relative front and rear axle motions are calculated by using formula 3.21:

$$\Delta z_{b_{f,r}} = z_b \pm \Delta z_{pitch_{f,r}} \tag{3.21}$$

The required vehicle parameters for these equations are shown in Table 3.1.

Table 3.1 : Vehicle Parameters.

Parameter	Symbol	Value
Sprung mass [kg] (half vehicle)	m_b	997
Front mass of entire vehicle [kg] (entire vehicle)	$m_{bf} + m_w$	1196

Parameter	Symbol	Value
Rear mass of entire vehicle [kg] (entire vehicle)	$m_{br} + m_w$	958
Unsprung mass [kg] (each wheel)	m_w	40
Front sprung mass [kg] (half vehicle)	m_{bf}	558
Rear sprung mass [kg] (half vehicle)	m_{br}	439
Wheelbase [m]	l	2,944
Front wheelbase [m]	l_f	1,2963
Rear wheelbase [m]	l_r	1,6477
Front spring stiffness of sprung mass [N/m]	k_{bf}	111000
Rear spring stiffness of sprung mass [N/m]	k_{br}	67000
Front damping coefficient of sprung mass [Ns/m]	c_{bf}	3500
Rear damping coefficient of sprung mass [Ns/m]	c_{br}	2800
Spring stiffness of unsprung mass [N/m]	k_w	234000
Actuator accumulator spring stiffness [N/m]	k_{act}	35000
Damping coefficient of unsprung mass [Ns/m]	c_w	0
Pitch moment of inertia [kg·m^2] (entire vehicle)	J_y	3800
Longitudinal velocity of the vehicle [km/h]	v	60
Front suspension compression ratio [-]	i_f	0,59
Rear suspension compression ratio [-]	i_r	0,67

After these assumptions and required equations are known, all vehicle parameters have been modified according to the test vehicle. However, when the simulations and experiments have been compared, it was realized that they were different from each other. Therefore, in Simulink model some modifications have been made. In the following section, these adaptations are explained.

3.1.2 Improvements of initial Simulink model

The adaption of the initial model obtained from Volkswagen AG into the required model is merely summarized in this section. As a matter of fact, this process is highly time-consuming. On account of this, the following two objectives have been set:

- The model needs to represent the actual vehicle as accurate as necessary to understand the movements of the vehicle influenced by the actuator and its controller.
- Hereby, the focus will be on the front body that assumingly affects the driver primarily (front axle is closer than rear axle to the driver).

The information gained by these simulations is meant to show a tendency of the applied controller model. A validation and further adjustments of these results need to be done with the test vehicle.

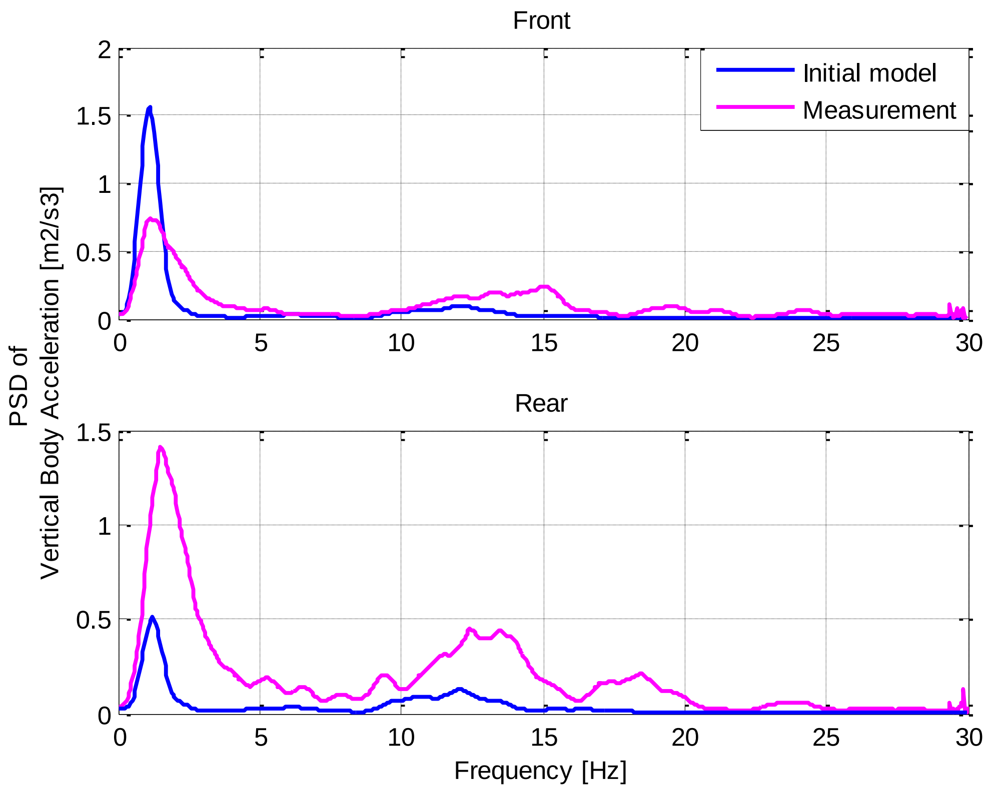

Figure 3.7 : Measurement and initial simulation model comparison.

Figure 3.7 compares the PSD diagrams of the Simulink model and the measurement with the test vehicle (on rough roadway explained in section 3.1.4 ., with 60 km/h and State-Space controller). The results of both diagrams are evidently highly different. These figures display an early state of the adapted Simulink model, which already includes all parameters, which were known at that time.

The following deals with the most important changes that were made to optimize the inadequate Simulink model.

One of the relevant inputs is the roadway excitation, to receive correct PSD diagrams. This test roadway was modified recently. As shown in Figure 3.8, the initial and modified roadway data are substantially different from each other. Consequently, the initial roadway data, which was loaded in the initial Simulink model at the beginning, has been updated according to the modified one.

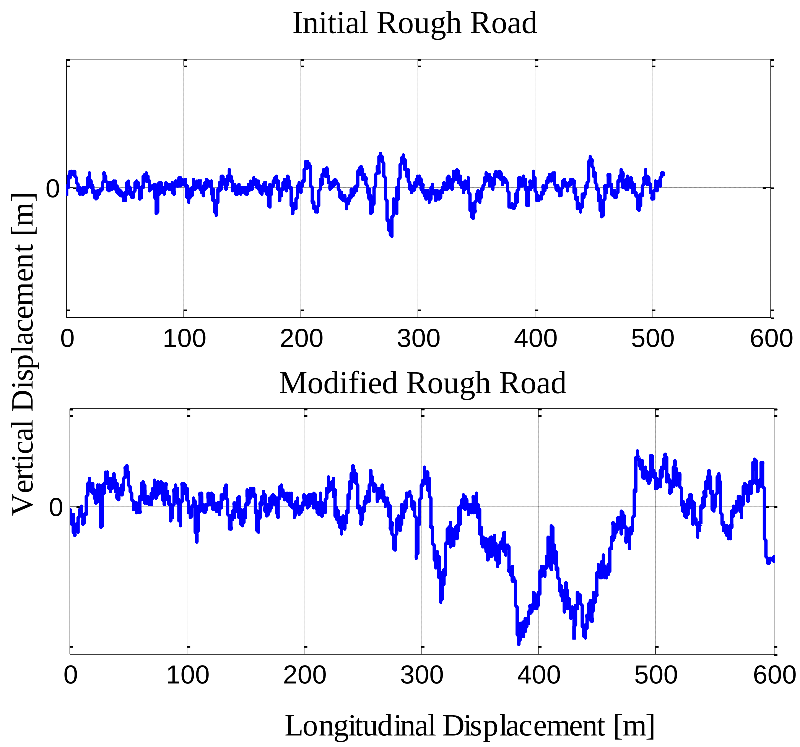

Figure 3.8 : Different road excitations.

As another important input, the vehicle velocity can be mentioned. In reality, the purpose is to drive at a speed of exactly 60 km/h (≅ 16.6667 m/s). During tests, in spite of using a speedometer, the velocity is variable. Moreover, there is a difference between the displayed value on the instrument board and the actual speed. It is possible to realize this variability by examining the results of sensor outputs, which relate to the driving speed. E.g. they can be displayed in the following form (measured every 0.005 sec):

- 16.040 m/s
- 16.036 m/s
- 16.066 m/s
- 16.079 m/s
- 16.201 m/s
- ….

Therefore, the proper simulation velocity has been calculated by using formula 3.22:

$$v_{new} = \frac{\sum \text{all velocity vector outputs}}{\text{length of the velocity vector}} = 16.084\ [\frac{m}{s}]. \quad \textbf{(3.22)}$$

For this reason, the previously assumed velocity of 16.6667 m/s matches a discrepancy of 3.5%.

Another optimization was achieved by examining the weights of the front and rear masses (altogether about 70kg), which were adjusted afterwards in the MATLAB/Simulink model. After all modifications, the new center of gravity and pitch moment of inertia were calculated.

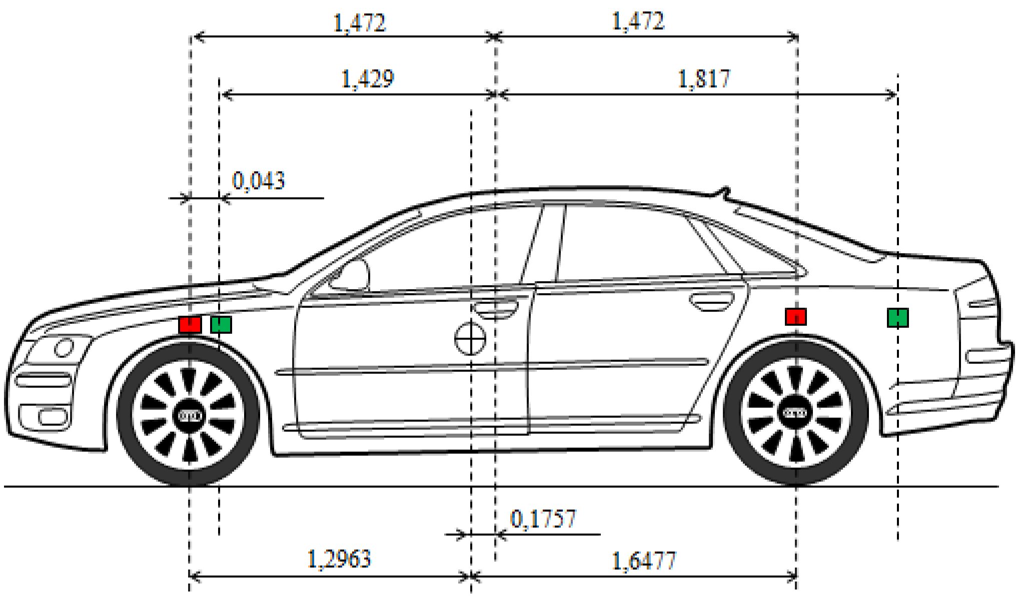

Figure 3.9 : Front and rear sensor acceleration sensor positions.

Further improvement was achieved by integrating the proper front and rear sensor acceleration positions in the model (see Figure 3.9). The adapted model uses the red marked positions, but in reality these acceleration sensors are installed in the green marked positions. (In this thesis the expression “front and rear body acceleration” refers to this given sensor positions.)

The comparison of the damper characteristics shows certain differences as well (see Figure 3.10). The previous damper characteristics in the MATLAB/Simulink model had to be replaced with the correct values, which represent the test vehicle.

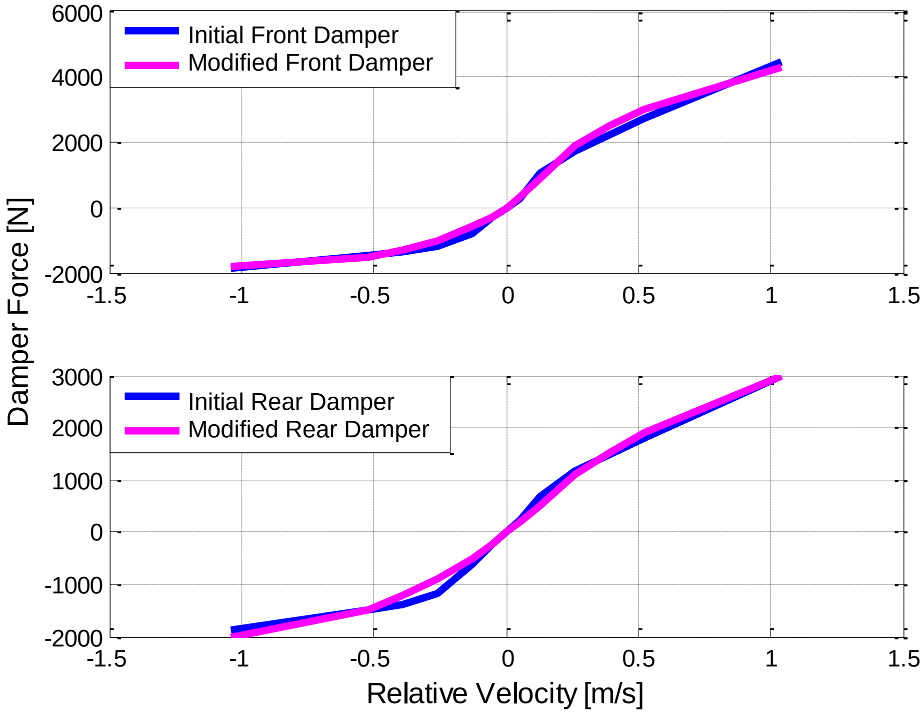

Figure 3.10 : Different damper characteristics.

These are the most important quantities that have been changed. Although, some of these properties do not appear to be significant on their own, altogether they generate an important impact on the simulations. Figure 3.11 depicts the PSD diagrams of vertical vehicle body accelerations. Additional to the curves of the measurement and the first adapted Simulink model as in Figure 3.7, it includes the enhanced adapted Simulink model. These results of the adapted simulation display an acceptable accuracy compared to the behavior of the test vehicle. Hence, it is possible to compare different controller models before testing them in reality.

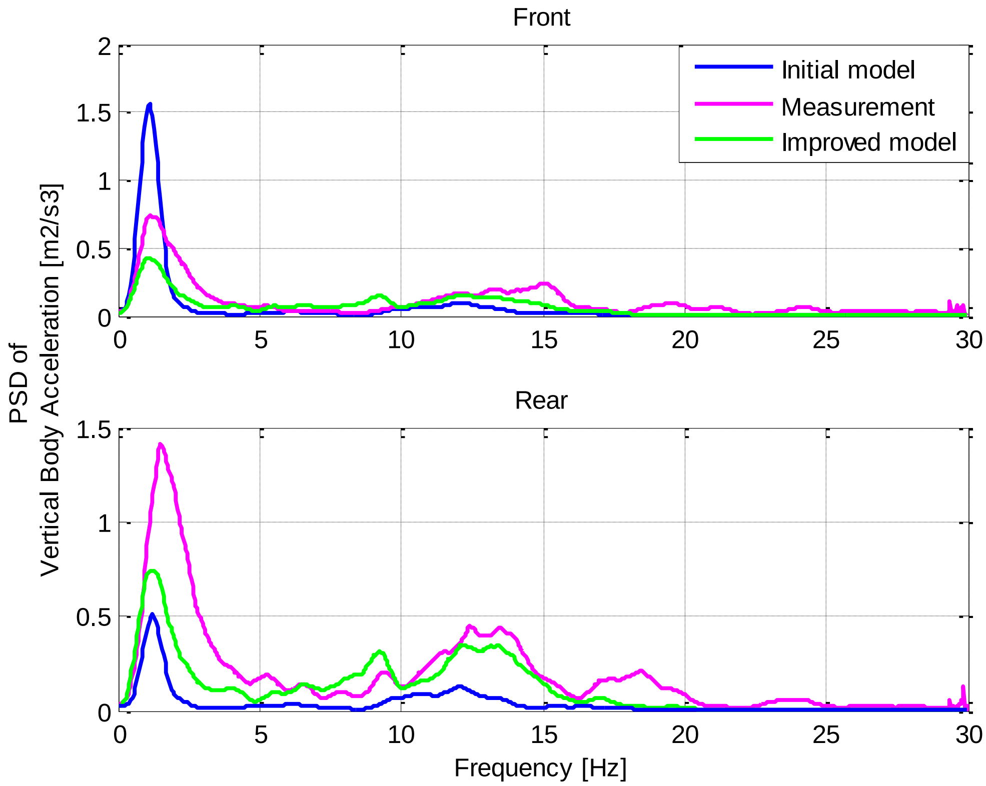

Figure 3.11 : PSD diagrams of vertical vehicle body accelerations.

3.1.3 Simulink model

According to previously explained adjustments of vehicle parameters, the Simulink model has been modified. In this section, the layout of this model will be shown. As mentioned before, this Simulink model was obtained from Volkswagen AG database. The focus of this thesis was to develop the controller models and to improve the initial Simulink model as illustrated in section 3.1.3

The entire vehicle model is depicted on Figure 3.12. It consists of six types of so-called “blocks”

- Body
- Controller
- Spring
- Damper
- Wheel
- Input and output data.

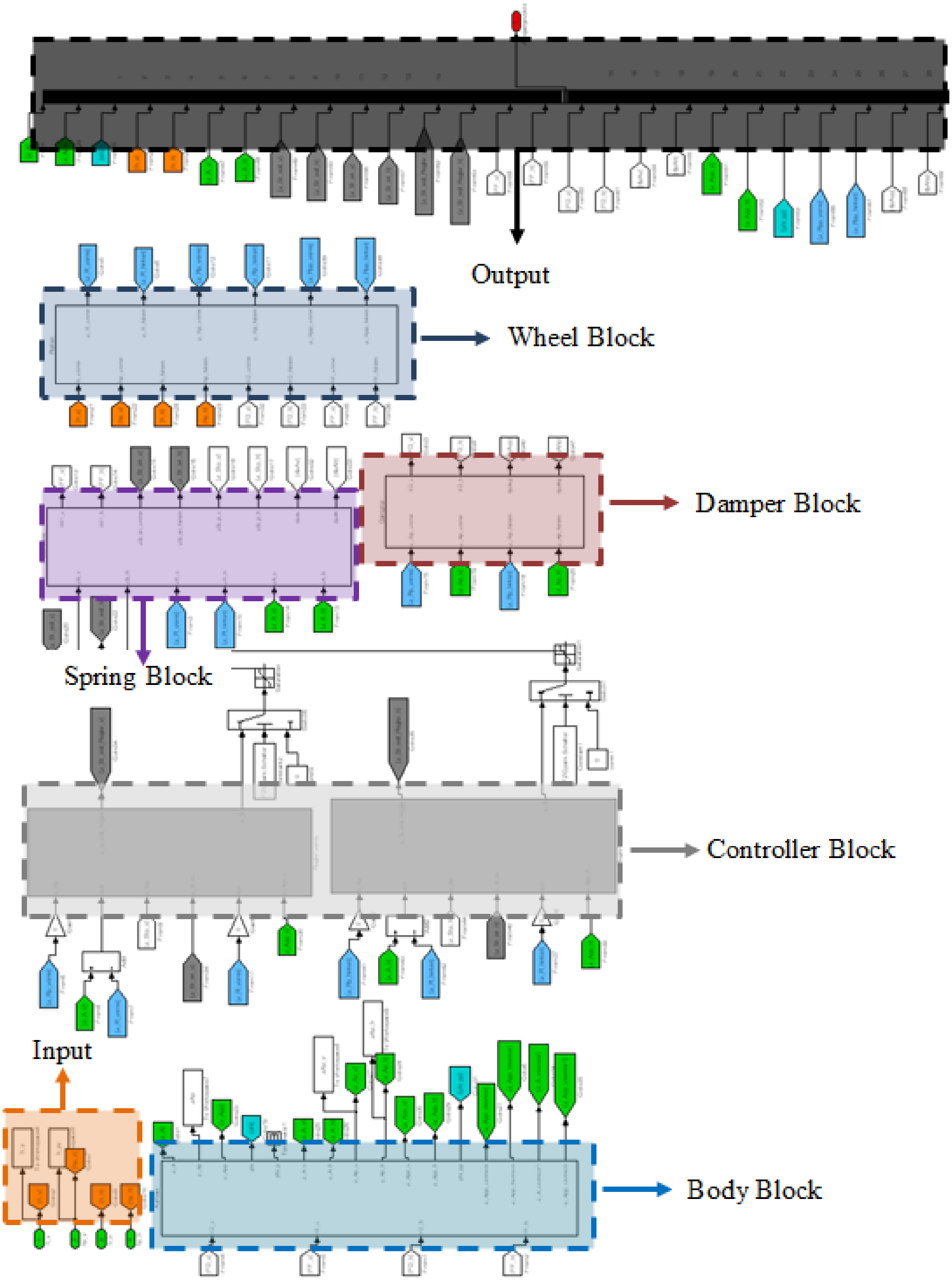

Figure 3.12 : Layout of vehicle model (MATLAB/Simulink).

In order to acquire the vertical body acceleration, the body block shown in Figure 3.13 is utilized. In this block at first, as explained in the "equations of motions" part, the forces are added together in order to calculate the vertical acceleration of the center of gravity. Then, by taking into account the pitch moment of inertia, the accelerations of front and rear bodies are calculated. As input, body block uses spring and damper forces, which are calculated in their individual blocks.

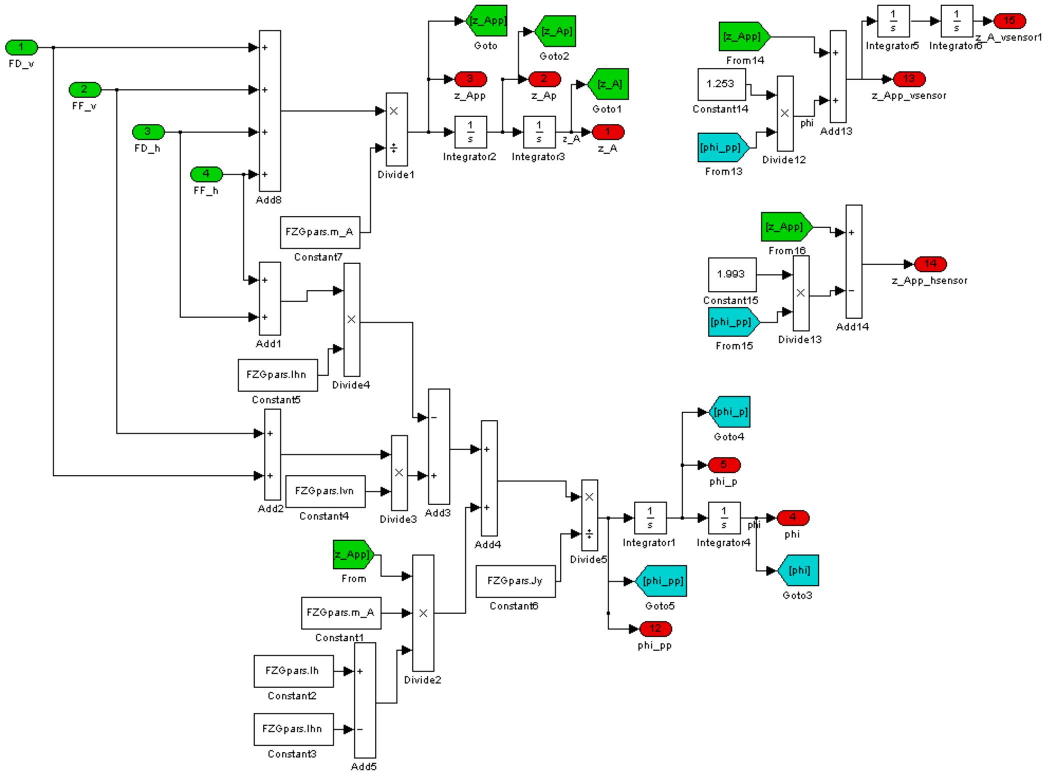

Figure 3.13 : Simulink body block.

In spring blocks (Figure 3.14 shows the front spring), the spring forces are calculated by taking into consideration the constraints of the actuator that is mentioned in formula 3.1 on page 30. The spring stiffness explained in section 3.1.1 (Suspension Compression Ratio) includes the previously explained suspension compression ratio "i".

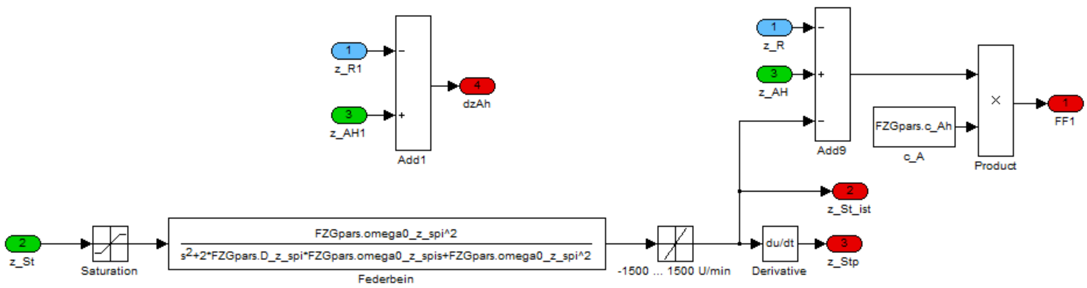

Figure 3.14 : Layout of spring model (MALAB/ Simulink).

The damper forces (see Figure 3.15) are calculated according to formula 3.6 by using the given damper characteristics as shown in Figure 3.10 and by applying the suspension compression ratio.

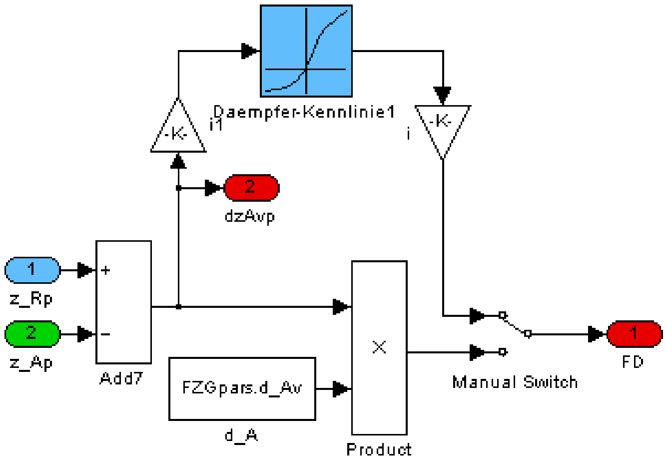

Figure 3.15 : Layout of damper model (MATLAB/Simulink)

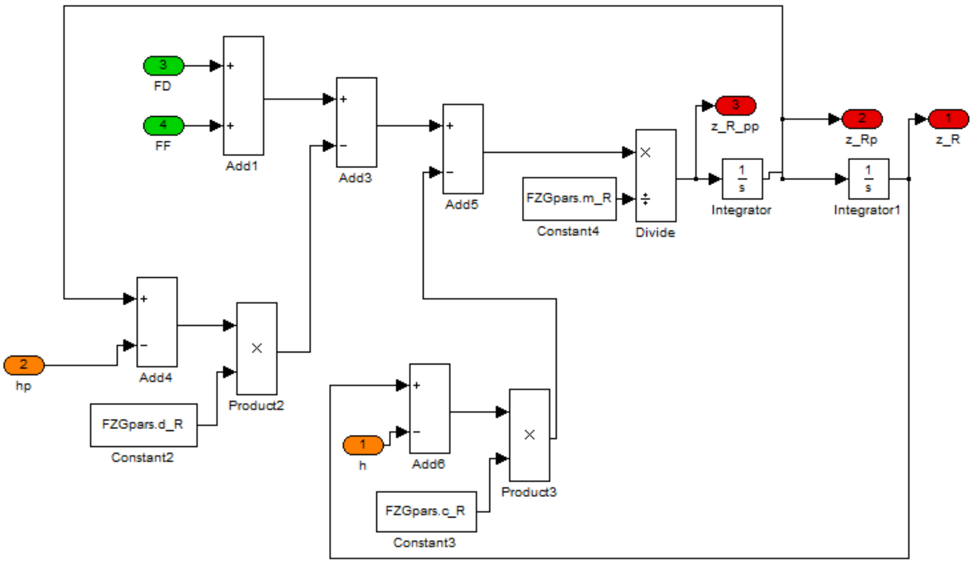

Figure 3.16 : Layout of wheel model (MATLAB/Simulink).

With the given forces and roadway inputs, the wheel motions are calculated as shown in Figure 3.16.

The input for the wheels and hereby the entire system “h” (corresponds h_v in the figure) is obtained from the input block by using the roadway unevenness (from workspace) in “x” and “z” directions and the longitudinal velocity of the vehicle as shown in Figure 3.17.

As input in simulations, the front left and rear left (a delayed form of front input) roadway data is used. Therefore, during the comparison of simulations and experiments, the front-left outputs have been taken into consideration.

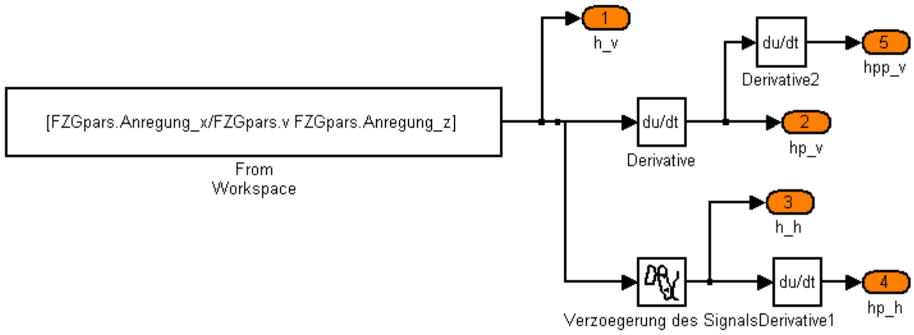

Figure 3.17 : Input block: Road roughness.

After using all downloaded parameters and blocks, at the end of the simulation, the required output parameters are obtained and used during the comparison of different controller strategies.

In the next section, three different types of roadways that were used in MATLAB/Simulink will be introduced.

3.1.4 Disturbance types and models

Different sources can induce vibrations (oscillations) to a vehicle [24]. Vehicle-induced disturbances (e.g. because of motor or unbalanced masses) are generally periodic and road-induced vibrations are mostly stochastic type. In this thesis, just road-induced disturbances have been taken into consideration.

In this section, two stochastic road profiles and singular disturbances (bumps) are presented. The reason of using singular disturbances is to determine whether the suspension deflections and actuator movements are plausible.

3.1.4.1 Stochastic road profiles

Usually, vehicles are induced by the public roads with stochastic vibrations. The velocity of the vehicle and the unevenness of the roadway determine the intensity of these vibrations [3]. In order to compare the simulations and measurement results, the measured real roadway profiles are used as input in these simulations. The rough road profile on Volkswagen AG test road and the smooth road on German country roadways have been recorded by a vehicle equipped with laser scanners, multi camera systems and sensors.

In Figure 3.18 and Figure 3.19, the soft and rough road profiles are depicted."x" denotes the longitudinal coordinate of the road and z the vertical in [m].

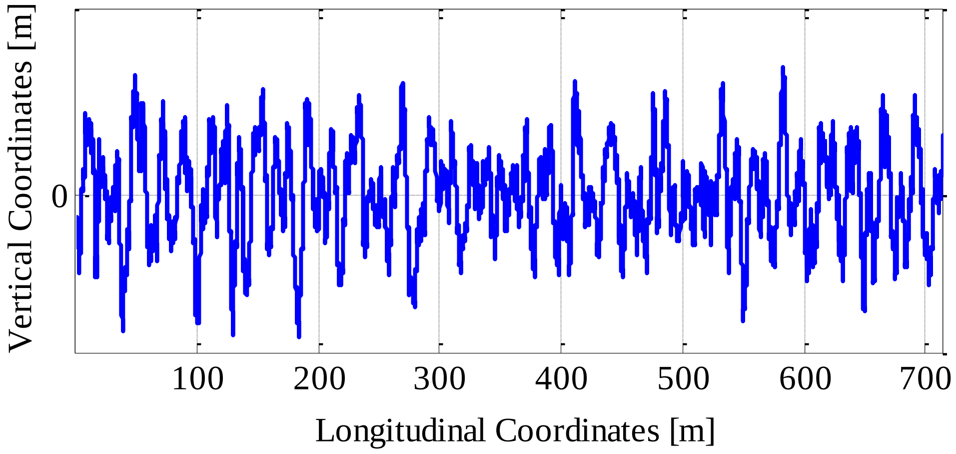

Figure 3.18 : Soft road profile

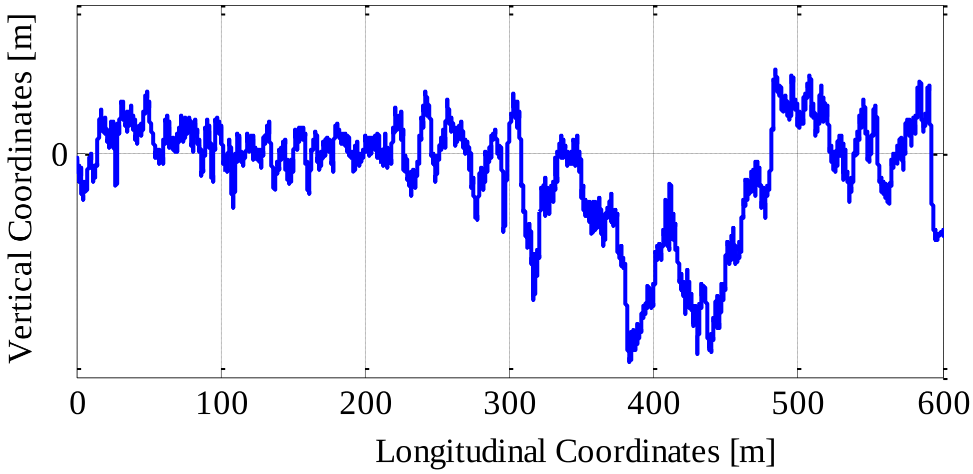

Figure 3.19 : Rough road profile.

3.1.4.2 Singular disturbance

The singular disturbance is used to examine the performance of suspension systems in addition to stochastic excitations signals [3]. In this thesis, a basic "bump" model is given as seen in Figure 3.20. "x" marks the longitudinal distance and "z" marks the height of the bumps in [m]. The longitudinal distance of a bump is approximately 2.1 m and the height is 0.05m.

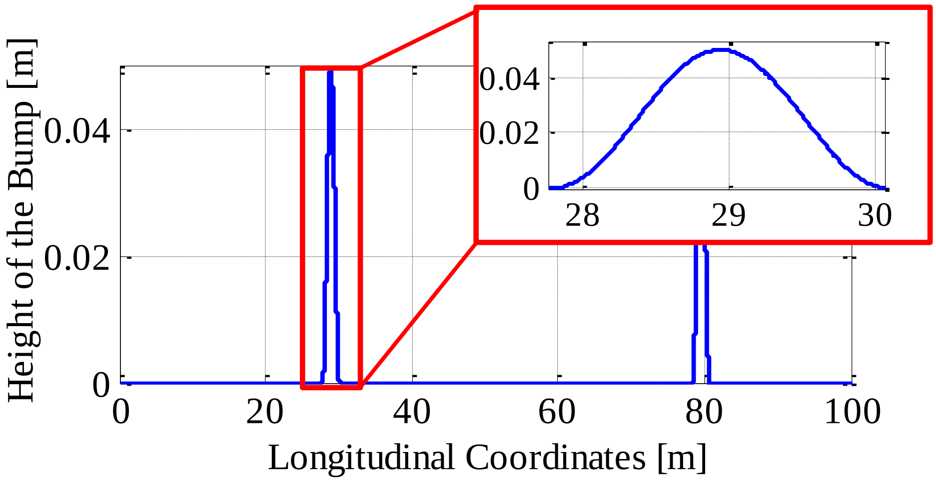

Figure 3.20 : Singular disturbance.

By using this type of road inputs in simulations, it is possible to interpret the appropriation of the actuator's control principle, through examining suspension working space or the actuator's vertical displacement.

After the required Simulink model is described and the assumptions are given, the 'Controller Models' which are the main part of this thesis, will be explained.

3.2 Controller Models

In this section, all controller models being worked on, will be explained. The control structure is always the same as in Figure 3.21.

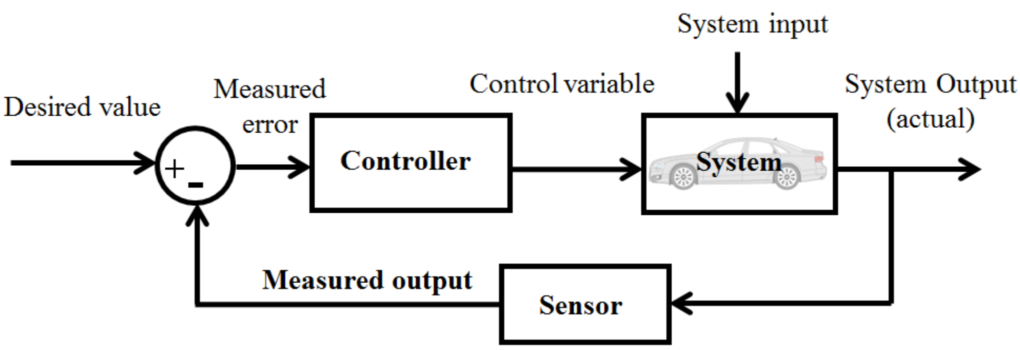

Figure 3.21 : The structure of a typical control system [36].

The vehicle vertical motions are controlled with a control variable. In slow-active suspensions, this value is "z_{act}", which represents the vertical displacement of the main spring seat, induced by the actuator. The purpose of applying any control strategies to the vehicle is to obtain the most convenient "z_{act}" value for ride comfort.

Therefore, in the following sections Skyhook, Groundhook, State-Space, P-Controller and a combination of Skyhook and State-Space controller will be explained with half-vehicle Simulink models. Since the model is half-vehicle, always two controller blocks will take part in it. One of them will regulate the front, while the other regulates the rear vehicle body motions. In these controller models, some neglects and simplifications have been assumed as in the "Simulation Model" section.

Firstly, the Skyhook control structure will be explained with its working principle, assumptions and Simulink block.

3.2.1 Skyhook controller model

For understanding Skyhook control, it is possible to think that there is an imaginary damper between the vehicle chassis and the sky (see Figure 3.22). With this imaginary damper chassis' motion will be reduced (with an imaginary hook).

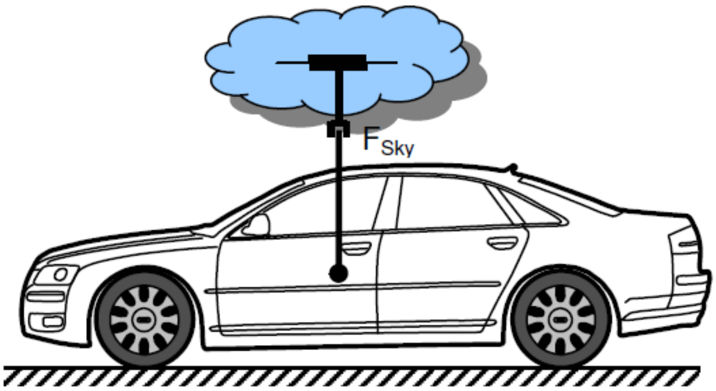

Figure 3.22 : The principle of Skyhook control [26].

It is supposed that instead of conventional damper, a device that is capable of generating any force "F_{sky}", is assembled and its force is controllable.

As shown in formula 3.23 and Figure 3.23, this strategy indicates that if the relative velocity of the body $(\dot{z}_{body} - \dot{z}_{wheel})$ is in the same direction as the body velocity '$\dot{z}_{body}$', then a damping force should be applied in order to reduce the body acceleration. On the other hand, if the two velocities are in the opposite directions, the damping force should be zero to keep the body acceleration at a minimum [1].

$$F_{sky} = \begin{cases} c_{sky} \cdot \dot{z}_{body} & (\dot{z}_{body} - \dot{z}_{wheel}) \cdot \dot{z}_{body} \geq 0 \\ 0 & (\dot{z}_{body} - \dot{z}_{wheel}) \cdot \dot{z}_{body} < 0 \end{cases} \quad \textbf{(3.23)}$$

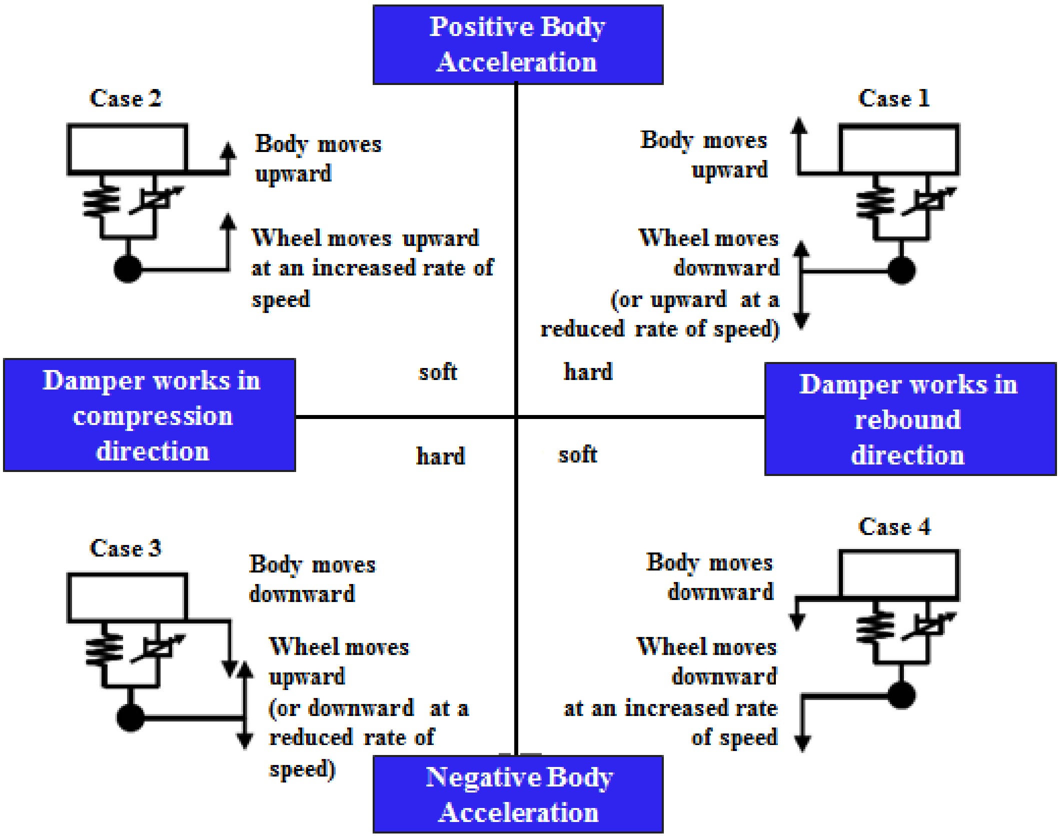

Figure 3.23 : Skyhook strategy for variable dampers [1] [26].

Relative vertical body velocity is calculated by using formula 3.24:

$$\dot{z}_{body} - \dot{z}_{wheel} = \Delta\dot{z}_{body} \tag{3.24}$$

When $\dot{z}_{body}$ and $(\dot{z}_{body} - \dot{z}_{wheel})$ have the opposite signs, the controller could only generate a force with an opposite sign to the desired force $c_{sky} \cdot \dot{z}_{body}$ in order to apply no force at all. Hence, the applied Skyhook force will be zero [39].

Skyhook control strategy is utilized with variable dampers in semi-active suspension systems. Since the damper force areas are limited, only in some kind of situations a Skyhook damping force will be generated as shown in Figure 3.24.

On the contrary, for active suspension there is no limited field to generate a Skyhook force. The main reason is that the control mechanism works on the spring seat, not the damper. There will be a continuously occurring force for each situation of active Skyhook control.

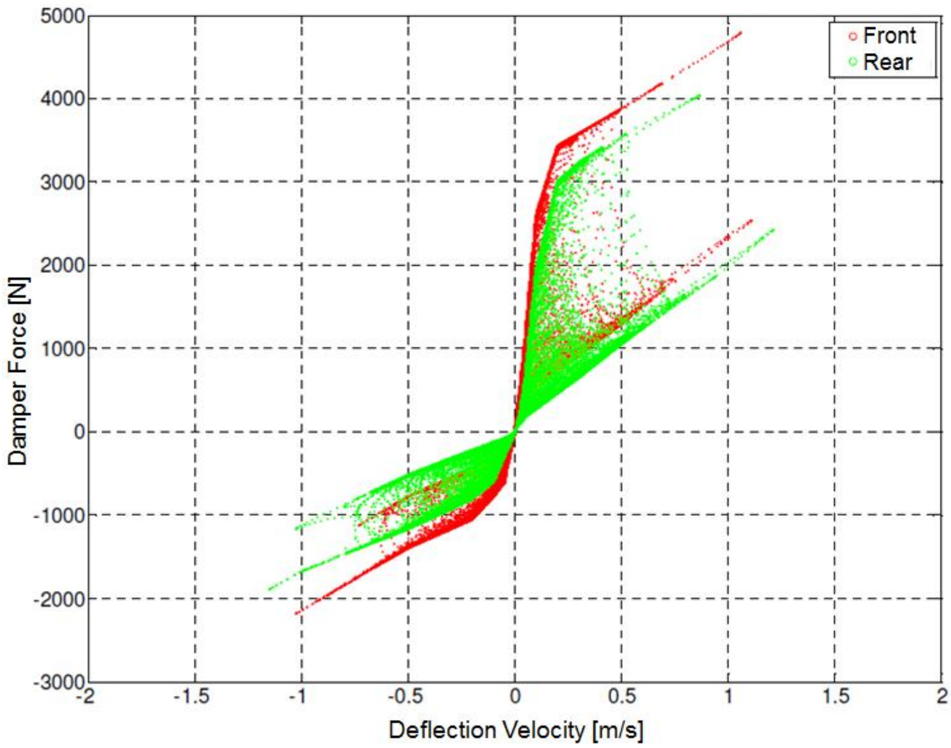

Figure 3.24 : An example of semi-active Skyhook damping [26].

Firstly, with the formula 3.25 the Skyhook force is calculated:

$$F_{sky} = c_{sky} \cdot \dot{z}_{body} \tag{3.25}$$

Here "c_{sky}" is an adjustable Skyhook value as in the semi-active systems. After the best suitable value is gained from tests or simulations, it will be implemented to the software of the vehicle. In the software program of the vehicle, the main spring seat movement "z_{act}" will be computed by using formula 3.26:

$$z_{act} = -F_{sky} / k_{body} \tag{3.26}$$

Once the desired "z_{act}" value is obtained, then the actual value will be calculated in the system due to the actuator's constraints. Eventually, the generated control force can be applied to the vehicle's suspension spring by the actuator, as shown in Figure 3.25.

As input, the vertical vehicle body velocity is used. After calculating the required Skyhook force, the main spring seat is moved upwards or downwards by the actuator.

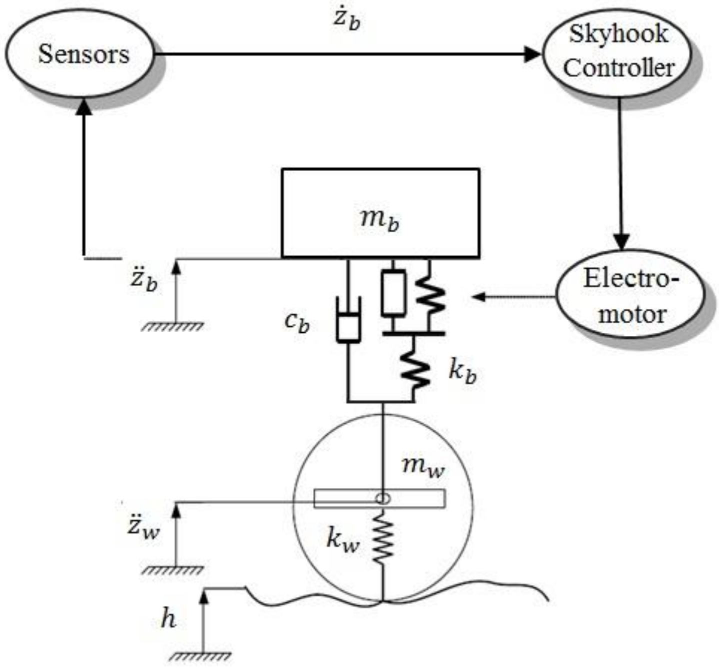

Figure 3.25 : Skyhook control sketch [40].

As shown in Figure 3.26, the required movement of the spring seat is calculated in the Skyhook controller block with the logic of formula 3.25.

The acceleration signal of the simulation is made similar to experimental acceleration data by applying a white-noise. Through a filter, the acceleration signal is converted to a velocity signal. By multiplying this acquired velocity signal with the Skyhook constant, the desired control value (z_St_soll_Regler) is obtained as shown in Figure 3.26.

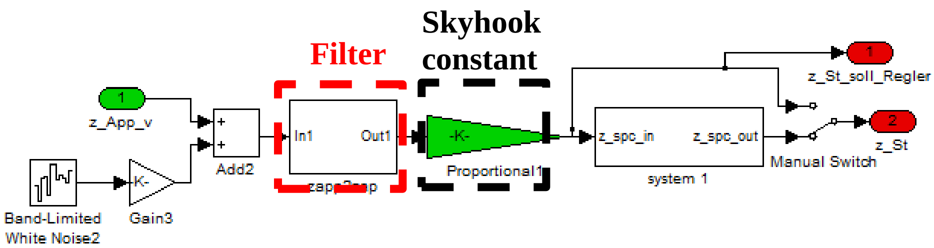

Figure 3.26 : Layout of Skyhook controller model (MATLAB/Simulink).

3.2.2 Groundhook controller

The principle of Groundhook control is similar to Skyhook control (Figure 3.27). The wheels are damped by an inertial system of ground as shown in Figure 3.28. The aim of this control is to reduce the wheel load fluctuations with the help of ground force "F_{Ground}". With this controller the handling of the vehicle is improved rather than driving comfort [30].

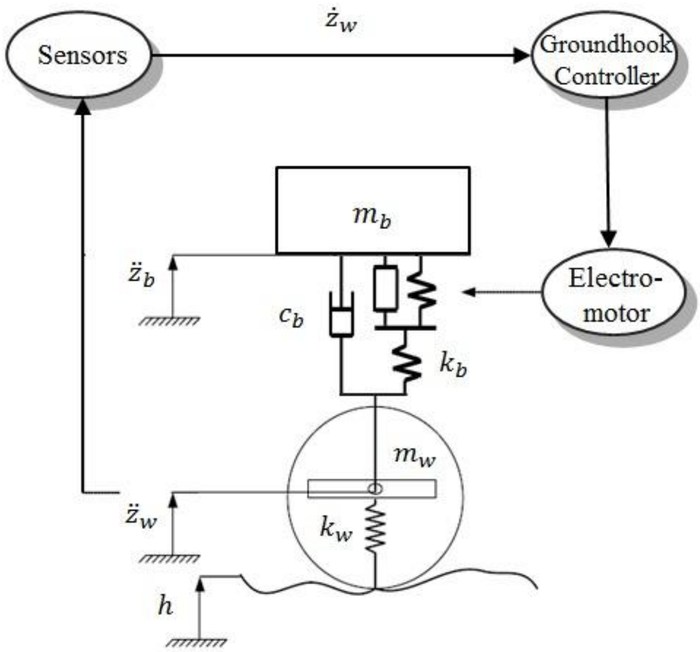

Figure 3.27 : Groundhook control sketch [40].

As seen in Figure 3.28, an imaginary groundhook force is produced with an adjustable damper. This force is calculated by using formula 3.27.

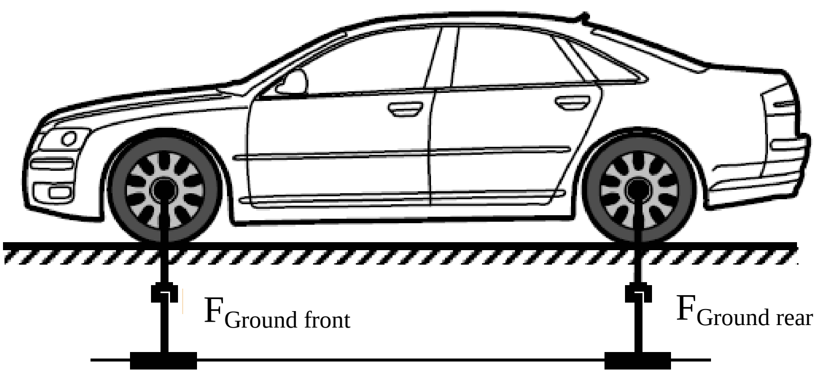

Figure 3.28 : The principle of Groundhook control [26].

$$F_{Ground} = \begin{cases} F_{act} = -c_{Ground} \cdot \dot{z}_{wheel} & (\dot{z}_{body} - \dot{z}_{wheel}) \cdot \dot{z}_{wheel} < 0 \\ F_{act} = 0 & (\dot{z}_{body} - \dot{z}_{wheel}) \cdot \dot{z}_{wheel} \geq 0 \end{cases} \quad \textbf{(3.27)}$$

Accordingly, as in Skyhook control, the actuator movement is calculated by using formula 3.28:

$$z_{act} = -F_{Ground}/k_{body} \quad \textbf{(3.28)}$$

All these knowledge is implemented to the Simulink model as seen in Figure 3.29

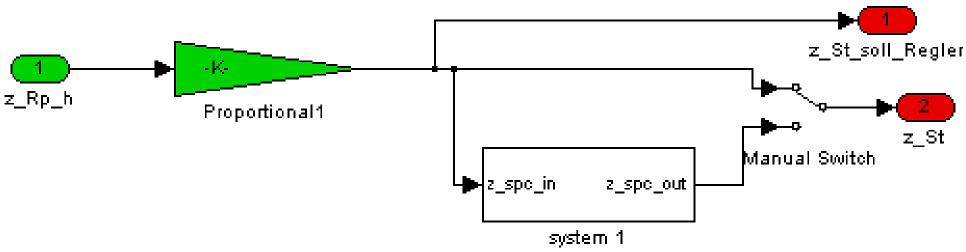

Figure 3.29 : Layout of Groundhook controller model (MATLAB/Simulink).

3.2.3 State-Space controller model

This control block has already been in the initial Simulink model, which was obtained from Volkswagen AG database. Since the objective is to find more effective State-Space parameters, this important controller algorithm is examined and applied.

The State-Space control is a control structure, which circulates, not only the output like "simple" controllers, but the entire state vector. Each state variable affects the control value with a proportional control “K_i” constant. In this way, the transmitted disturbance can be realized more quickly in the controlled system and it is possible to design faster controllers [35] [41].

First of all, control structure as shown in Figure 3.30 should be comprehended:

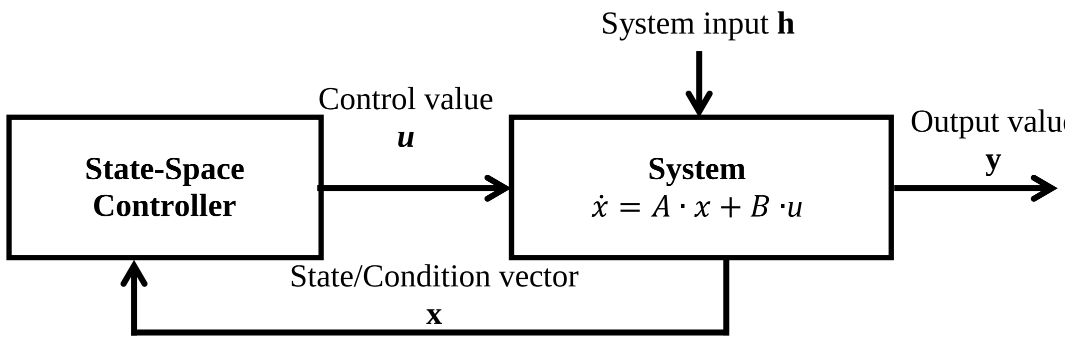

Figure 3.30 : Structure diagram of State-Space controller [35].

In this presentation;

x: State vector (a feedback which is sent to the controller and calculates the control variable for the spindle drive of the active spring leg.)

A : System matrix

B : Control vector

u : Control value (for this kind of suspensions is "z_{act}". I.e. the vertical displacement of the main spring seat induced by actuator)

h : System input. (I.e. the road roughness, which acts as a disturbance to the controlled system)

y : Output value (vertical body acceleration)

After describing the control structure, the control principle should be defined. For the realization of a State-Space control, it is necessary that the control system takes place in the State-Space representation.

In order to represent the control system in State-Space, firstly the equations of motions of a quarter vehicle should be formed.

$$\ddot{z}_b = -\frac{c_b}{m_b}\dot{z}_b + \frac{c_b}{m_b}\dot{z}_w - \frac{k_b}{m_b}\Delta z_b + \frac{k_b}{m_b}z_{act} \quad \textbf{(3.29)}$$

$$\ddot{z}_w = \frac{c_b}{m_w}\dot{z}_b - \frac{c_b}{m_w}\dot{z}_w + \frac{k_b}{m_w}\Delta z_b - \frac{k_w}{m_w}\Delta z_w - \frac{k_b}{m_w}z_{act} + \frac{c_w}{m_w}\left(\dot{h} - \dot{z}_w\right) \quad \textbf{(3.30)}$$

Afterwards, the dynamic behavior of the actuators spindle motor should be taken into consideration in the State-Space representation. It is assumed that it is in the form of PT_2 (explanation on page 24). This can be written by using the following transfer function in formula 3.31:

$$F(s) = \frac{\omega_{0,\mathrm{act}}^2}{s^2 + 2 \cdot D_{act} \cdot s \cdot \omega_{0,\mathrm{act}} + \omega_{0,\mathrm{act}}^2} \qquad \textbf{(3.31)}$$

The control system will be a MIMO (multiple input multiple output) system as shown in the following Figure 3.31.

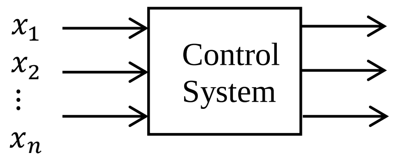

$$\begin{bmatrix} u_1 \\ u_2 \\ \vdots \\ u_m \end{bmatrix} = \begin{bmatrix} f_{11} & \cdots & f_{1n} \\ \vdots & & \vdots \\ f_{m1} & \cdots & f_{mn} \end{bmatrix} \begin{bmatrix} x_1 \\ x_2 \\ \vdots \\ x_n \end{bmatrix}$$

Figure 3.31 : Inputs and outputs delineation of State-Space controller.

From these equations (3.29 - 3.31) the State-Space representation can be derived, which results in the following form :

$$\begin{bmatrix} \ddot{z}_b \\ \ddot{z}_w \\ \Delta\dot{z}_b \\ \Delta\dot{z}_w \\ \ddot{z}_{act} \\ \dot{z}_{act} \end{bmatrix} = \begin{bmatrix} -\frac{c_b}{m_b} & \frac{c_b}{m_b} & -\frac{k_b}{m_b} & 0 & 0 & \frac{k_b}{m_b} \\ \frac{c_b}{m_w} & -\frac{c_b}{m_w} & +\frac{k_b}{m_w} & -\frac{k_w}{m_w} & 0 & -\frac{k_b}{m_w} \\ 1 & -1 & 0 & 0 & 0 & 0 \\ 0 & 1 & 0 & 0 & 0 & 0 \\ 0 & 0 & 0 & 0 & -2 \cdot D_{act} \cdot \omega_{0,act} & -\omega_{0,act}^2 \\ 0 & 0 & 0 & 0 & 1 & 0 \end{bmatrix} \cdot \begin{bmatrix} \dot{z}_b \\ \dot{z}_w \\ \Delta z_b \\ \Delta z_w \\ \dot{z}_{act} \\ z_{act} \end{bmatrix} + \begin{bmatrix} 0 \\ 0 \\ 0 \\ 0 \\ \omega_{0,act}^2 \\ 0 \end{bmatrix} \cdot z_{act,desired} \qquad \textbf{(3.32)}$$

Through this mathematical representation of the system that is shown in formula 3.32, it is possible to interpret the State-Space controller. With the regulation of the State-Space vector, it is possible to specify a desired behavior to the placement of the eigenvalues of the system matrix.

In MATLAB/Simulink the poles (eigenvalues) of the passive system are calculated. The two poles, which are closest to the imaginary axle, are the most important (dominant) poles for the system since they affect the stability and characteristic of the system most. By generating a new preferred PT_2 behavior, a new favored dynamic system can be achieved. This means the damping ratio and the natural frequency values of the desired structure can be assigned, as shown in the following MATLAB code:

$$Poles_{controlled}(5:6) \ = \ roots[1,2 \cdot D \cdot \omega_0, \omega_0^2]);$$

The poles of the passive and controlled systems are shown in Figure 3.32.

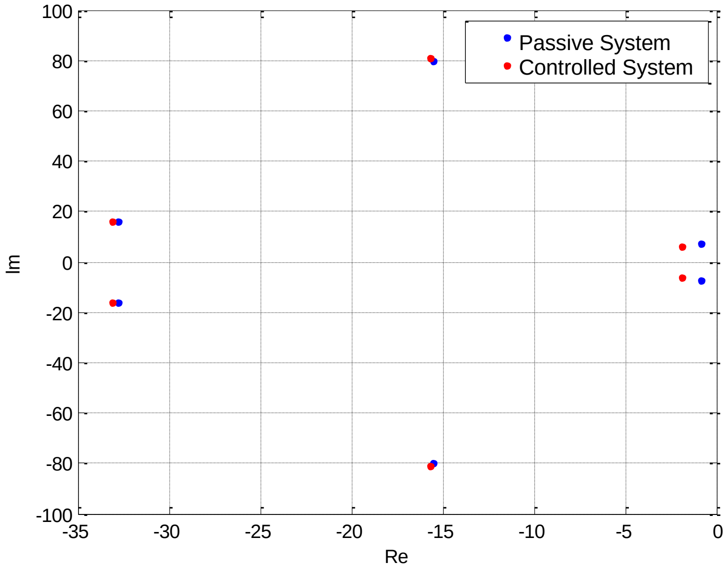

Figure 3.32 : Locations of Poles [35].

Two poles, which are closest to the imaginary axle, are the most important poles for the system because most likely they decide the stability and characteristic of the system.

According to feedback law of control, as shown in formula 3.33, "u" values should be obtained. In order to get "u" values firstly, "K" constants are acquired.

$$u(t) \ = \ -K \cdot x(t) \qquad \textbf{(3.33)}$$

For calculating the required "K" values, A and B matrixes are utilized:

$$\underline{\dot{x}} = (\underline{A} - \underline{B} \cdot \underline{K}) \cdot \underline{x} \qquad \textbf{(3.34)}$$

"$A - B \cdot K$" corresponds to the prescribed eigenvalues as shown in formula 3.35:

$$Poles_{new} = eigs(A - B \cdot K) \qquad \textbf{(3.35)}$$

Then with the Ackermann's correlation, the feedback gain matrix of controller "K" will be calculated in MATLAB via formula 3.36:

$$K = ACKER(A, B, Poles_{new}) \qquad \textbf{(3.36)}$$

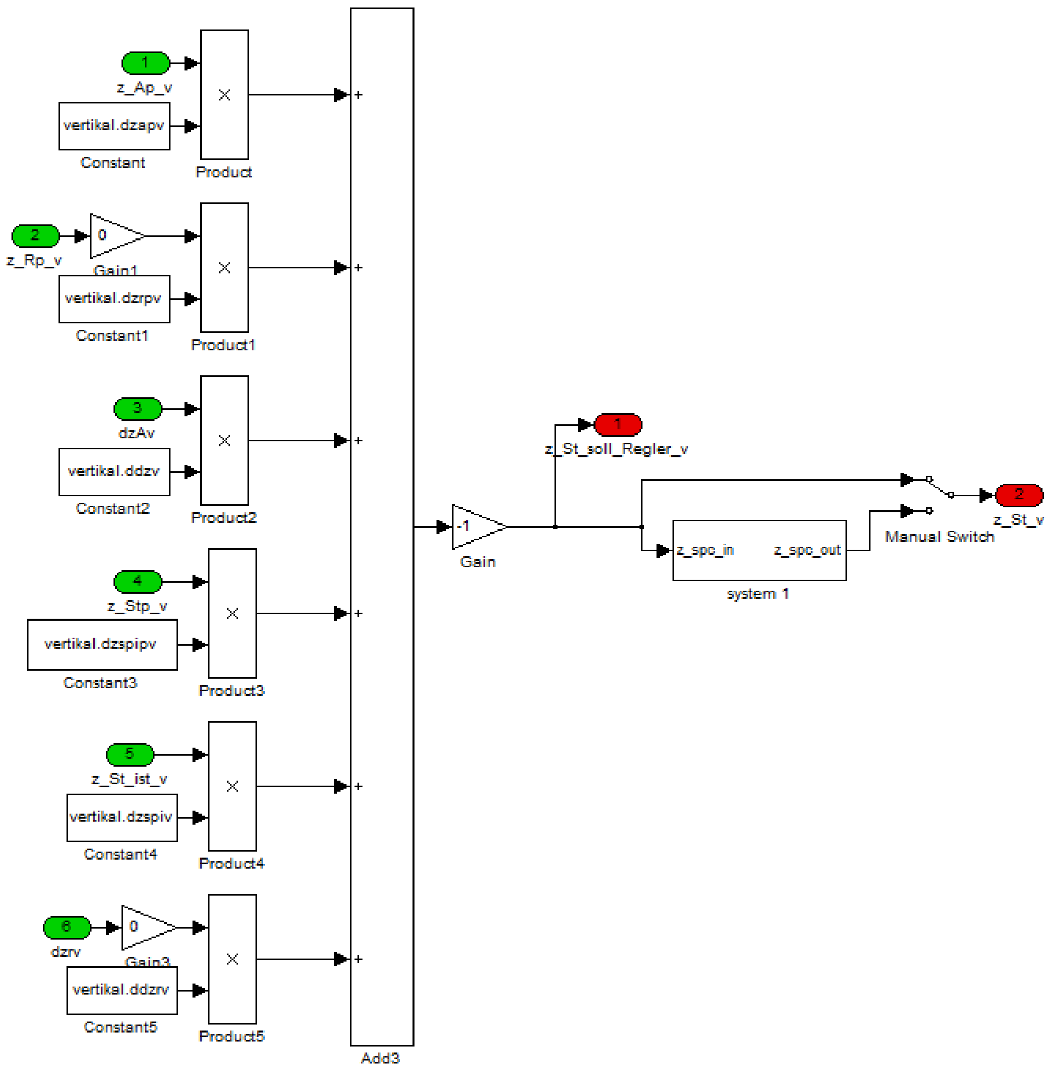

Figure 3.33 : Layout of State-Space controller in Simulink.

After calculating all "K" constants, the six state vectors "x_i" are multiplied with these constants, in order to get "z_{act}" i.e. the actuator motion "u".

This logic is adapted into the Simulink model as shown in Figure 3.33. While calculating the actuator motion with respect to the implemented regulation, it is necessary that only measurable and logical quantities will be in the state vector. For this reason, some assumptions have been made. For example, due to the actuator limits (5 Hz), using "$\dot{z}_w$" and "z_w" (2^{nd} and 6^{th} input in Figure 3.33) values in State-Space controller block is not feasible on account of their high frequencies (frequencies of wheels are generally higher than 5 Hz). Therefore, they are assumed as zero for the control system:

$$z_w = \dot{z}_w = 0 \tag{3.37}$$

3.2.3.1 Combination of Skyhook and State-Space Controller Model

This combination includes two control strategies, as depicted in Figure 3.34.

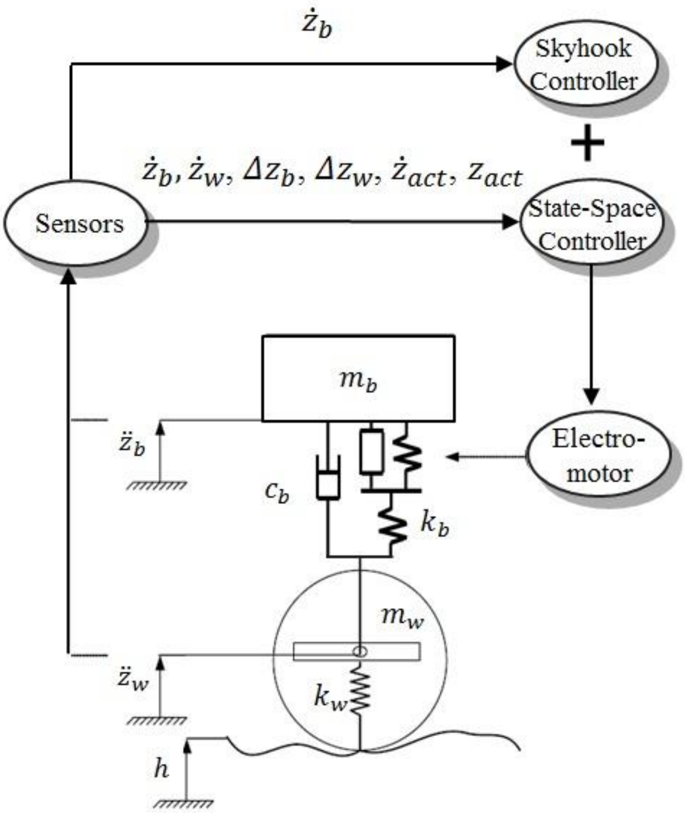

Figure 3.34 : Control sketch of the combined controller [40].

The Skyhook controller obtains the vertical body velocity and computes its own corresponding control value. Simultaneously, the State-Space controller (explained in section 3.2.3) utilizes vertical body and wheel velocities ($\dot{z}_b$, $\dot{z}_w$), suspension and wheel deflections (Δz_b, Δz_w), vertical actuator movement (z_{act}) and vertical actuator velocity ($\dot{z}_{act}$) as inputs and computes its own control value. Once these two control values are computed, the resulting desired z_{act} value will be acquired by adding both together. According to this desired control value, the desired motor torque of the electromotor is calculated by its spindle position controller. Consequently, electromotor triggers the main spring's seat of the body.

This explained control logic is applied to the model as shown in Figure 3.35. The design of the combined controller corresponds to the structure of the State-Space controller, illustrated in Figure 3.33, and to the Skyhook structure in Figure 3.26. After the control values of both control strategies are calculated and added to a new resulting control values, the output is stored in the variable “z_St_soll_Regler”.

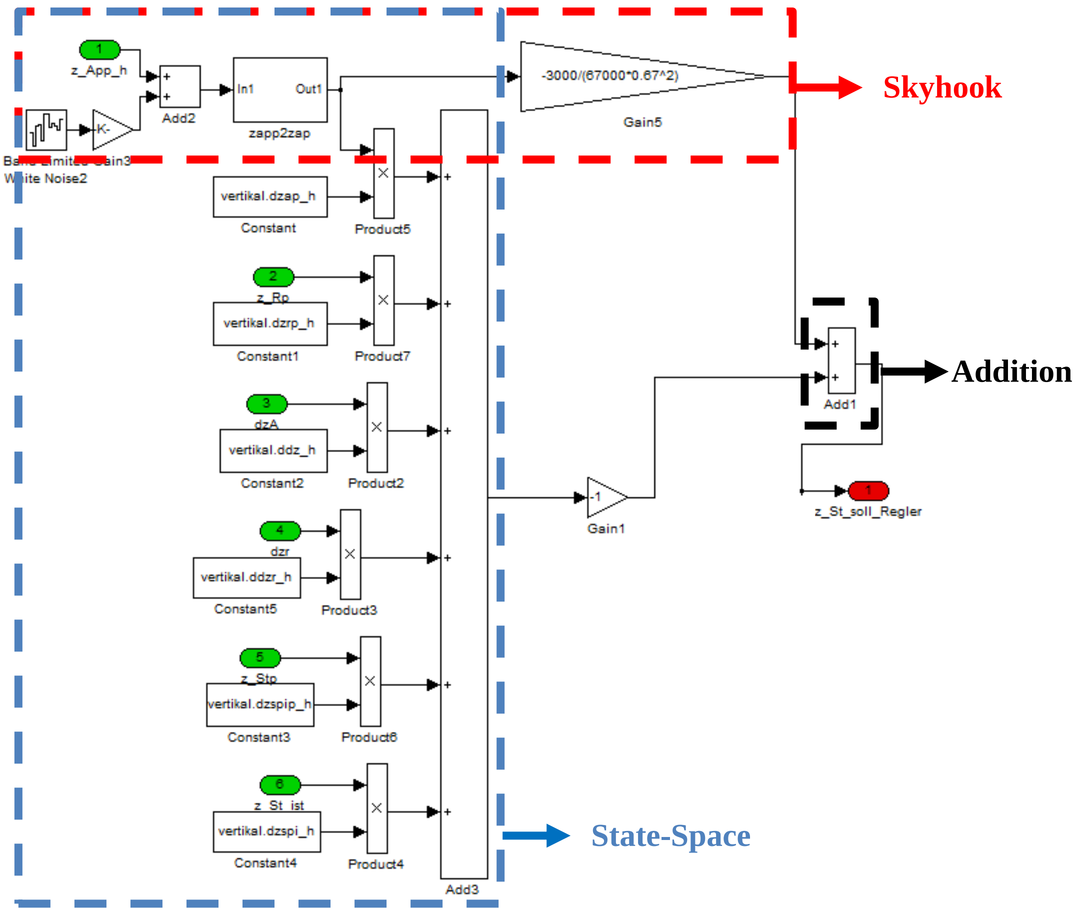

Figure 3.35 : Layout of the combined controller in Simulink.

3.2.4 P-Controller

The P-Controller (Proportional) provides a linear feedback control system in which the output signal is proportional to the input signal (error signal) [36].

The purpose of this thesis is to reduce the vertical body acceleration in order to obtain a better ride comfort. Therefore, the error signal is the difference between the actual and desired acceleration, which is assumed as zero [m/s^2].

During the calculation of control value the formula 3.38 is used:

$$\ddot{z}_{desired} - \ddot{z}_{actual} = e \qquad \textbf{(3.38)}$$

After obtaining this error, the control value is calculated by using formula 3.40 [36]:

$$z_{act} = K_p \cdot e \qquad \textbf{(3.39)}$$

Figure 3.36 illustrates the principle of this P-Controller. Due to the fact that the desired value is zero, the resulting error signal corresponds to the negative actual body acceleration (formula 3.38). The P-Controller multiplies this error with the P-constant (K_p) and transmits the control value to the actuator (electromotor), which generates the related displacement. The new adjusted body acceleration is measured again by the acceleration sensor.

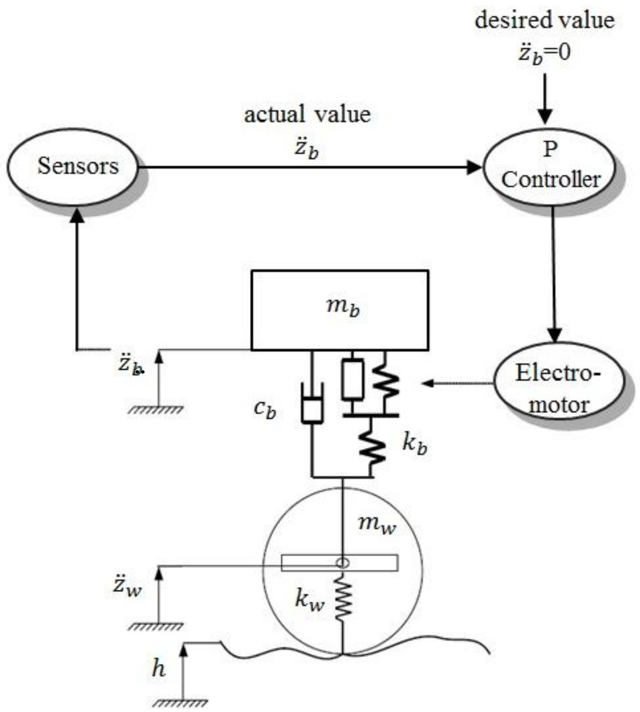

Figure 3.36 : Control sketch of P-Controller for simulations [40].

Figure 3.37 shows the Simulink model of P-Controller. The mentioned "$\ddot{z}_{\mathrm{desired}}$" value is assumed as „0". "z_App" represents the actual vehicle body acceleration and it is multiplied with a negative "K_p" value in order to get "$-\ddot{z}_{actual}$".

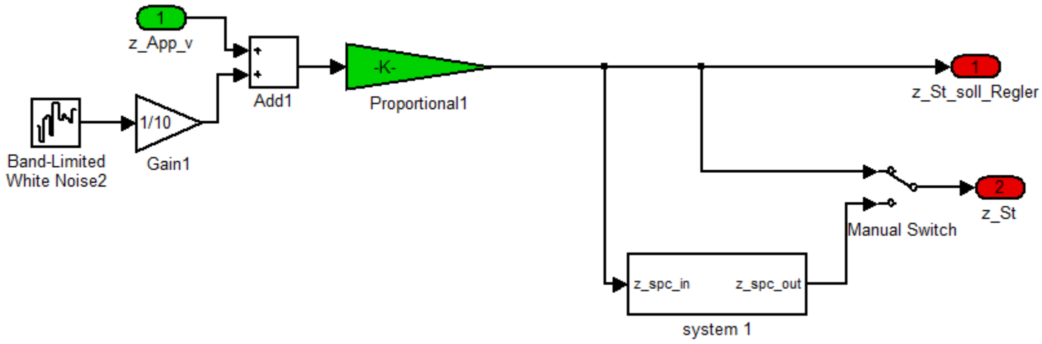

Figure 3.37 : Layout of P-Controller block in Simulink.

4. RESULTS AND DISCUSSIONS

In this section, the simulation and experimental results will be presented. In order to obtain the best ride comfort possible, initially, the best control parameters have been determined for each controller model. Therefore with different control parameters, several simulations were run to understand the reaction logic of the controller and hereby the behavior of the test vehicle. Afterwards, supported by the results of the simulations, the controller strategies are validated in the test vehicle.

These experimental tests have been performed on the Volkswagen AG rough roadway (presented previously on page 46). The controller models (page 47), developed in MATLAB/Simulink were implemented in the test vehicle via dSPACE, an interface to the vehicle's electronic control unit. Furthermore, the obtained signals (Table 4.1) by the sensors of the vehicle were recorded by dSPACE (the test vehicle was already equipped with these sensors).

Table 4.1 : Acquired sensor data of test vehicle

Parameter	Unit
Actual moment of electromotor	Nm
Actual total spring seat motion	m
Desired moment of electromotor	Nm
Desired total spring seat motion	m
Desired spring seat motion against yaw moment	m
Desired spring seat motion for leveling	m
Desired spring seat motion against vertical road roughness	m

Parameter	Unit
Electricity current	A
Longitudinal driving speed	m/s
Spring deflection	m
Wheel velocity	km/h
Vertical body acceleration	m/s^2
Vertical wheel acceleration	m/s^2

Firstly, the results of a common passive suspension system, which represents the basis for all further examinations, will be shown and appraised.

4.1 Passive Suspension System (Simulation and Measurements)

The simulation model of the passive suspension system does not generate any actuator movements and is consequently determined as zero (see Figure 4.1). The simulation shows the expected behavior.

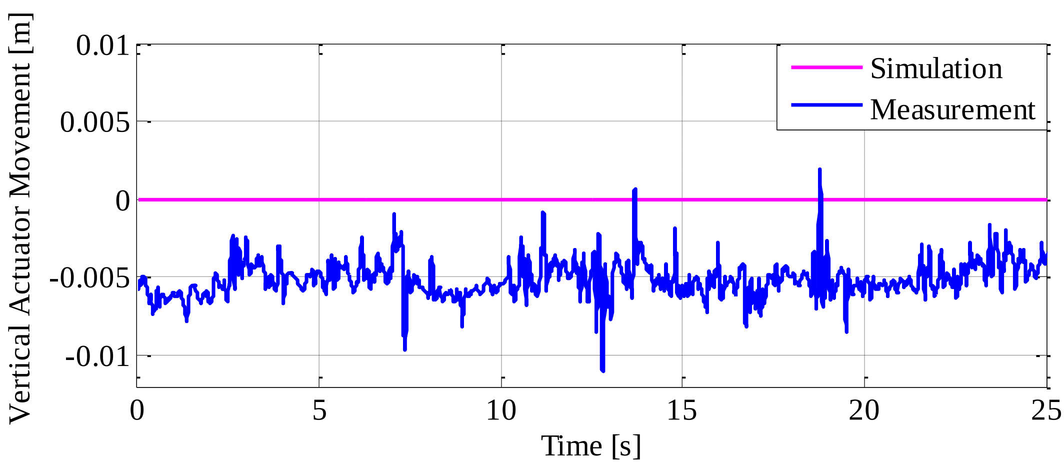

Figure 4.1 : Actuator movements (passive suspension).

In contrast to this, the actual movement of the actuator in the test vehicle shows a deviating behavior due to the following reasons:

- Stochastic movement: Apart from improving the ride comfort on a rough road, there are further objectives, which are provided by additional control strategies. In this case, they are the automatic level and horizontal control. The stochastic movements caused by the horizontal controller are shown by the green curve in Figure 4.2.

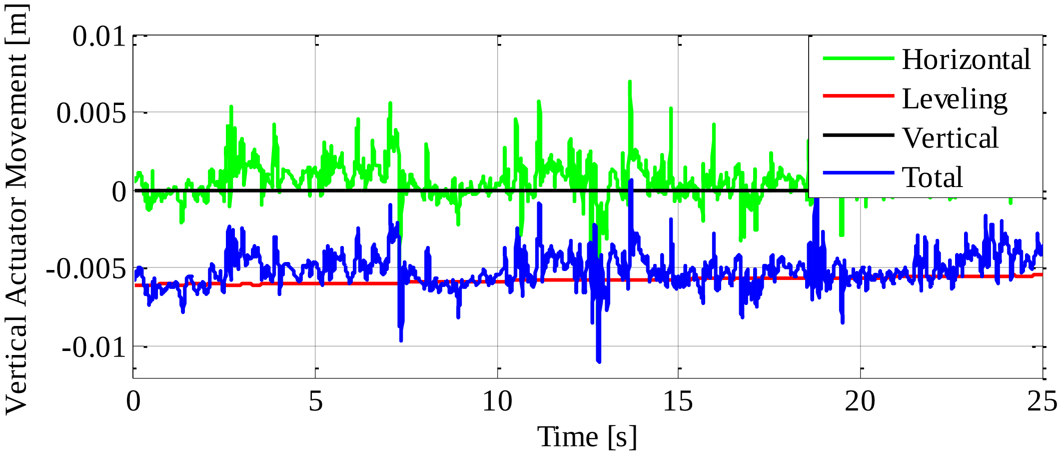

Figure 4.2 : Actual actuator movements (passive suspension).

- Offset: This offset is caused by the leveling control, which ensures the maintenance of a constant ride height (regardless of load condition) causes this offset (5 mm). Disabling these additional controllers is not allowed, because the vehicle can be damaged. As expected, there are no movements caused by the vertical controller as in the simulations.

The resulting body acceleration of the simulated and measured vehicle shows a similar trend as depicted in Figure 4.3. Despite the fact that time plots of the body acceleration are mostly difficult to interpret from the point of view of ride comfort, they are presented in order to understand the impact of the control strategy on the vehicle.

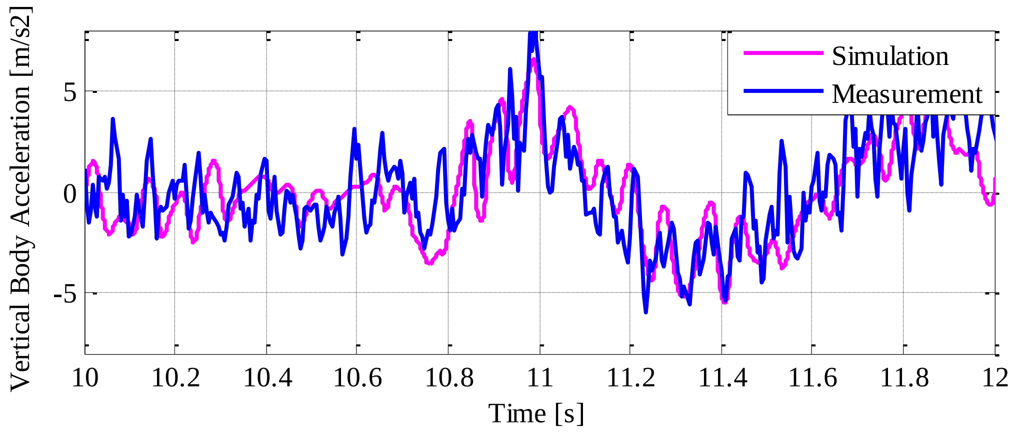

Figure 4.3 : Vertical body accelerations (passive suspension).

A more suitable and objective evaluation of the ride comfort is possible with a PSD diagram (see Figure 4.4). The vehicle characteristics of the simulation are equivalent to a PSD peak point of 1,33 $\frac{m^2}{s^3}$ and those of the measurement to a PSD peak point of 2,34 $\frac{m^2}{s^3}$. (This discrepancy between simulations and measurements, in which different PSD peak points represent the same suspension system, is not relevant for the objective of this thesis as shown in the following sections.)

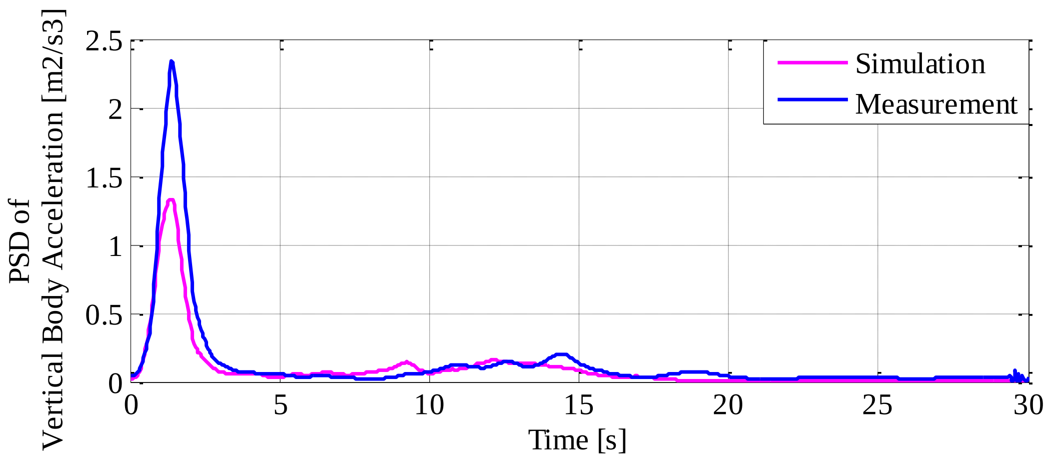

Figure 4.4 : PSD diagrams (simulated passive suspension).

4.2 Skyhook Controller

4.2.1 Simulations

In order to understand the vehicle's diverse responses to the Skyhook controller and its different constants, a loop has been written in MATLAB/Simulink. This loop contains several Skyhook values from '500' to '20000' and it analyses the impact of these values on the vehicles movements.

Figure 4.5 shows the time plot of the desired actuator movement of four exemplary Skyhook constants. A Skyhook constant of '500' generates a minimal actuator movement (see Figure 4.6). By increasing the Skyhook constants to '2000', '10000' or '20000', the desired actuator movement increases proportionally. The Skyhook constant of '20000', for instance, shows a desired actuator movement of more than 20 cm in some situations.

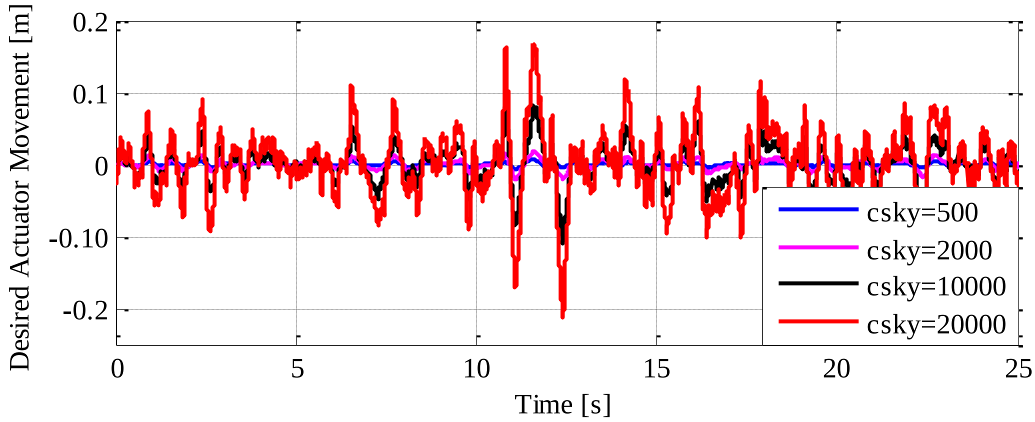

Figure 4.5 : Desired actuator movements (simulated Skyhook controller).

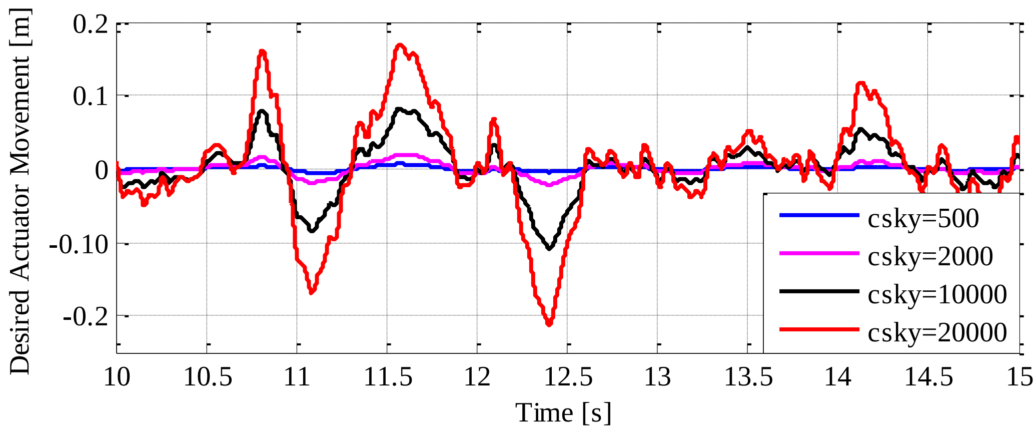

Figure 4.6 : Large-scaled desired actuator movements.

Due to the actuator constraints, the actual actuator movements differ from the desired actuator (see Figure 4.7). Hence, the maximum movement (Skyhook constant '20000') of the actuator is reduced to realistic values of maximum 7 cm.

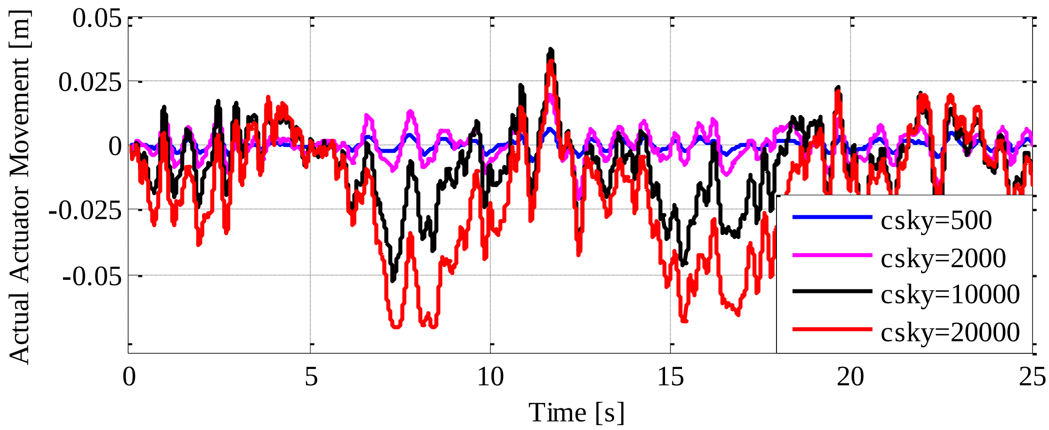

Figure 4.7 : Actual actuator movements (simulated with Skyhook controller).

A section, which displays the general characteristics of the front body acceleration, is displayed in Figure 4.8.

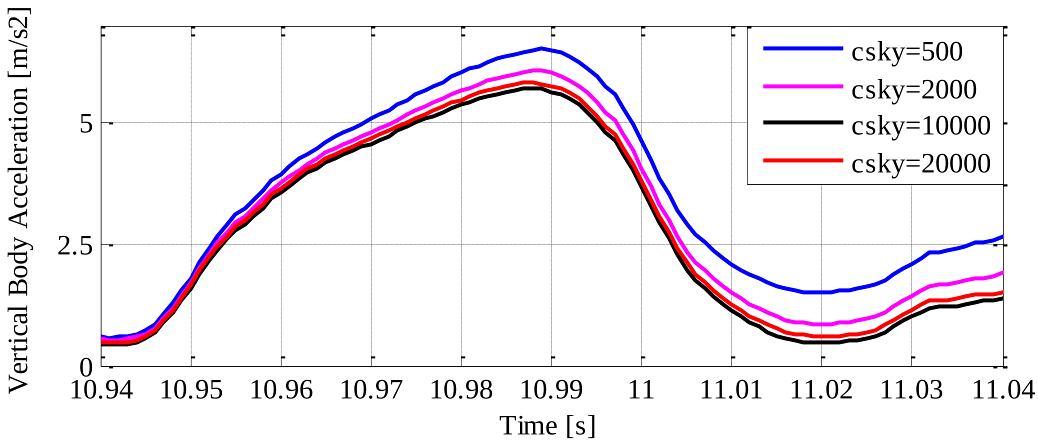

Figure 4.8 : Vertical body accelerations (simulated Skyhook controller).

The Skyhook constant of '500' causes the highest and the Skyhook constant of '10000' causes the lowest front body acceleration. A Skyhook constant of '20000' generates the second best behavior.

The resulting PSD diagrams confirm these characteristics (see Figure 4.9). With a Skyhook constant of '500', the worst ride comfort results are obtained. In this case the peak value of the PSD diagram corresponds with 1,05 $\frac{m^2}{s^3}$. The use of the Skyhook constants '2000' and '10000' illustrates that increasing constants generate minor PSD peaks (0,55 $\frac{m^2}{s^3}$ and 0,35 $\frac{m^2}{s^3}$). On the other hand a Skyhook constant of '20.000' matches a PSD peak of 0,38 $\frac{m^2}{s^3}$.

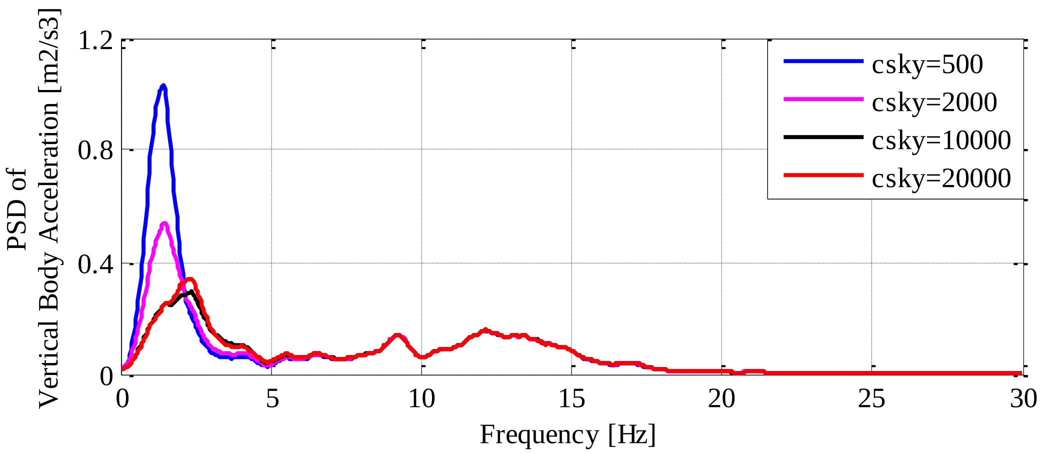

Figure 4.9 : PSD diagrams (simulated Skyhook controller).

Therefore, a loop (as mentioned on page 66) is utilized to obtain the lowest peak value with the Skyhook controller. Figure 4.10 depicts the correlation between the peak points of the PSD diagrams and the Skyhook constants.

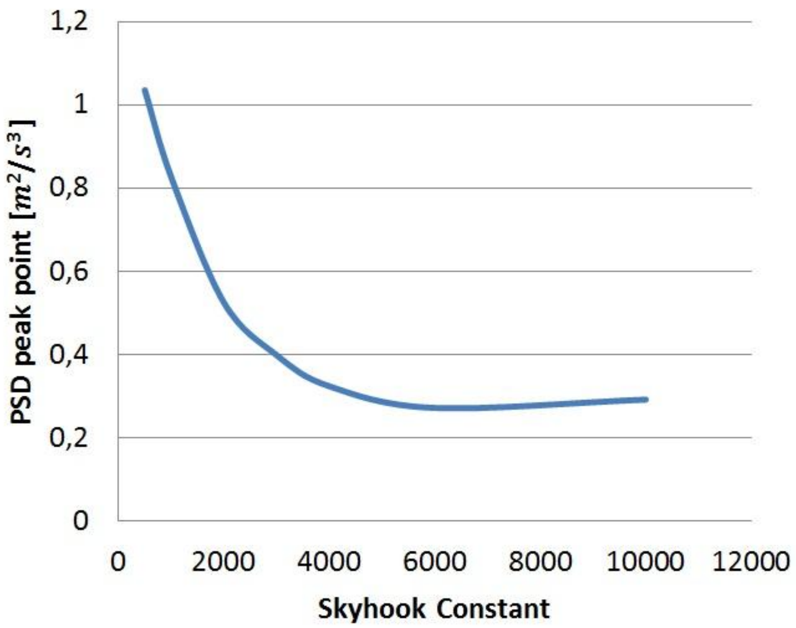

Figure 4.10 : Effect of Skyhook constants on PSD peak points (simulated).

As can be seen the peak points of the PSD diagrams are decreasing up to a value of 0,27 $\frac{m^2}{s^3}$ with a Skyhook constant of ‘6000’. This minimum point illustrates that, regarding ride comfort, boundaries are set to the maximum enlargement of the Skyhook constant. Further increasing of this constant provokes a deterioration of the PSD value.

An analysis of the actuator movements, vertical body acceleration and PSD diagrams leads to the following conclusion:

With a ‘500’ Skyhook constant the actuator moves less than required. In contrast, a Skyhook constant of ‘20000’ forces the system to move more than required. As a result, the vehicle becomes very sensitive to road roughness and reacts strongly, which causes disturbances for the passengers. This reaction points to the fact that there is an optimum constant in a Skyhook model, which needs to be acquired. According to Figure 4.10 it is approximately ‘6000’ in this simulation.

4.2.2 Measurements

Several Skyhook parameters were used in order to identify the optimum constant (as explained in the section above) for the test vehicle. Because of the high electrical consumption of the actuator, the experimental measurements could not have been accomplished with a Skyhook constant of ‘10000’ or higher.

Figure 4.11 and Figure 4.12 shows the resulting actuator movement of some of these experimental tests. The desired and actual actuator movements are similar to the simulated movements in MATLAB/Simulink (Figure 4.6 and Figure 4.7 on page 67): A higher Skyhook constant induces a higher actuator movement.

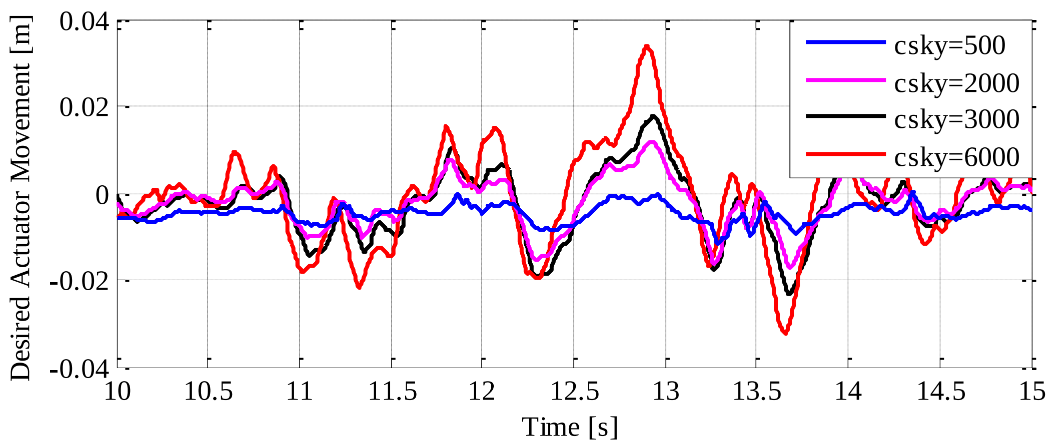

Figure 4.11 : Desired actuator movements (measured Skyhook controller).

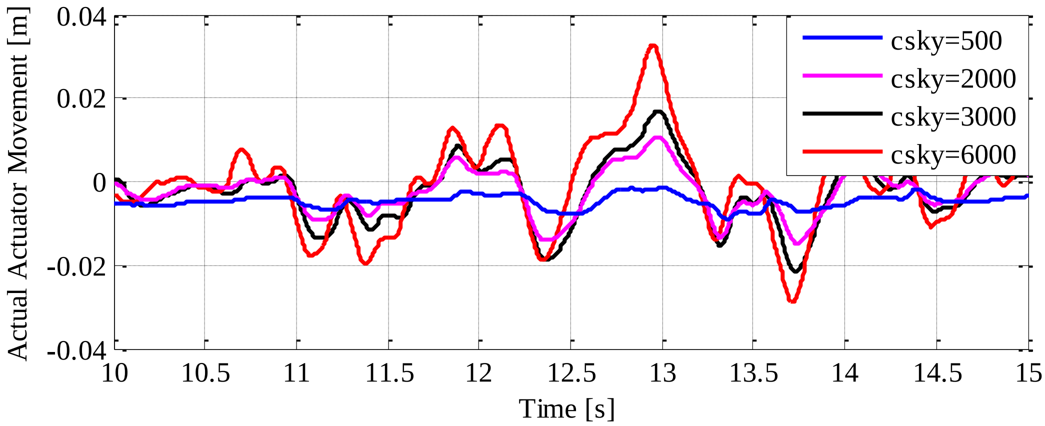

Figure 4.12 : Actual actuator movements (measured Skyhook controller).

With the PSD diagram as displayed in Figure 4.13, an evaluation of these Skyhook values is possible. The use of the Skyhook constant '500' is equivalent to a maximum PSD peak of 1,78 $\frac{m^2}{s^3}$.

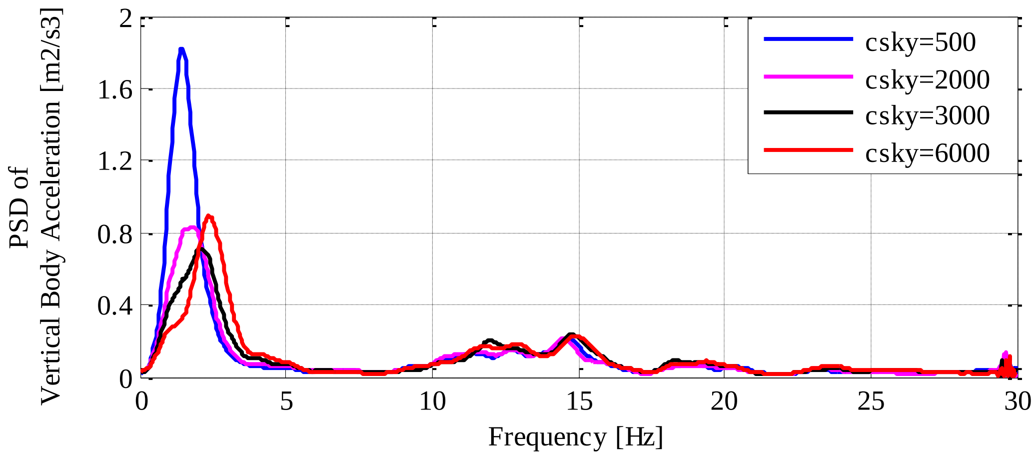

Figure 4.13 : PSD diagrams (measured Skyhook controller).

As expected by the results of the simulation, the PSD value is decreasing with higher values up to 0,69 $\frac{m^2}{s^3}$ when using a Skyhook constants of '3000'. A higher Skyhook constant of '6000' corresponds with 0,83 $\frac{m^2}{s^3}$. This value indicates that the minimum PSD peak has already been reached as shown in Figure 4.14. Based on the shape of the curve, it can be assumed that the optimum Skyhook constant for ride comfort is approximately '3000'. In summary, it can be stated that when using a Skyhook controller this value represents the best ride comfort achievable.

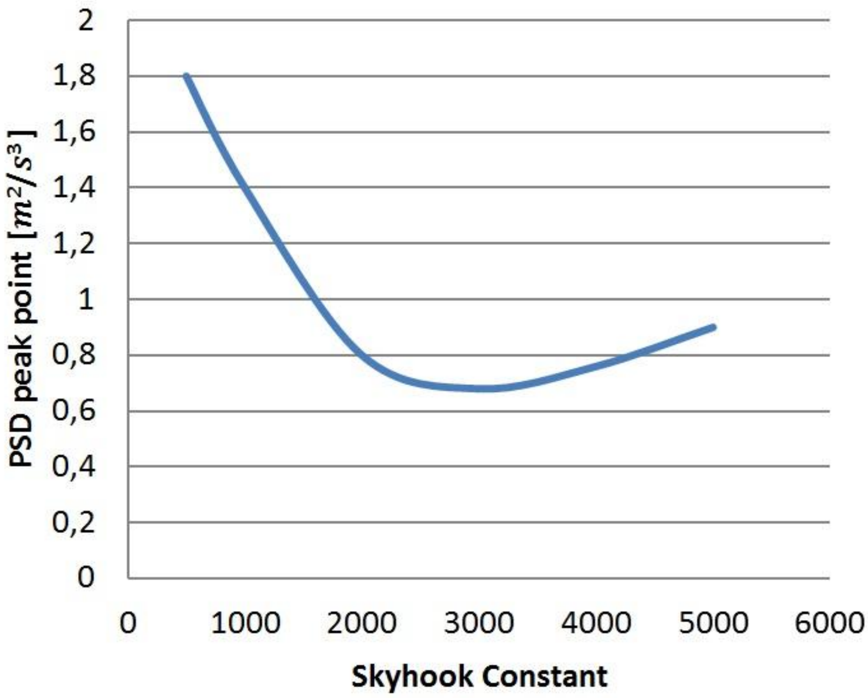

Figure 4.14 : Effect of Skyhook constants on PSD peak points (measured).

4.3 Groundhook Controller

4.3.1 Simulations

As explained in the chapter ‘Controller Models’ (page 47), the Groundhook control strategy is developed in order to get better handling and safety. Using the Groundhook control is in general not appropriate for a better ride comfort. Nevertheless, due to its relation with the Skyhook controller strategy it will be presented in the following. It enables to understand the reactions of the vehicle based on the actuator movements.

As seen on Figure 4.15 and Figure 4.16, a higher control constant triggers a proportionally greater actuator movement. The Groundhook values ’500’, ‘1000’ and ’1500’ correspond to a maximum desired actuator movement of 2,1 cm, 4,2 cm and 6,3 cm. In consequence of the actuator constraints, the actual actuator movements correlate with an absolute maximum of 0,6 cm 1,2 cm and 1,8 cm.

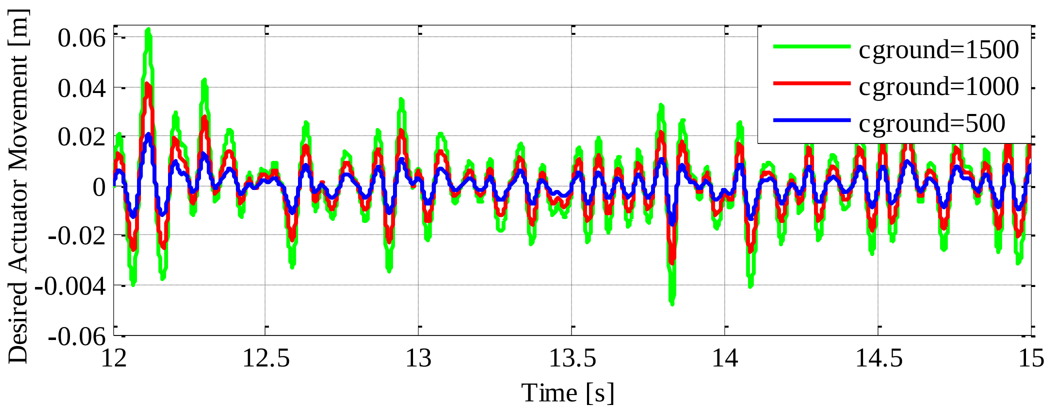

Figure 4.15 : Desired actuator movements (simulated Groundhook controller)

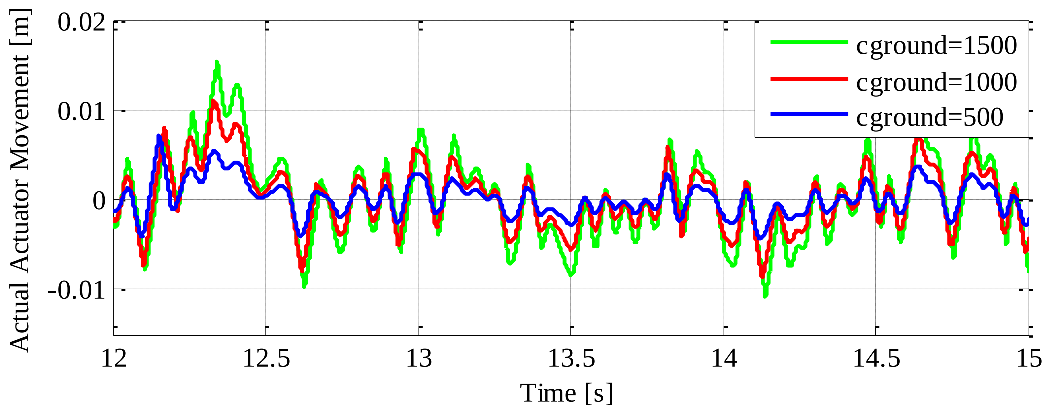

Figure 4.16 : Actual actuator movements (simulated Groundhook controller).

Generally, in the Skyhook controller strategy, a higher constant is equivalent to an enlarged actuator movement and reduced vertical body acceleration.

In contrast to the Skyhook controller strategy, the control variable 'vertical wheel velocity' is used in the Groundhook controller strategy instead of 'vertical vehicle velocity'. Usually wheels fluctuate more than the vehicle body and if bigger control constants are applied in this controller, then greater reactions of the vehicle will be obtained even during small roughness. On account of this, the front body acceleration and thereby the ride comfort is deteriorated as displayed in Figure 4.17.

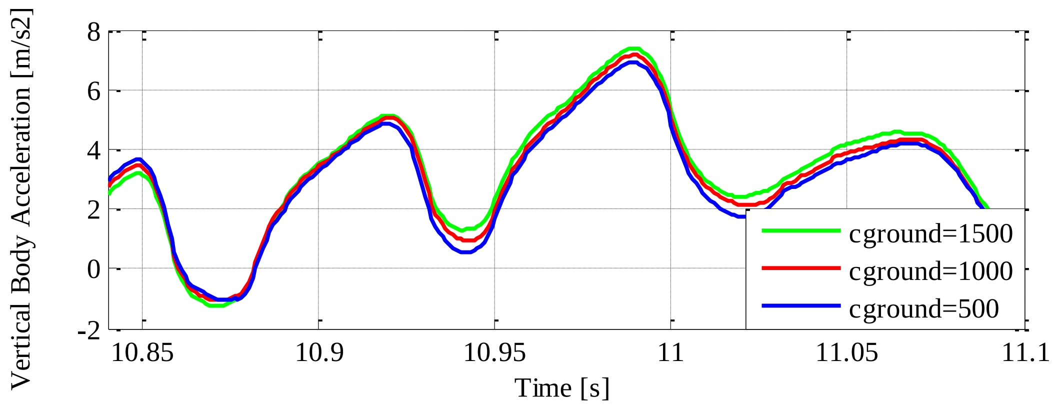

Figure 4.17 : Vertical body accelerations (simulated Groundhook controller)

The graphical illustration of this correlation is shown on the PSD diagram in Figure 4.18. While the lowest value provides the best ride comfort (1,52 $\frac{m^2}{s^3}$) with the Groundhook strategy, the biggest constant causes the worst result (2,23 $\frac{m^2}{s^3}$).

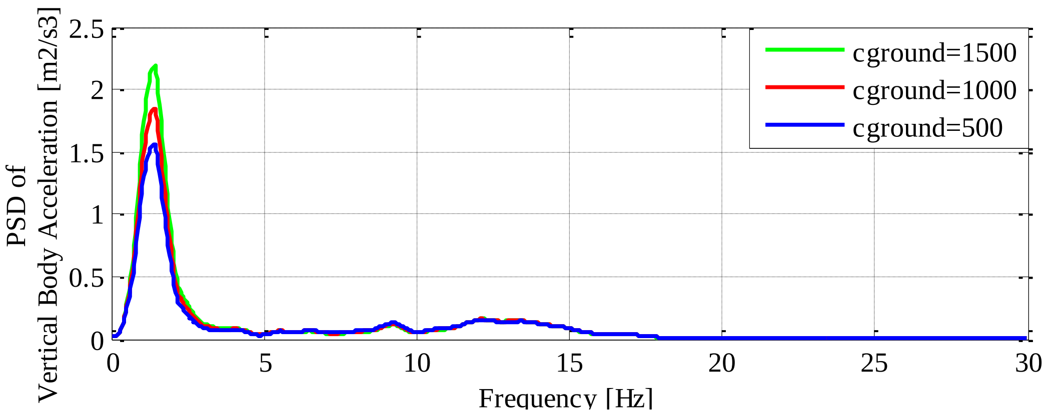

Figure 4.18 : PSD diagrams (simulated Groundhook controller).

After examining the desired and actual actuator movements in a simulated system, the experimental tests have been made with these control values as shown in the following section.

4.3.2 Measurements

The actuator movement results of the tests confirm the simulated results (see Figure 4.19): A high Groundhook constant leads to a bigger movement of the actuator. On account of the actuator constraints the actual movements are smaller than the desired ones (see Figure 4.20).

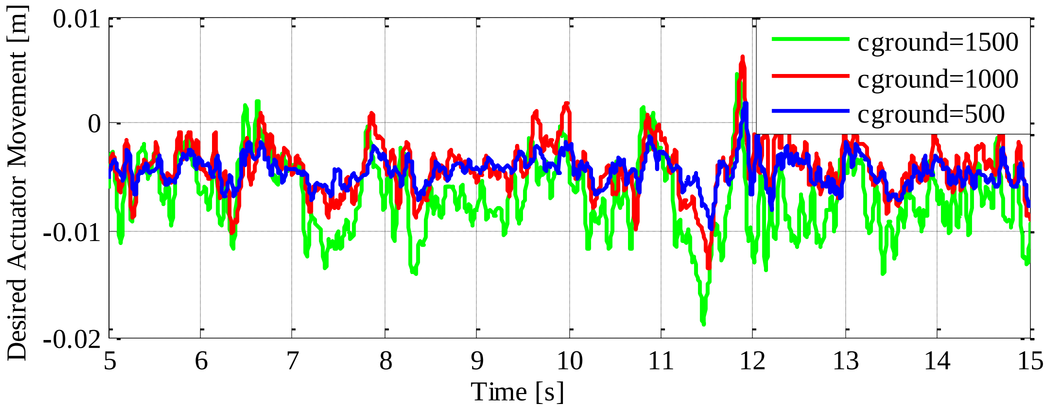

Figure 4.19 : Desired actuator movements (measured Groundhook controller)

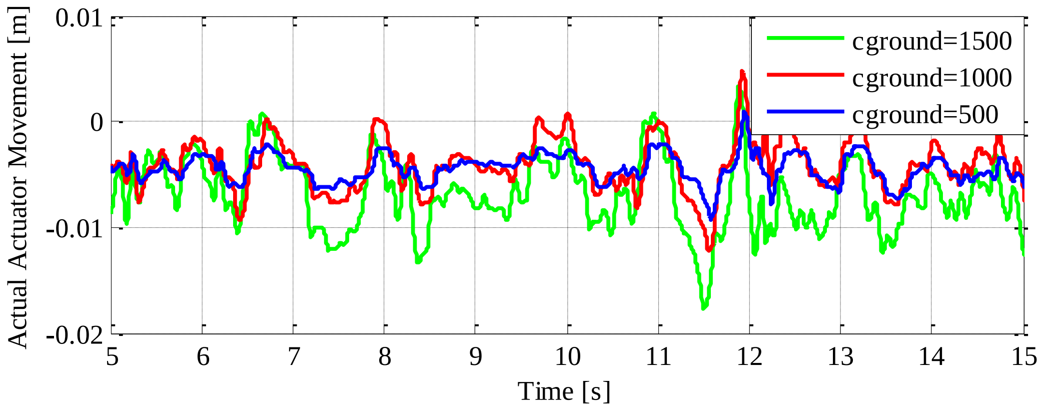

Figure 4.20 : Actual actuator movements (measured Groundhook controller).

As one would expect according to the simulation, a bigger movement of the actuator, evoked by the 'vertical wheel velocity', effects the ride comfort negatively (see Figure 4.21). The Groundhook constant of '500' corresponds with a maximum PSD value of 2,78 $\frac{m^2}{s^3}$ and a constant of '1500' causes a maximum PSD value of 4,01 $\frac{m^2}{s^3}$.

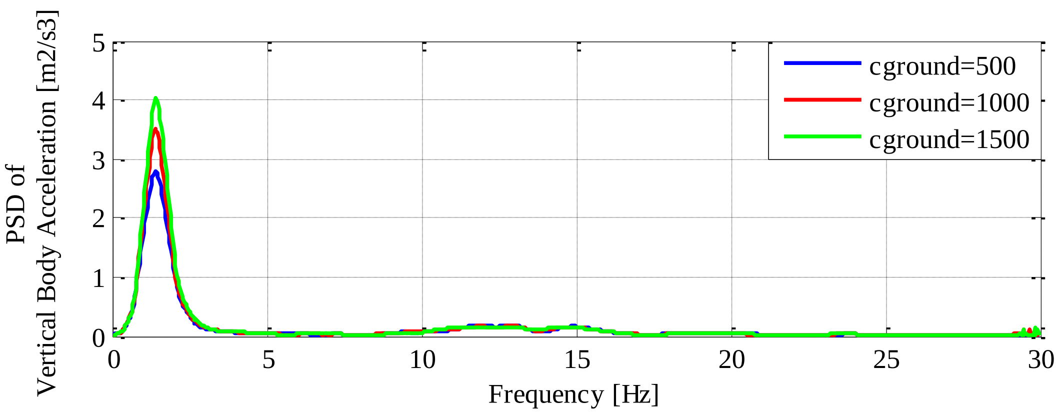

Figure 4.21 : PSD diagrams (measured Groundhook controller).

In contrary to the Skyhook controller strategy, a higher controller value disturbs the system intensified. For this reason, the best constant for ride comfort in this controller strategy is obtained with the lowest value.

4.3.3 Comparing measurements of Groundhook and Skyhook

In the following, the best Skyhook value (from tests=3000) and the two extreme Groundhook controller constants (500 and 1500) are compared in a PSD diagram of vertical body acceleration for ride comfort (Figure 4.22) and in a PSD diagram of vertical wheel acceleration for safety (see Figure 4.23).

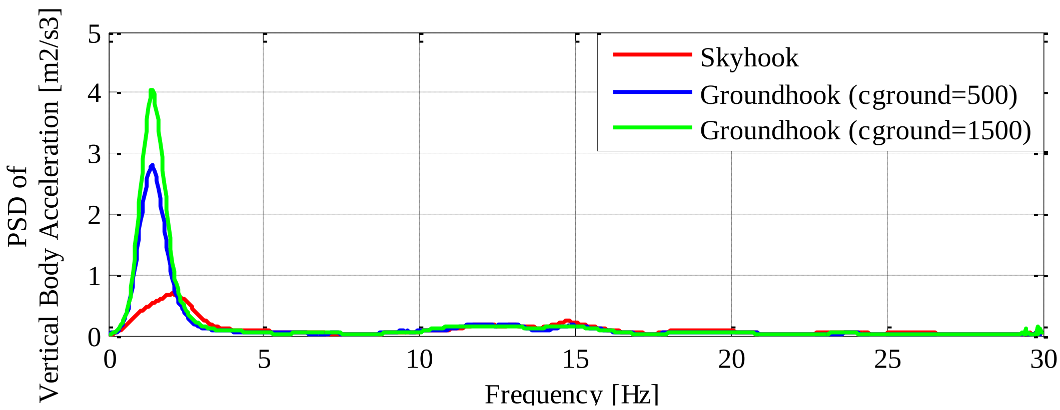

Figure 4.22 : PSD diagrams of measured Groundhook and Skyhook controllers.

As illustrated in Figure 4.23, the Groundhook control strategy is suitable to enhance the handling safety of the test vehicle: The small PSD values, which are in the diagram between approximately 13 Hz – 16 Hz imply that the wheel fluctuations are smaller in general and hereby, a better contact is given to the road surface. In summary, it can be said that the lowest control value (500) provides the best safety and at the same time, the best ride comfort.

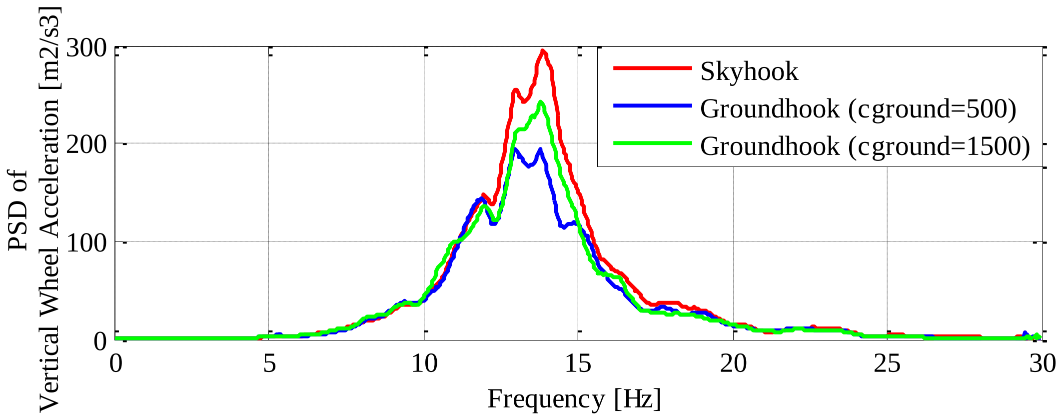

Figure 4.23 : PSD diagrams of wheel accelerations (measurements).

4.4 State-Space Controller

4.4.1 Simulations

For a better understanding of a State-Space controller, several simulations are made with different control parameters. In this section, three exemplary pairs of values are presented:

1. f = 0,3 Hz and D = 1,5
2. f = 1,0 Hz and D = 0,3
3. f = 1,3 Hz and D = 0,3

Figure 4.24 and Figure 4.25 displays the desired and the actual actuator movements (due to the actuator constraints) in consequence of these control parameters. The operating principle of a State-Space controller is more complex than the operating principle of a Skyhook or Groundhook controller. Due to this fact, there is no direct identifiable correlation between these values and the actuators motions.

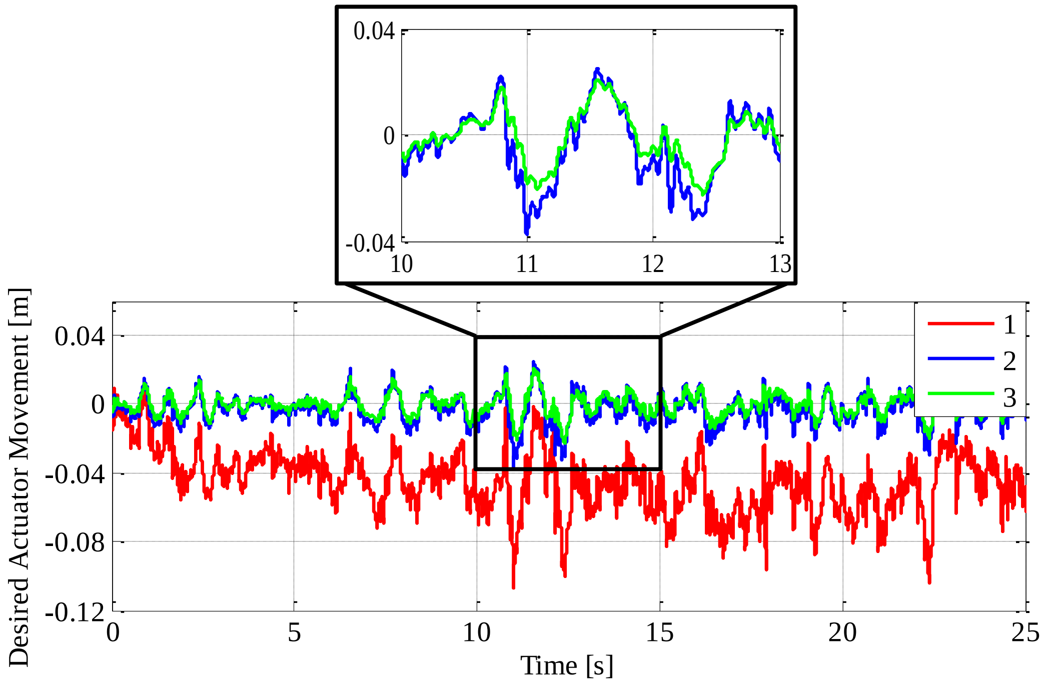

Figure 4.24 : Desired actuator movements (simulated State-Space controller).

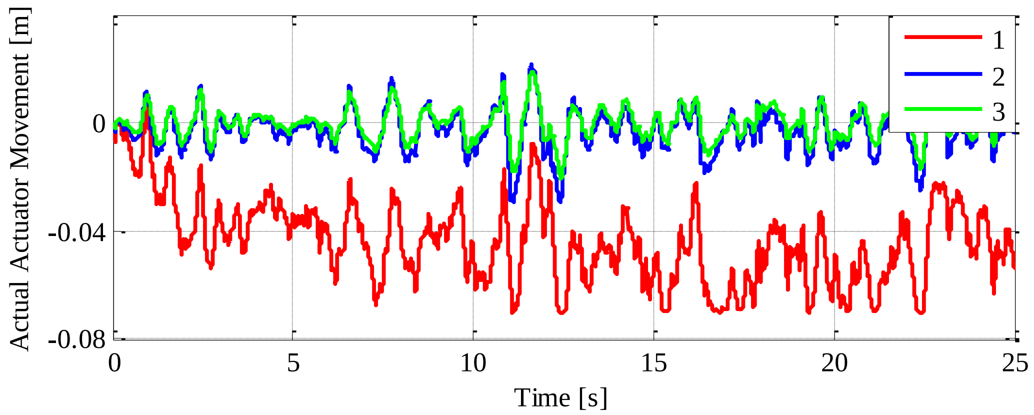

Figure 4.25 : Actual actuator movements (simulated State-Space controller).

For a better understanding of State-Space controllers, it is necessary to compare the poles of these three modified systems with the poles of the passive system as shown in Figure 4.26.

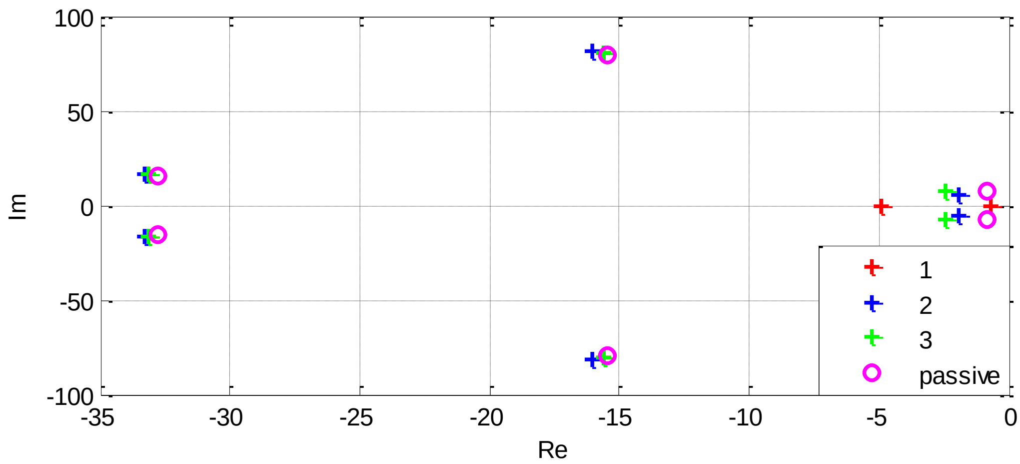

Figure 4.26 : Location of Poles (simulated State-Space controller).

Basically, the poles near by the imaginary axis effect the movement of the vehicle body the most. By predetermining these values, the vehicle is forced into a new motion by the actuator and its controller settings. Hence, the actuator movements in Figure 4.24 correspond to the intended pole positions and consequently the new modified system.

For instance, the third option (f=1,3 Hz and D = 0,3) generates a lower actuator movement than the second controller option (f = 1,0 Hz and D = 0,3) (see Figure 4.24). That implies that the new poles and hereby the adjusted behavior of the third system are easier to accomplish.

Another interesting issue is the displayed actuator movement induced by the first pair of values (f = 0,3 Hz and D = 1,5), in which the actuator seems to remain at a value around -5 cm (Figure 4.24 or Figure 4.25). There are two reasons of this behavior:

- The initial vertical position: During the test, the roadway input starts at a positive value of the vertical road roughness as shown in Figure 4.27. As a result, the actuator moves towards the displayed position (Figure 4.24).
- The extreme damping ratio of 1,5 (Figure 2.17 on page 25), which causes a very slow reaction.

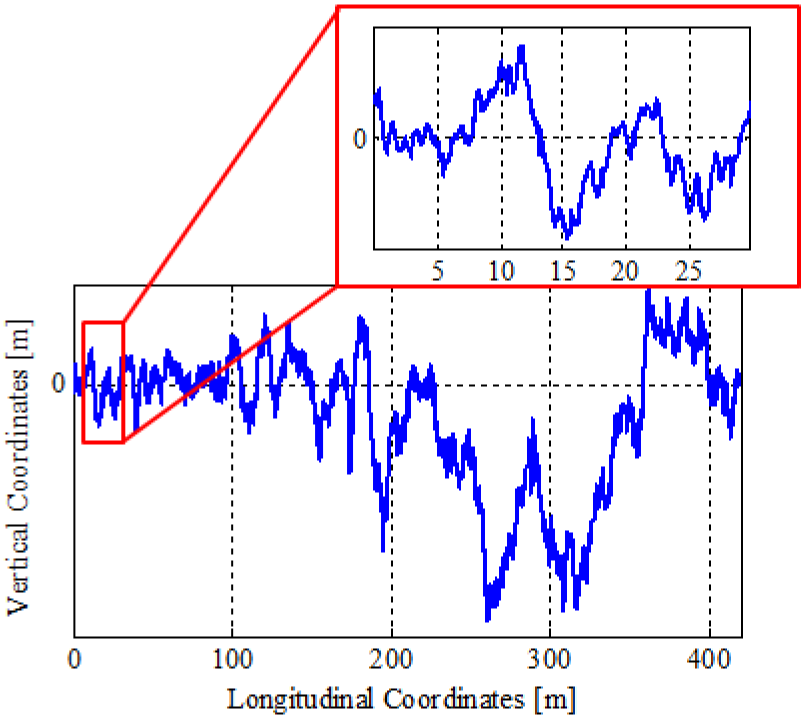

Figure 4.27 : Roadway input (simulated State-Space controller).

An analysis of the examined constants is only achievable by evaluating the PSD diagrams (see Figure 4.28). The peak points in a PSD diagram of the three value of pairs correspond with 0,17 $\frac{m^2}{s^3}$, 0,38 $\frac{m^2}{s^3}$ and 0,55 $\frac{m^2}{s^3}$.

These examined constants illustrate, that even basically similar values may have a great impact on the controller and hereby on the vehicle movement. Furthermore, the circumstance of two variables (D and f) complicates the process to gain the optimum variables for best ride comfort.

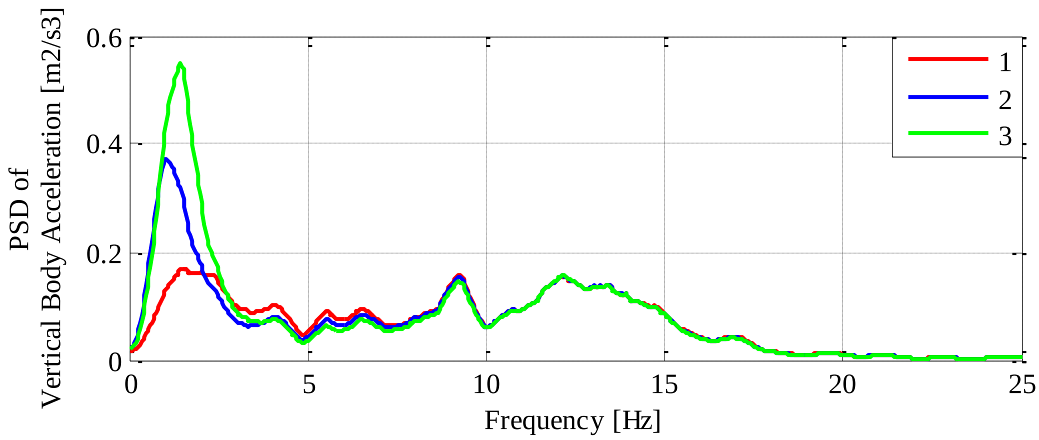

Figure 4.28 : PSD diagrams (simulated State-Space controller).

On account of the reasons mentioned on page 78, the controller settings of the first option (f = 0,3 Hz and D = 1,5) cannot be considered. Therefore, in summary, it can be stated that the constants f = 0,3 Hz and D = 1,0 generate the lowest body acceleration (0,38 $\frac{m^2}{s^3}$) which can be achieved with a State-Space controller in this simulation.

4.4.2 Measurements

The information gained by the simulation need to be verified as before by the test vehicle, whereby the examined pairs of values correspond with the simulation parameters (see page 77). As depicted in the previous section, an evaluation of the actuator's motions is unrewarding. However, for the sake of completeness both figures are shown. Figure 4.29 and Figure 4.30 delineates the offset of the actuator position due to the controllers slowness (damping ratio of 1,5) and the initial roadway input (first option).

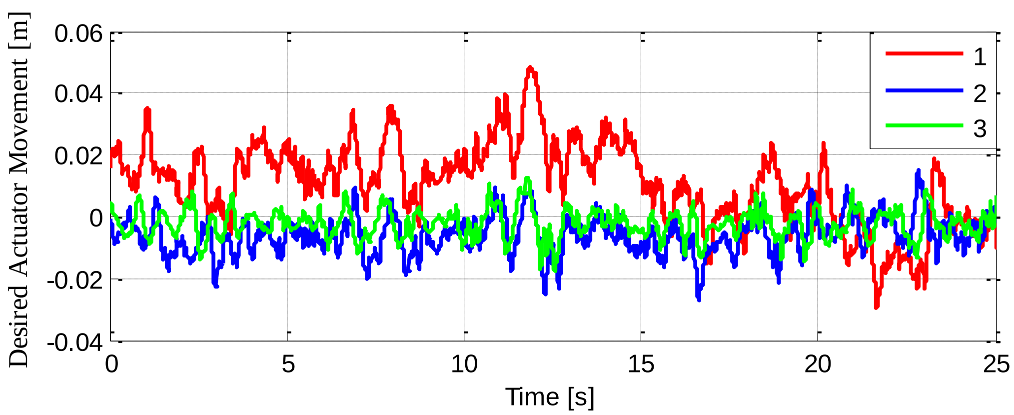

Figure 4.29 : Desired actuator movement (measured State-Space controller).

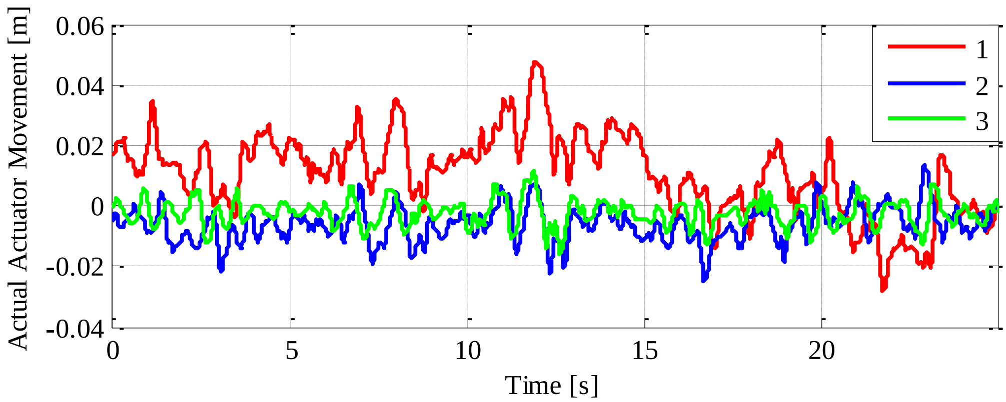

Figure 4.30 : Actual actuator movement (measured State-Space controller).

The evaluation of the PSD diagrams clarifies the impact of the three different pairs of values on the ride comfort (see Figure 4.31). The peak points in a PSD diagram of the four value of pairs correspond with 0,57 $\frac{m^2}{s^3}$, 0,66 $\frac{m^2}{s^3}$ and 0,81 $\frac{m^2}{s^3}$.

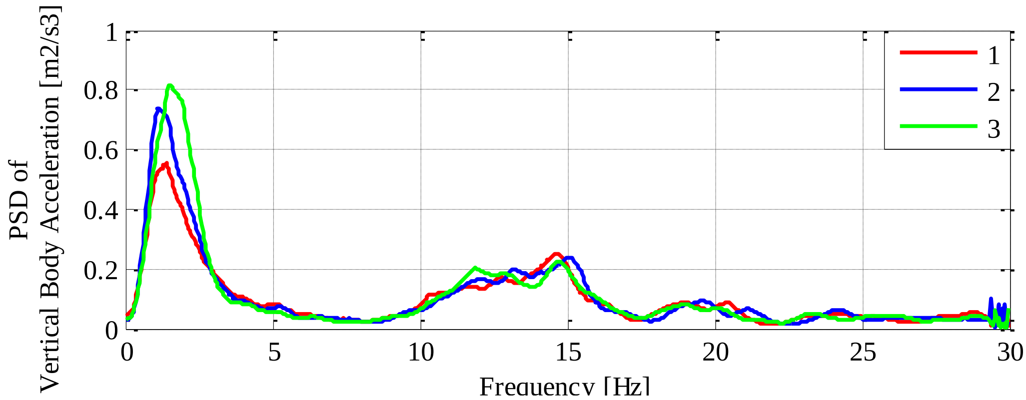

Figure 4.31 : PSD diagrams (measured State-Space controller).

On the basis of these results, it can be concluded that the constants f = 1,0 Hz and D = 0,3 provide the best ride comfort (0,66 $\frac{m^2}{s^3}$) which could be gained by the State-Space controller in the test vehicle.

4.5 P-Controller

4.5.1 Simulations

As explained in the section ‘Controller Models’ (see page 47) the main target of the P-Controller is to eliminate or minimize the vertical body acceleration itself.

The predictable proportionality between the P-constants and the desired actuator motions is illustrated in Figure 4.32. The P-constant of “500” generates an actuator movement, which is five times enlarged than the movement of the P-constant “100”.

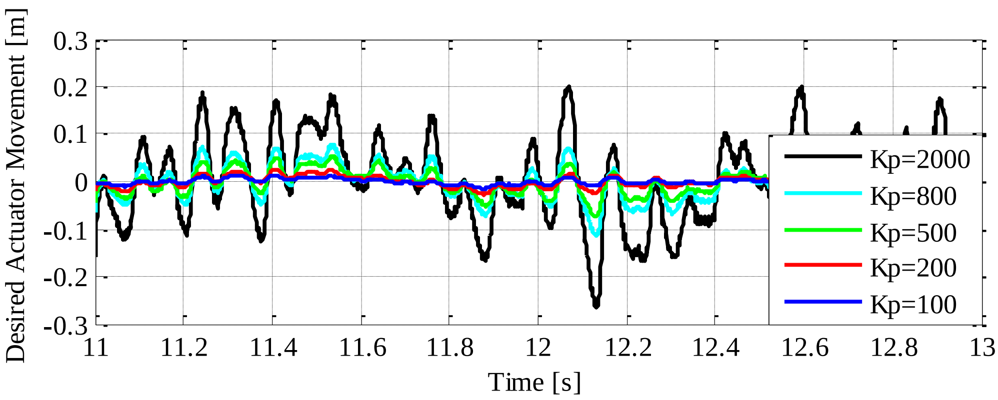

Figure 4.32 : Desired actuator movement (simulated P-Controller).

The actual actuator motions show similar characteristics as well (see Figure 4.33). However, what attracts attention, are the higher P-constants. Because of the actuator constraints, these constants cannot provide the desired proportional reaction motions. Furthermore, the smooth movement seems to turn into a rather restless movement with increasing constants: With a constant of ‘2000’, the actuator is permanently in motion with its maximum speed.

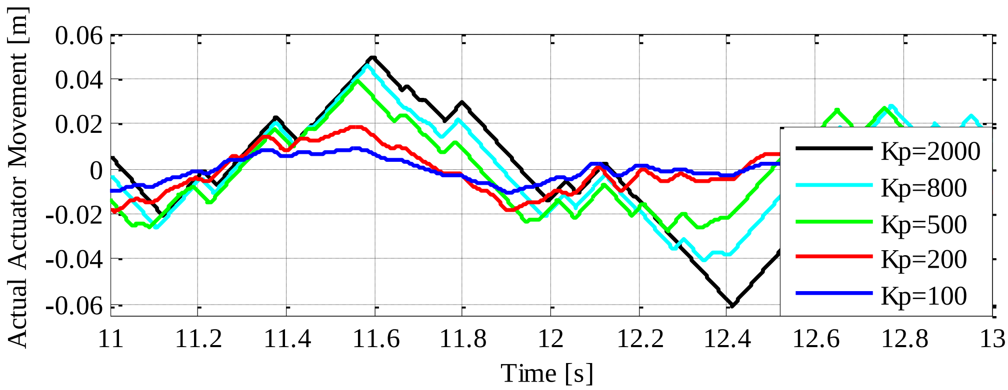

Figure 4.33 : Actual actuator movement (simulated P-Controller).

The PSD diagram, shown in Figure 4.34, supports this correlation. A P-constant of ‘100’ is equivalent to a PSD peak point of 1,12 $\frac{m^2}{s^3}$ and a greater P-constant, for instance “200”, generates a lower PSD peak point of 0,98 $\frac{m^2}{s^3}$. A surprisingly low PSD peak point (0,17 $\frac{m^2}{s^3}$) is provided by the greatest P- constant (2000).

This remarkable result will be further investigated in the next section, which deals with the application of this controller in the test vehicle.

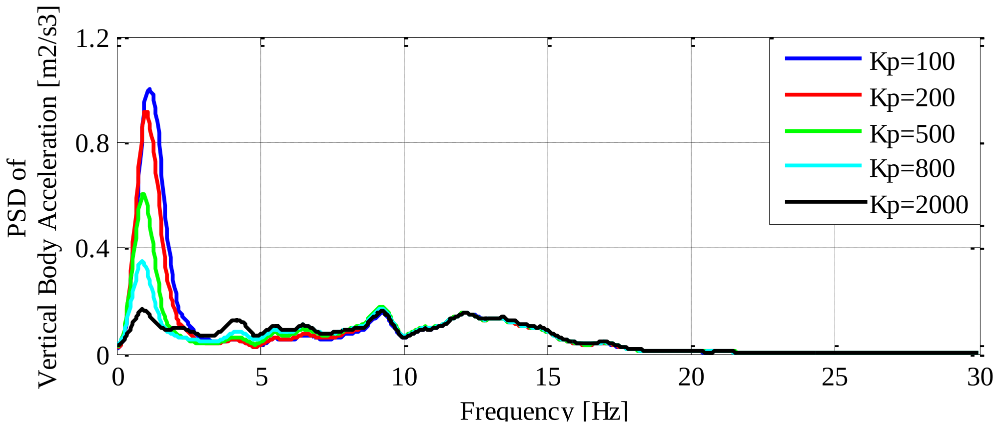

Figure 4.34 : PSD diagrams (simulated P-Controller).

4.5.2 Measurements

Figure 4.35 and Figure 4.36 show the actuator movement in consequence of the P-constants '100' and '200'. Unfortunately, the examination of higher values needed to be aborted due to the high electrical consumption, which has become excessive while testing. However, the motions of the actuator correspond with the simulated system: An increased P-constant generates an enlarged actuator movement.

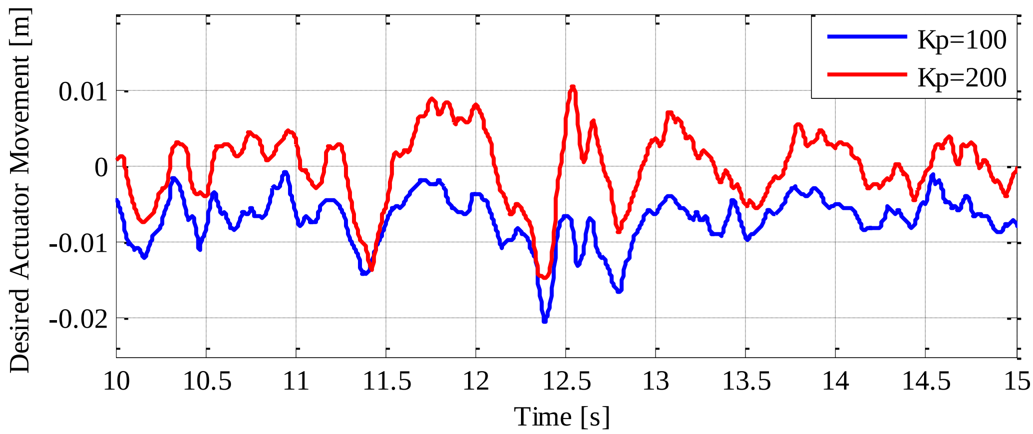

Figure 4.35 : Desired actuator movements (measured P-Controller).

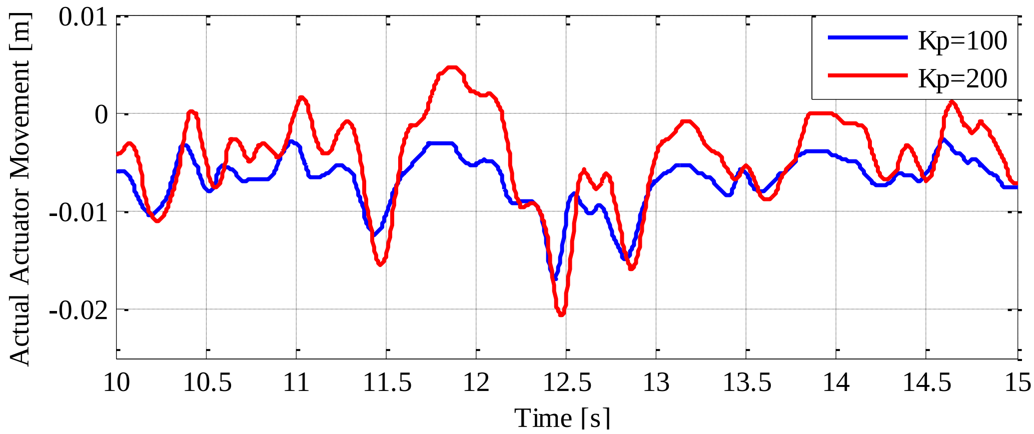

Figure 4.36 : Actual actuator movements (measured P-Controller).

Furthermore, the simulation's results are valid for the interpretation of the vertical body acceleration's PSD's, as illustrated in Figure 4.37. The P-constants of "100" and "200" correspond with a PSD peak value of 1,34 $\frac{m^2}{s^3}$ and 0,95 $\frac{m^2}{s^3}$. As a result of the higher P-constant, the vertical body acceleration decreases.

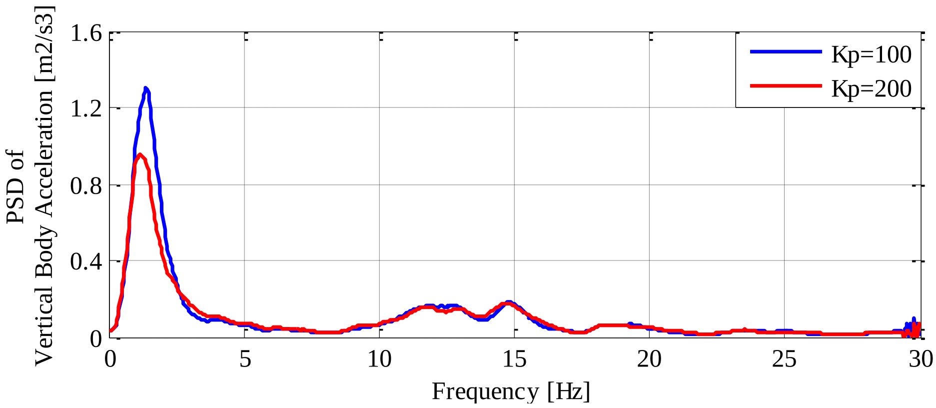

Figure 4.37 : PSD diagrams (measured P-Controller).

Summarizing the above, it can be said that a simple P-Controller, which is minimizing the vertical body acceleration itself, shows interesting potential: The higher the P-constant, the better the provided ride comfort. However, the very good results gained by the simulation could not be verified with the test vehicle. The best parameter, which could be obtained for this controller model, is thereby '200'.

4.6 Combination of Skyhook and State–Space Controller

4.6.1 Simulations

In order to achieve further improvements, additional controller models need to be examined. Another option is a combination of different control strategies, as shown in this section. A new combined controller model will be presented, which uses a rather uncomplicated approach. So far, the best ride comfort in this thesis for the test vehicle could be achieved by the State-Space controller (f = 1,0 Hz and D = 0,3) as depicted in Figure 4.31. The second behavior was generated by the Skyhook controller (with c_{sky}=3000). Consequently, State-Space and Skyhook controller have been combined in order to achieve a better ride comfort.

The controller models calculate their desired actuator movements independently and afterwards resulting values are added as detailed in the 'Controller Models' section (page 58). The consequence of this is an enhanced actuator motion as illustrated in

Figure 4.38 and Figure 4.39. Another fact worth mentioning is the similarity between desired and actual movement. It indicates that the calculated motions are within the limits of the actuator's constraints: They can be generated in the required form.

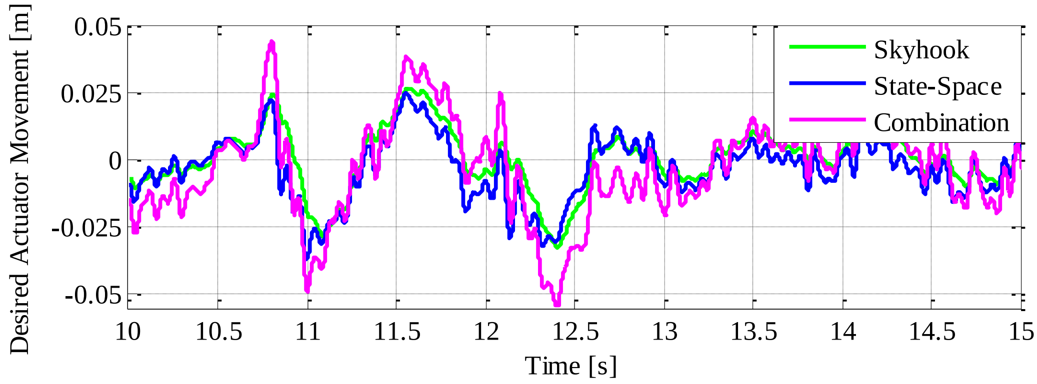

Figure 4.38 : Desired actuator movements (simulated combined controller).

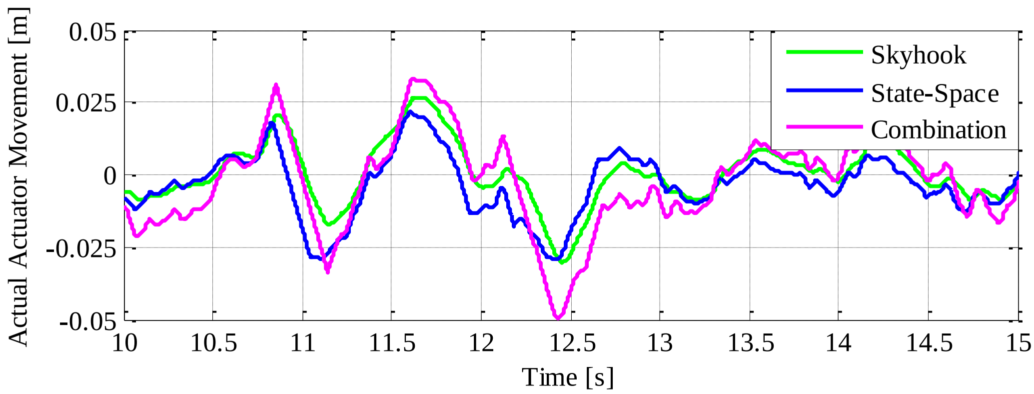

Figure 4.39 : Actual actuator movements (simulated combined controller).

The analysis of the PSD diagram shows, that the positive effect of this new combined controller on the ride comfort is unexpectedly high in comparison to the other controllers (see Figure 4.40). The maximum peak point in the PSD diagram of the combination of Skyhook (c_{sky}=3000) & State-Space (f=1 Hz, D=0,3) equals 0,18 $\frac{m^2}{s^3}$.

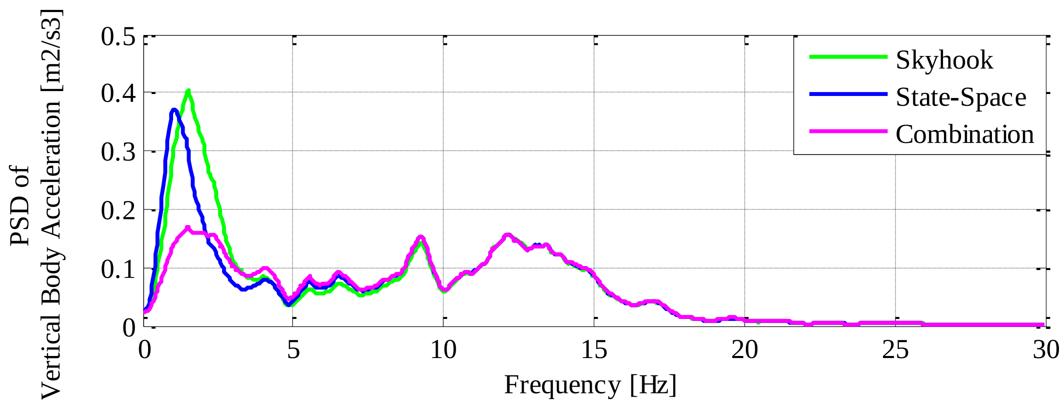

Figure 4.40 : PSD diagrams (simulated combined controller).

4.6.2 Measurements

The time plots of the actuator show the expected behavior: The combined model generates the maximum movement not only in the simulations but as well in the tests. Moreover, desired and actual movements shown in Figure 4.41 and Figure 4.42 are very similar.

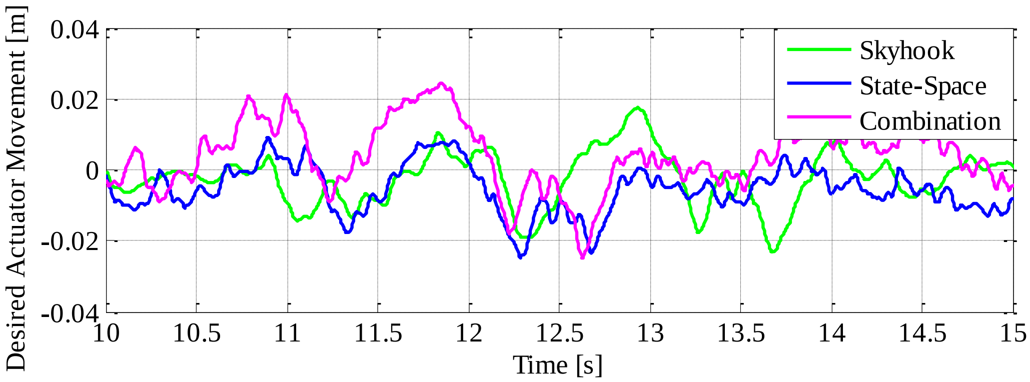

Figure 4.41 : Desired actuator movement (measured combined controller).

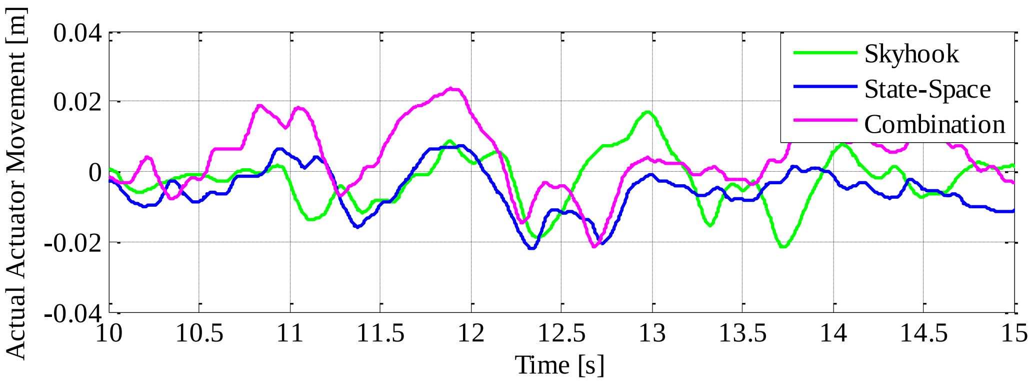

Figure 4.42 : Actual actuator movement (measured combined controller).

The performance of this controller model is remarkable, as illustrated in Figure 4.43.

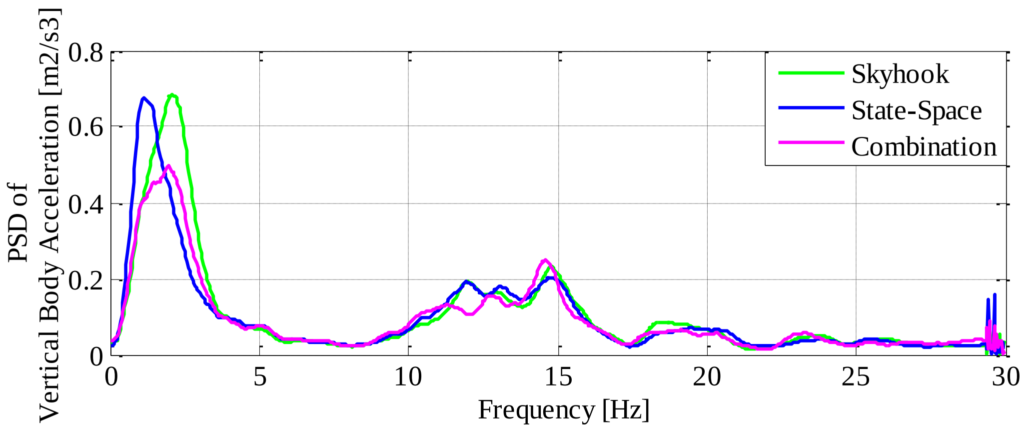

Figure 4.43 : PSD diagram (measured combined controller).

Another notable fact is the subjective improvement of the ride comfort (human perception), which is even more developed than the objective improvement (PSD values). In summary it can be said, that the combined controller based on a State-Space controller and a Skyhook controller provides the best ride comfort of all examined control strategies.

4.7 Summary of Results

The main objective of this thesis is to establish the best controller strategy for the test vehicle possible. As explained at the beginning of this thesis (see page 10), the most important characteristic value for interpreting the ride comfort of a vehicle and its suspension system is displayed in a PSD diagram. Therefore, this summary deals with the evaluation of different controller models by analyzing their resulting PSD peak points. However, it contains not only the results of test vehicle but also data from the simulations, which served as basis to generate the best controller parameters.

Figure 4.44 depicts the PSD peak points of all examined controller models with their best constants respectively. As illustrated a passive suspension system generates a PSD peak point of 2,34 $\frac{m^2}{s^3}$ during the tests. As expected, in contrast to the other controller strategies, the ride comfort is worsened by the use of a Groundhook controller to a value of 2,78 $\frac{m^2}{s^3}$. It reflects the circumstance, that the Groundhook controller forces solely the wheels to perform a minimum vertical movement (enhanced driving safety). A deterioration of the body acceleration is not aspired, but taken into account.

A very interesting controller proves to be the P-Controller, which minimizes the vertical body acceleration itself. This controller shows an astonishing performance in the simulations by lowering the PSD peak point up to 0,17 $\frac{m^2}{s^3}$ (P-Controller constant = 2000). Unfortunately, the examination of higher values in the vehicle needed to be aborted due to the electrical consumption of the actuator, which has become excessive.

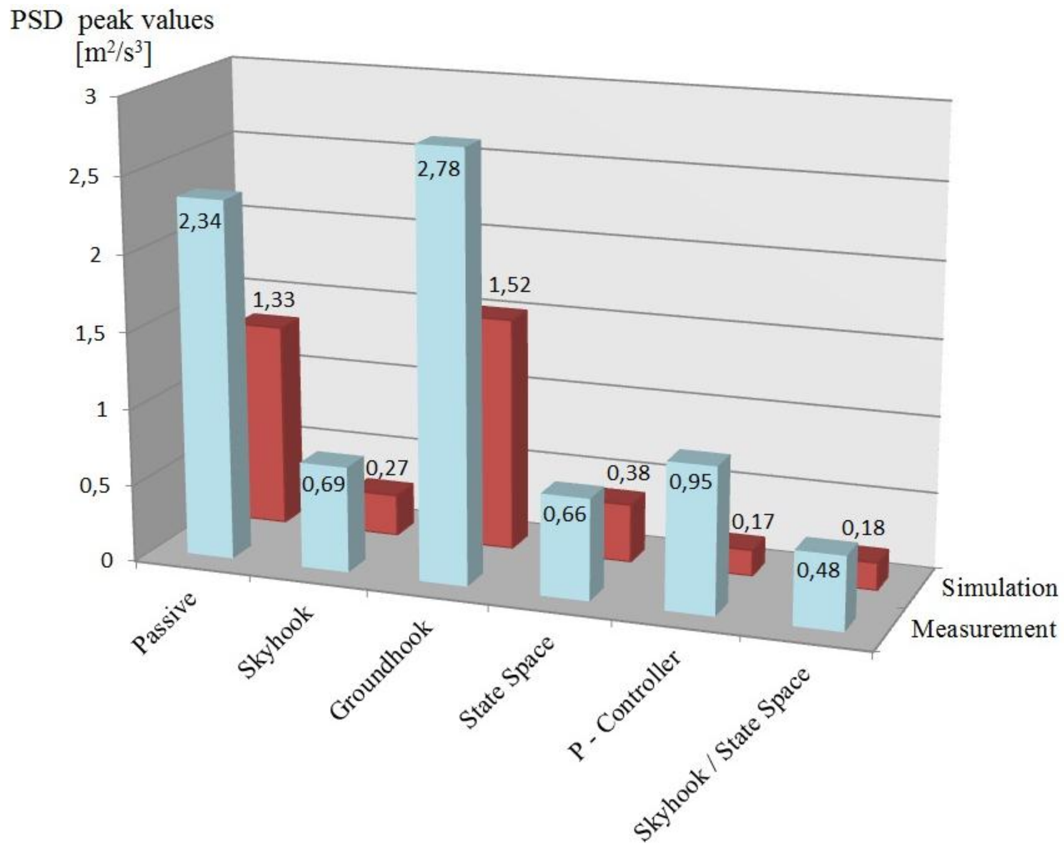

Figure 4.44 : Comparison of PSD peak points of examined controllers.

This is the very reason why the highest examined constant in the test vehicle for this strategy is merely '200', representing a PSD peak point of 0,95 $\frac{m^2}{s^3}$. Consequently, the high expectations regarding the P-Controller model cannot be fulfilled.

The Skyhook controller on the other hand shows a very promising behavior. Compared to a passive suspension system the PSD peak point is reduced to one third which corresponds with 0,69 $\frac{m^2}{s^3}$ (Skyhook constant of 3000).

This very good behavior can be exceeded by the State-Space strategy when using the following constants: f = 1,0 Hz; D = 0,7. In this case the system attributes correspond with a maximum PSD value of 0,66 $\frac{m^2}{s^3}$.

With the aim of further improvements, the first two controller models, which showed the best characteristics are combined: The Skyhook controller with a constant of 3000 and the State-Space controller with its constants f = 1,0 Hz and D = 0,7. These controllers calculate their desired actuator movements independently and add the resulting values. With a PSD value of 0,48 $\frac{m^2}{s^3}$ this combined strategy shows the best ride comfort of all examined controll strategies. Although the difference to the results of the State-Space controller seems to be moderate, the impact on the subjective feeling in the test vehicle appears substantial.

Additionally Figure 4.44 illustrates that the simulation shows an acceptable accuracy compared to the behavior of the test vehicle, even though the absolute values are not identical. Table 4.2 demonstrates that the trend calculated by simulation is confirmed by reality i.e. the PSD peak point of the measured Skyhook controller corresponds to a reduction of 71 % compared to the measured passive system. Equivalently, the simulated Skyhook controller corresponds to a reduction of 80 % compared to the simulated passive system.

Table 4.2 : Improvement of controller types.

	Measurement M		**Simulation S**	
Controller	**PSD Peak Point [m^2/s^3]**	**Improvement compared to passive system**	**PSD Peak Point [m^2/s^3]**	**Improvement compared to passive system**
Passive	2,34	-	1,34	-
Skyhook (constant S= 6000) (constant M= 3000)	0,69	71 %	0,27	80 %
Groundhook (constant = 500)	2,78	-19 %	1,52	-14 %
State-Space (f = 1,0 Hz; D = 0,3)	0,66	72 %	0,38	71 %
P-Controller (constant S = 2000) (constant M = 200)	0,95	59 %	0,17	87 %
Skyhook (constant = 3000) **/ State-Space** (f = 1,0 Hz; D = 0,3)	0,48	79 %	0,18	86 %

The shown PSD diagrams and values have been plotted by using a smoothened PSD calculation through an ‘m - file’ in MATLAB. However, for the human well-being there are some appointed frequency weightings. In order to interpret the comfort feeling of human accurately, ISO 2631-1 and VDI2057, which are explained in the following section, should be taken into consideration.

4.8 Evaluation of Human Exposure to Whole-Body Vibration

According to ISO 2631-1 and VDI 2057, vertical body acceleration's RMS values should be evaluated with human sensitivity, when examining the ride comfort: The frequency-weighted acceleration '$a_w(t)$' is "the variable derived from the instantaneous acceleration signal '$a(t)$' and enables to interpret human well-being.

The related weighting factors (see Figure 4.45) that will be used, are explained in VDI as following:

- W_k: Assessment of well-being while sitting or standing for the vertical axis z
- W_f: Assessment of low-frequency vertical vibrations which could result in kinetosis
- W_e: Rotational vibrations about three axes x, y and z, for seated position, for assessment of well-being.

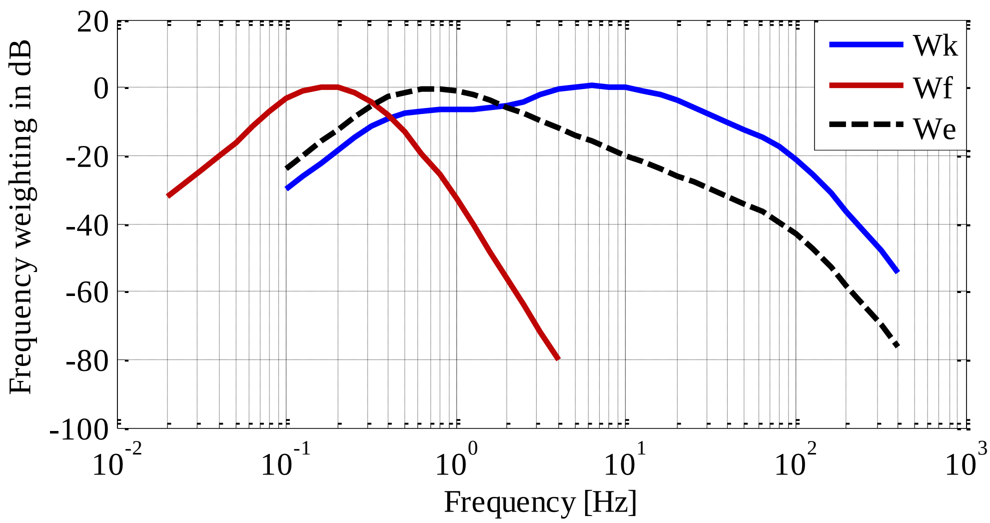

Figure 4.45 : Frequency weightings according to ISO.

According to VDI 2057, when the frequency spectrum is attainable in the form of unweighted spectral power density G(f), the partial energy- equivalent frequency-weighted acceleration 'a_{wi}' is calculated by using formula 4.1, for each frequency component:

$$a_{wi} = W_i \cdot \sqrt{G_i \Delta f_i} \qquad \textbf{(4. 1)}$$

In this formula:

- 'a_{wi}' is partial frequency-weighted acceleration for the frequency interval Δf_i
- 'G_i' is average spectral power density in the frequency interval
- 'Δf_i' is bandwidth of the frequency interval i
- 'W_i' is value of the function of the frequency weighting for the frequency interval [23].

The energy-equivalent mean value of the frequency-weighted acceleration of the complete spectrum 'a_w' is calculated from the partial frequency-weighted accelerations by using formula 4.2:

$$a_w = \sqrt{\sum_{i=1}^{m} a_{wi}^2} \qquad \textbf{(4. 2)}$$

e.g. to determine the assessment of well-being W_k the following resulting (from formula 4.1 and 4.2) formula applies:

$$a_{w}\_W_k = \sqrt{\sum_{i=1}^{m} (W_{ki} \cdot \sqrt{G_i \Delta f_i})^2} \qquad \textbf{(4. 3)}$$

$a_w\_W_k$, $a_w\_W_f$ and $a_w\_W_e$ display a rather specific interpretation of the vehicles characteristics. A general evaluation of the ride comfort can be gained by:

$$Total = \sqrt{(a_w\_W_k)^2 + (a_w\_W_f)^2 + (a_w\_W_e)^2} \qquad \textbf{(4. 4)}$$

The results of these calculated frequency-weighted accelerations, based on the measurements, are presented in Figure 4.46.

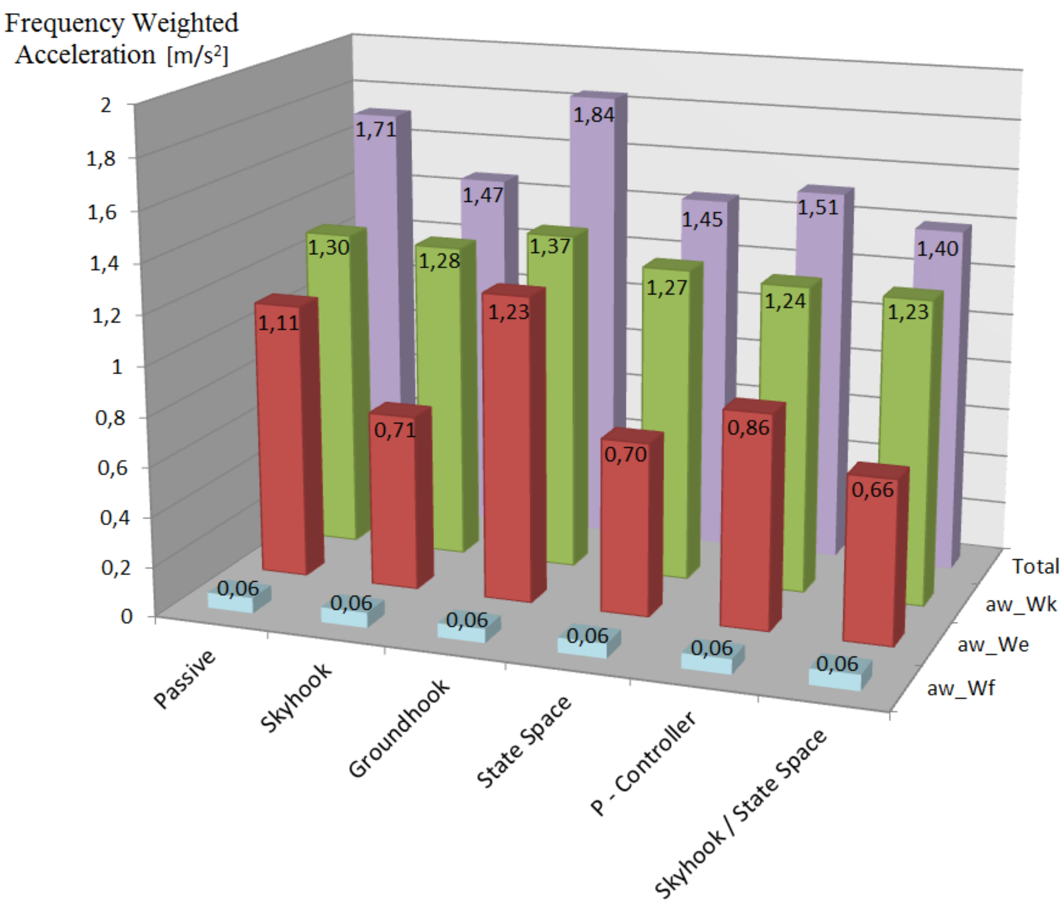

Figure 4.46 : Frequency weighted accelerations (measurements).

As illustrated the frequency weighted acceleration ($a_w\_W_f$) of the passive system is 0,06 $\frac{m}{s^2}$. Furthermore, it is notable that there is no or merely an insignificant impact of the differing controller strategies on the assessment of low-frequency vertical vibrations.

The value $a_w\_W_e$ represents the subjective impact of rotational vibrations (such as roll motion) on the human well-being. The following attributes are worth pointing out:

- The frequency-weighted accelerations show the same tendencies as the peak values of the PSD diagrams (compare Figure 4.44). The passive system provides a weighted acceleration of 1,11 $\frac{m}{s^2}$. As expected, the Groundhook controller deteriorates (1,23 $\frac{m}{s^2}$) and the P–Controller improves the human well-being (0,86 $\frac{m}{s^2}$). As illustrated before, the Skyhook (0,71 $\frac{m}{s^2}$) and the State-Space (0,70 $\frac{m}{s^2}$) strategy are able to generate a further improvement.

Consequently, the combined Skyhook / State–Space system provides the lowest and hereby the best value of 0,66 $\frac{m}{s^2}$.

- A comparison of $a_w\_W_k$, $a_w\_W_f$ and $a_w\_W_e$ shows that the values of $a_w\_W_e$ are varying the most: The smallest value correlates with 0,66 $\frac{m}{s^2}$ and the biggest with 1,23 $\frac{m}{s^2}$. This implies that the active suspension and the examined controllers affect mostly the rotational vibrations.

The assessment of well-being while sitting $a_w\_W_k$ shows mostly a similar tendency compared to the values $a_w\_W_e$. The Groundhook (1,37 $\frac{m}{s^2}$) controller provides a worse behavior than the passive system (1,30 $\frac{m}{s^2}$). The best performance can be achieved, as before, by the combined Skyhook / State–Space controller (1,23 $\frac{m}{s^2}$). In contrast to prior results, the P-Controller (1,24 $\frac{m}{s^2}$) generates a lower value than the Skyhook (1,28 $\frac{m}{s^2}$) or the State-Space strategy (1,27 $\frac{m}{s^2}$). Another fact worth mentioning is the minor difference between the biggest and lowest value (1,37 $\frac{m}{s^2}$ and 1,23 $\frac{m}{s^2}$): The impact on the characteristics of $a_w\_W_k$ is considerably smaller than the impact on the characteristics of $a_w\_W_e$.

The summarized results calculated by formula 4.4 show the same order of controllers providing the best ride comfort as assumed by the results of the PSD peak points:

6. Groundhook controller: 1,84 $\frac{m}{s^2}$

5. Passive system: 1,71 $\frac{m}{s^2}$

4. P-Controller: 1,51 $\frac{m}{s^2}$

3. Skyhook controller: 1,47 $\frac{m}{s^2}$

2. State–Space controller: 1,45 $\frac{m}{s^2}$

1. combined Skyhook / State–Space controller: 1,40 $\frac{m}{s^2}$

Due to the fact, that the relevant elements of this calculation show mostly the same tendency as the calculated PSD peak points, this result is expected.

4.9 Error Discussions (Discrepancy of Model and Test Results)

In this master thesis, mainly the most convenient controller design for a slow-active suspension system is examined. Firstly, the investigations were done with simulations and then with a prototype vehicle. The probable reasons for the discrepancies between simulations and tests are mentioned in this section.

One of the reasons can be the simulation model assumptions as half vehicle model. The mentality of using a half vehicle model is the assumption of driving only on the rough roadway without curves or bends. This means that the roll motion is neglected. Therefore, the right input of the roadway is also neglected and only the left input is used in simulations. There could be some errors arising from this reason.

Another reason can be the negligence of wheel damping. In wheel blocks of the Simulink model, the damping coefficient or characteristics are assumed as zero. Furthermore, in Simulink model there is no tire model or rubber bearing model, which can influence the transmitted force to the vehicle body.

Another reason is the difference of controller block in the vehicle and in the simulations. In Simulink model, always a vertical controller design has been examined while in the test vehicle there are some other controllers as automatic level (offset explained in section 4.1) and horizontal controller. Figure 4.47 shows only an example of controller's desired actuator values from the tests. There are three main parts to affect the total desired actuator value as shown in the figure.

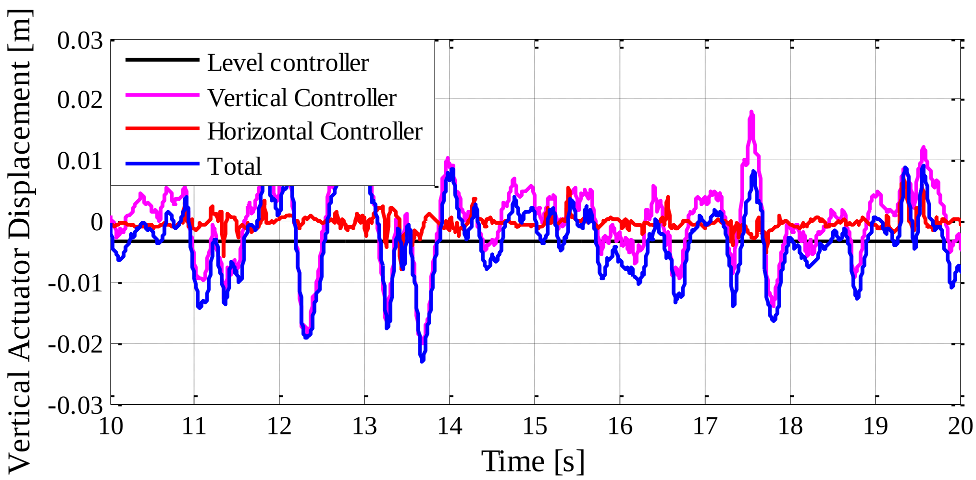

Figure 4.47 Desired actuator movement (with Skyhook controller -c_{sky}=3000-).

The total desired movement of the actuator is calculated by using formula 4.5:

$$z_{vertical} + z_{horizontal} + z_{level} = z_{Act\_total} \quad \textbf{(4.5)}$$

In simulations, the effects of horizontal and level controllers are neglected. Therefore, there can be a discrepancy between simulations and tests.

5. CONCLUSIONS AND RECOMMENDATIONS

The objective of this thesis was to design a controller strategy for an active electromechanical suspension system in order to enable the best ride comfort behavior in the test vehicle.

First of all, a MATLAB/Simulink model has been created, which represents the most relevant dynamic properties of the vehicle for the purpose of reducing the number of tests in reality, as those take more time and are riskier. This simulation is based on a half vehicle model that has been obtained from the Volkswagen AG database. By modifying the vehicle parameters and adjusting the initial model, a suspension behavior could be generated, that displays an acceptable accuracy compared to the examined test vehicle.

At first, several different control strategies have been evaluated in MATLAB/Simulink for understanding the reaction logic of the controller and hereby its impact on the test vehicle. Subsequently, the best control parameters have been determined for each controller model in order to get the best ride comfort possible. Within the scope of this work the following controller have been analyzed:

- passive (no vertical controller),
- Groundhook controller,
- P-Controller (minimizing the vertical body acceleration itself),
- Skyhook controller,
- State-Space controller,
- Combination of Skyhook and State-Space controller.

Finally, supported by the results of the simulations, the controller strategies were validated in the test vehicle. Thereby, the controller constants needed to be adjusted due to the fact that the simulation provides a qualitative characterization in which absolute values may differ (compared to the test vehicle).

The significant findings resulting from this work, show that the Groundhook strategy (PSD peak point = 2,78 $\frac{m^2}{s^3}$) deteriorates the ride comfort in comparison to the passive suspension system (2,34 $\frac{m^2}{s^3}$), since the controller strategy is focusing on driving safety and not on ride comfort.

The P-Controller shows an astonishingly effective performance in the simulations by lowering the PSD peak point up to 0,17 $\frac{m^2}{s^3}$. However, caused by the excessive electrical consumption of the actuator in the test vehicle, the examination of higher P-Controller constants needed to be aborted. Nevertheless, the feasible P-Controller constants were able to improve the ride comfort moderately (0,95 $\frac{m^2}{s^3}$). Although the results of the tests and especially of the simulations illustrated a very promising behavior, further examinations of this interesting control strategy could not be conducted due to lack of time. For this reason, additional analyses are advised.

The Skyhook controller (0,69 $\frac{m^2}{s^3}$) on the other hand is able to enhance the ride comfort substantially. This already good behavior can be exceeded by the State-Space strategy (0,66 $\frac{m^2}{s^3}$), especially when combining it with a Skyhook controller (0,48 $\frac{m^2}{s^3}$). The combined State-Space / Skyhook strategy generates a ride comfort in the test vehicle, which seems even more enhanced than anticipated from the objective PSD values. Consequently, the application of this controller strategy is recommended for the active electromechanical suspension system.

However, for future work there are several effects to consider, while working with this combined controller. The performance of this control strategy illustrates a potential, which needs to be further refined and thereby exploited. For this purpose, the following research may be advantageous:

(i) As mentioned before, this control algorithm represents the combination of the two superior controller models of this thesis. It was assumed that the control parameters, which provide the best dynamic behavior in Skyhook and State-Space (individually), would also generate the best dynamic characteristic in this combined controller. Nevertheless, differing parameters may enable an even more enhanced dynamic performance.

(ii) Instead of adding the resulting actuator displacements (100% Skyhook + 100% State-Space) another combining structure could be more rewarding (e.g. 60 % Skyhook + 90% State-Space).

(iii) A combination of Skyhook, State-Space and an additional controller (e.g. P-Controller) might be beneficial.

REFERENCES

[1] **Heißing, B. and Ersoy, M.**, 2011, *Chassis Handbook - Fundamentals, Driving Dynamics, Components, Mechatronics, Perspectives.* Wiesbaden : Vieweg+Teubner.

[2] **Hrovat, D.**, 1997, *Survey of advanced suspension developments and related optimal control applications.* Great Britain : Automatica, Vol. 33, No. 10, page 1781–1817.

[3] **Koch, G.**, 2011, *Adaptive Control of Mechatronic Vehicle Suspension.* s.l. : Dissertation, Technische Universität München.

[4] **Boekestyn, Alex, et al.**, 2011, *Advanced Chassıs systems Report.* Stamford, UK : IHS SupplierBusiness.

[5] **Cho, Byung Kwan.**, 1999, *Active suspension controller design using MPC with preview information.* s.l. : KSME International Jouranl . 1999, Vol.13, No.2.

[6] **Heißing, B.**, 2007, *Fahrwerkhandbuch.* Wiesbaden : Vieweg Verlag.

[7] **Eulenbach, Dr.-Ing. Dieter.**, 2000, *Nivomat The Automatic Level Control System with Spring Function and Damping Function.* Eitorf/ Germany : Technical Academy of Esslingen (Mannesmann Sachs AG).

[8] **Url-1** <*http://www.citroenet.org.uk/miscellaneous/hydraulics/hydraulics-13.html*>, accessed at 07.09.2011.

[9] **Url-2** <*http://www.psa-peugeot-citroen.com/modules/suspension/anglais/parent.swf*>, accessed at 05.10.2011.

[10] **Savaresi, S. M., et al.**, 2010, *Semi-active suspension control design for vehicles.* Amsterdam : Butterworth-Heinemann.

[11] **Url-3** <*http://www.bose.de/DE/de/learning-centre/suspension-problem*>, accessed at 09.12.2011.

[12] **Muenster, M., et al.**, 2008, *Electromechanical Active Body Control.* F2008-03-057 : s.n.

[13] **Merker, T., Girres, G. and Thriemer, O.**, 2002, Active Body Control (ABC) The DaimlerChrysler Active Suspension and Damping System.

[14] **Muenster, M., et al.**, 2009, *Electromechanical Active Body Control.* s.l. : ATZ.

[15] **Abdalla, M. O., Al Shabatat, N. and Al Quaisi, M.**, 2009, *Linear matrix inequality based control of vehicle active suspension system.* Jordanien : Vol. 47, p. 121 – 134, Vehicle System Dynamics,.

[16] **Hestermeyer, T.**, 2006, *Strukturierte Entwicklung der Informationsverarbeitung fuer die aktive Federung eines Schienenfahrzeugs, PhD thesis.* University of Paderborn : s.n.

[17] **Becker, M., et al.**, 1996, *Development of an active suspension system for a Mercedes-Benz coach.* Dearborn, Michigan : IEEE International Symposium on Computer-aided Control System Design.

[18] **Merker, T., et al.**, 2001, *Das SL- Fahrwerk – Dynamik und Komfort vereint.* s.l. : ATZ Sonderausgabe.

[19] **Schindler, A.**, 2009, *Neue Konzeption und erstmalige Realisierung eines aktiven Fahrwerks mit Preview-Strategie.* Dissertation, Universität Karlsruhe : s.n.

[20] **Mehra, R. K., et al.**, 1997, *Active suspension using preview information and model predictive control.* s.l. : pages 860 – 865, IEEE International Conference on Control Applications.

[21] **Akbari, A.**, 2009, *Multi-Objective H∞/GH2 preview control of active vehicle suspensions.* s.l. : Dissertation, Technische Universitaet Muenchen.

[22] **Reimpell, J.**, 1995, *Fahrwerktechnik: Grundlagen.* 3.überarbeitete Auflage, Würzburg : Vogel.

[23] **ISO 2631-1**. *Mechanical vibration and shock – Evaluation of human exposure to whole-body vibration.* s.l. : 2nd edition, International Organization for Standardization, 1997.

[24] **Mitschke, M. and Wallentowitz, H.**, 2004, *Dynamik der Kraftfahrzeuge, 4. Auflage.* Berlin Heidelberg : Springer.

[25] **VDI *guideline 2057***, 2002, *Human exposure to mechanical*.

[26] **Rieckmann, A.**, 2009, *Potentialanalyse semi-aktiver Fahrwerke mit Vorausschau.* s.l. : Studienarbeit, Technische Universität Braunschweig.

[27] **Streiter, R. H.**, 1996, *Entwicklung und Realisierung eines analytischen Regelkonzeptes für eine aktive Federung.* s.l. : Dissertation, Technische Universität Berlin.

[28] **Mitschke, M. and Wallentowitz, H.**, 2001, *Dynamik der Kraftfahrzeuge.* Berlin : Springer.

[29] **Tims, H. E.**, 2005, *Vehicle Active Suspension System Sensor Reduction.* s.l. : Dissertation, The University of Texas at Austin.

[30] **Guglielmino, E., et al.**, 2008, *Semi-active suspension control - Improved vehicle ride and road friendliness.* London : Springer.

[31] **Gao, G. S. and Yang, S. P.**, 2006, *Semi-active control performance of railway vehicle suspension featuring magnetorheological dampers, pages 1–5.* Shijiazhuang, China : 1st IEEE Conference on Industrial Electronics and Applications.

[32] **Jordan, T. C. and Shaw, M. T.**, 1989, *Electrorheology.* s.l. : Vol. 24, No. 5, page. 849–878, IEEE Transactions on Electrical Insulation.

[33] **Chung, S. K. and Shin, H.-B.**, 2004, *High-voltage power supply for semi-active suspension system with ER-fluid dampe.* s.l. : Vol. 53, No. 1, page 206 – 214, IEEE Transactions on Vehicular Technology.

[34] **Url-4** <*http://www.kfztech.de*>, accessed at 09.09.2011.

[35] **Zeipert, S.**, 2009, *Potentialanalyse von Regelstrategien für aktive Fahrwerke mit Vorausschau.* s.l. : Diplomarbeit (Master Thesis), Technische Universitaet Braunschweig.

[36] **Serge Zacher, Manfred Reuter.**, 2011, *Regelungstechnik für Ingenieure (13., überarbeitete und erweiterte Auflage).* Germany : Vieweg + Teubner.

[37] **Duda, H., Berkner, S. and Hoffmann, J.**, 2002, *Querdynamikregelung für PKW mit aktivem Fahrwerk, Steuerung und Regelung von Fahrzeugen und Motoren.* s.l. : VDI-Berichte Nr. 1672, Page 343-352., Vols. Page 343-352.

[38] **Url-4** <*http://www.et.uni-magdeburg.de*>, accessed at 16.08.2011.

[39] **Karnopp, D.**, May 1974, Vibration Control Using Semi-Active Force Generators. *Journal of Engineering for Industry.*.

[40] **Wang, Y.-H. and Shih, M.-C.**, 2007, *Semi-Active Suspension Control In A Passenger Car Using A Ga-Fuzzy.* Tainan City, 701 Taiwan : National Cheng-Kung University.

[41] **Lunze, J.**, 2008, *Regelungstechnik 2- Mehrgrößensysteme, Digitale Regelung.* Berlin Heidelberg : Springer-Verlag.

CURRICULUM VITAE

Name Surname:	Sevsel Gamze KABIL
Place and Date of Birth:	Besiktas, 21.02.1986
Address:	Palanga Cad. Yildiz Subay Lojmanlari Turgutreis Blok D:18 Besiktas/Istanbul
E-Mail:	gamzekabil@hotmail.com
B.Sc.:	Yıldız Technical University, (2004-2009)
M.Sc.:	Istanbul Technical University, (2009-2012)